

2941 2  
P  
**N91-14666**  
90-0

**BLOCK ROTATIONS, FAULT DOMAINS AND CRUSTAL  
DEFORMATION IN THE WESTERN U.S.**

**FINAL REPORT**

**09-15-87/02-28-90**

**Prepared by Amos Nur  
Geophysics Department  
Stanford University  
Stanford, CA 94305-2215**

**For  
NASA  
Goddard Space Flight Center  
Research Grant No: NAG 5 926**

This report contains a brief summary, new results, a list of publications and reprints for the project on "Block Rotations, Fault Domains and Crustal Deformation in the Western United States".

## SUMMARY

The aim of the project was twofold :

- 1) Develop a 3D model of crustal deformation by distributed fault sets.
- 2) Test the model results in the field.

### 1. Block Rotation Modeling in 3D

In the first part of the project, Nur's 2D model (1986) was generalized to 3D. In Nur's model the frictional strength of rocks and faults of a domain provides a tight constraint on the amount of rotation that a fault set can undergo during block rotation. Domains of fault sets are commonly found in regions where the deformation is distributed across a region. The interaction of each fault set causes the fault bounded blocks to rotate. The following paragraphs briefly summarize the work that has been done towards quantifying the rotation of fault sets in a 3D stress field.

Estevez et al. (1990) developed a block rotation algorithm to analyze the 3D rotation path of faults, which describes the subsequent orientation of rotating, fault bounded blocks of a domain. The algorithm computes the rotation path in either the  $\sigma_n - \tau$  space of the Mohr circle, or the Wulff stereoprojection representations. The former demonstrates the mechanical behaviour of faults during rotation whereas, the latter provides a geometrical picture of the rotating faults in space. The most important results of this study are:

- a) Fault rotation may occur under "unstable" stress conditions (that is, slip and rotation of preexisting, poorly oriented faults may promote further slip and rotation).
- b) Rotating faults may change their style of faulting as deformation continues.

Scotti et al. (1990) analyzed the geometry of distributed deformation across the domains of Southern California. The results show that active faults of the domains considered, can slip in accordance with friction criteria, in a homogeneous and stationary stress field, in spite of their diverse orientation and fault behaviour. The most important conclusions of the first part of this study are:

- a) Reactivated fault sets are usually not well oriented in the stress field.
- b) Even very poorly oriented fault sets can be reactivated in a stationary stress field.

In the second part of the study Scotti et al. (1990) analyzed the behaviour of rotating faults using the algorithm of Estevez et al. (1990). All three stress regimes were considered: normal, reverse and strike-slip. The results show that, for specific stress conditions and initial fault geometries, extreme changes in fault behaviour are possible during fault rotation. As an example the authors investigated the faulting history of the West Transverse Ranges, southern California. The 3D block rotation model predicts, in accordance with geological information, that the fault set of this domain may have been initially reactivated as normal faults. Upon rotation the fault set became strike-slip in nature and finally it rotated into the present-day high angle

reverse behaviour. The most important conclusions of the second part of this study are:

- a) Fault sets become poorly oriented due to block rotation.
- b) In general, faults and blocks will rotate about a mixture of vertical and horizontal axis. Therefore a vertical component of rotation is indeed expected in all three stress regimes.
- c) Fault behaviour may change considerably as a fault set rotates in a stationary stress field.

Scotti and Nur (see abstract) developed a graphical algorithm to help visualize block rotation in 3D. The algorithm runs on an Ardent computer and utilizes its 3D Dore graphics package. This is an ongoing project aimed at developing a mechanical platform, on which both kinematics and mechanics of the block rotation model can be readily visualized and its implications understood. The final product will be a video tape, summarizing the 2D and 3D model results, as well as showing some applications to actual field examples (West Transverse Ranges, Mojave Desert, Lake Mead etc.).

## 2. Field examples

In the second part of the project, field studies were carried out in Israel, Nevada and China. These studies combined both paleomagnetic and structural information necessary to test the block rotation model results.

Li et al. (1990; 1989) present two field examples of block rotation: one from northwestern China and another from the North Nevada Rift Region. In the first field study, the authors found a discordance between the observed declination and expected declinations from the stable craton. Because the region is characterized by distributed reverse and strike-slip faults, the authors attribute the  $30^{\circ} - 40^{\circ}$  declination anomaly to counterclockwise tectonic rotation of the fault bounded blocks. In the second field study, paleomagnetic data from mid-Miocene dikes and flows indicate that some crustal blocks have rotated  $\sim 20^{\circ}$  counterclockwise relative to stable North America. Rotation of blocks may have been accommodated along a system of right-lateral northwest-trending faults distributed across the region. The most important conclusions from these two field studies are:

- a) Vertical axis rotation of crustal blocks in normal faulting environments does occur, as predicted by the 3D block rotation model.
- b) Because regions of distributed deformation are characterized by tectonic block rotation, it is essential to study the paleomagnetic signature of dykes and single fault set domains before inferring stress directions from them.

The ambiguity between tectonic block rotation or stress field rotation is further addressed in Ron et al. (1989a). In this field study, the authors analyzed both paleomagnetic measurements and structural information from the Lake Mead fault system, Nevada. This region is characterized by distributed sets of strike-slip and normal faults. Multiple generations of faults have been identified. The main conclusions of this study are:

- a) To unravel the combination of tectonic rotation of blocks and stress field rotation it is essential to combine structural and paleomagnetic studies.
- b) Because of both tectonic rotation of blocks and stress field rotation, at least two generations of faults have contributed to crustal deformation in this region, as predicted by the block rotation model.

The existence of multiple generations of faults is further documented in field examples from Israel (Ron et al.; 1989b). As explained by Nur et al.

(1989a; 1989b; 1987), these and previous field studies provide a consistent picture that substantiates the block rotation model results. In accordance with the model, field studies demonstrate that faults and attending fault bounded blocks slip and rotate away from the direction of maximum compression when deformation is distributed across fault sets. Slip and rotation of fault sets may continue as long as the earth's crustal strength is not exceeded. More optimally oriented faults must form, for subsequent deformation to occur. Eventually the block rotation mechanism may create a complex pattern of intersecting generations of faults.

## NEW RESULTS

### 1. 3D BLOCK ROTATION IN THE WEST TRANSVERSE RANGES: THE KEY TO STRUCTURAL HISTORY AND BASIN DEVELOPMENT.

Oona Scotti and Amos Nur.

(AAPG annual convention, 1990)

#### Abstract

Block rotation is widespread in regions of distributed shear. As rigid block-faulted domains rotate, "gaps" open up along their boundaries and sedimentary basins may develop. The evolution and the geometry of these basins is controlled by the slip history of the faults that bound them. To unravel their history, a 3D model was developed that combines the kinematics of block rotation with the mechanics of faulting.

As an example we present a 3D computer simulation for the history of rotation of the West Transverse Ranges domain, Southern California. A set of pre-existing faults, striking N-NE, is allowed to slip and rotate in accordance with known friction criteria. Rotation is assumed to occur in the strike slip stress regime. The principal stress axes are assumed fixed in the present day orientation throughout the deformation. Therefore, as faults slip and blocks rotate the sense of motion along the faults changes. This simulation predicts, in agreement with the observations, a initial period of normal motion along the reactivated faults. Upon fault slip and block rotation the same faults go through a phase of strike slip. With further slip and rotation they eventually become the E-W striking, oblique reverse faults that characterize the present day tectonics of this domain.

The model shows that a single set of faults can experience both dip slip and strike slip motion throughout its deformation history within a strike slip stress regime. It is not necessary to appeal to complex and arbitrary changes in the orientation of the stress field. Only by combining a 3D block rotation model with structural and paleomagnetic data it may be possible to unravel the complex tectonics of distributed deformation and basin evolution.

## 2. BLOCK ROTATION IN 3D.

Raul Estevez, Oona Scotti and Amos Nur

(in preparation...)

### **Abstract**

Based on Mohr's Circles stress representation, *Coulomb-Navier criterion* for faulting and Wulff's stereographic projections, the basic mathematical tools for the description of block rotations in 3-D have been developed. These tools allow to follow the creation and dynamic evolution of individual faults within a bounded rotating fault domain. Mapping relations between Mohr's and geographic Wulff's representations let us "visualize" the state of stress and the geographic location of individual faults at each rotation event, as well as the direction of slip associated with these episodes. Three different models are considered for system stress increase and drop before and after each rotation occurs, corresponding to shear, normal and thrust faulting. Using parameter values, commonly found in the literature, theoretical models show several remarkable features, including, 1) the possibility of changes in faults's principal regimes (strike-slip, normal, thrust), 2) the existence of "unstable states" allowing rotations in the absence of major, if any, contributions from the system's stresses, and 3) notable differences in the evolution of stresses acting on the domain and those acting on individual faults during rotations.

## PUBLICATIONS

- Yianping Li, John Geissman, Amos Nur, Hagai Ron and Qing Huang; "Counterclockwise Block Rotation in the North Nevada Rift Region: Paleomagnetic Evidence", *Geology*, 18, 79-82, 1990.
- Yianping Li, Robert Sharps, Michael McWilliams, Amos Nur, Yongan Li, Qiang Li and Wei Zhang; "Paleomagnetic results from Late Paleozoic dikes from the northwestern Junggar Block, northwestern China", *Earth and Planetary Science Letters*, 94, 123-130, 1989.
- Amos Nur, Hagai Ron and Oona Scotti; "Kinematics and Mechanics of Tectonic Block Rotation", in *Slow Deformation and Transmission of Stress in the Earth*, eds. S.C.Cohen and P.Vanicek, *Geophysical Monograph: 49/IUGG Series: 4*, 1989a.
- Amos Nur, Hagai Ron and Oona Scotti; "Mechanics of distributed fault and block rotation", in *Paleomagnetic Rotations and Continental Deformation* by Kluwer Academic Publishers, eds. C.Kissel and C.Laj, 209-228, 1989b.
- Amos Nur and Hagai Ron; "Block Rotations, fault domains and crustal deformation", *Annales Tectonicae*, 1, 1, 40-47, 1987.
- Hagai Ron, Amos Nur and Attila Aydin; "Stress Field Rotation or Block Rotation: an Example from the Lake Mead Fault System", submitted to *Geology*, 1989a.
- Hagai Ron, Amos Nur and Y. Eyal; "Multiple Strike Slip Fault sets: a Case Study from the Dead Sea Transform", submitted to *Tectonics*, 1989b.
- Oona Scotti, Amos Nur and Raul Estevez; "Distributed deformation and block rotation in 3D", submitted to *Journal Geophysical Research*, March 1990.

# Distributed deformation and block rotation in 3D

Oona Scotti, Amos Nur, Raul Estevez\*

Rock Physics Laboratory  
Department of Geophysics  
Stanford University  
Stanford California 94305  
March 1, 1990

## ABSTRACT

In this paper, we address how block rotation and complex distributed deformation in the Earth's shallow crust may be explained within a stationary regional stress field. Distributed deformation is characterized by domains of sub-parallel fault-bounded blocks. In response to the contemporaneous activity of neighboring domains some domains rotate, as suggested by both structural and paleomagnetic evidence.

Rotations within domains are achieved through the contemporaneous slip and rotation of the faults and of the blocks they bound. Thus, in regions of distributed deformation, faults must remain active in spite of their poor orientation in the stress field. Traditional friction models cannot account for this mechanism. To solve this problem we developed a model that tracks the orientation of blocks and their bounding faults during rotation in a 3D stress field. Mechanically, we considered Coulomb criteria for rock fracture, as an upper bound, and fault slippage, as a lower bound, between which block rotation is expected.

In our model, the effective stress magnitudes of the principal stresses ( $\sigma_1$ ,  $\sigma_2$ ,  $\sigma_3$ ) are controlled by the orientation of fault sets in each domain. Therefore, (1) adjacent fault sets with differing orientations may be active and may display differing faulting styles, and (2) a given set of faults may change its style of motion as it rotates within a stationary stress regime. The style of faulting predicted by our model depends on a dimensionless parameter  $\phi = (\sigma_2 - \sigma_3)/(\sigma_1 - \sigma_3)$ . Thus, we present a model for complex distributed deformation and complex offset history requiring neither geographical nor temporal changes in the stress regime.

We apply the model to the Western Transverse Range domain of Southern California. There, it is mechanically feasible for blocks and faults to have experienced up to  $75^\circ$  of clockwise rotation in a  $\phi = 0.1$  strike-slip stress regime. The results of our model suggest that this domain may first have accommodated deformation along preexisting NNE-SSW faults, reactivated as normal

---

\*now at Universidad de los Andes, Mérida, Venezuela

faults. After rotation, these same faults became strike-slip in nature. Subsequent rotations could have resulted in the present day E-W high angle reverse faults. This history agrees with both prominent structural phases documented for post-Oligocene activity and paleomagnetically inferred rotations of this domain.

# CRUSTAL DEFORMATION BY BLOCK ROTATION

## 1. The problem

Distributed crustal deformation is characterized by sub-parallel sets of faults (Freund, 1970; Freund, 1971; Garfunkel, 1974; Luyendyk et al., 1980; Ron et al., 1984; and others). Sets are distinguished from their neighbors by orientation and often by faulting style as well. In a region like Southern California, throughgoing faults often mark the boundaries of these domains such as the San Andreas and Garlock fault shown in Fig. 1.

If the regional stress field is homogeneous and stationary throughout a region like Southern California (Zoback et al., 1987), then how can we have active fault sets in such varying orientations? At least three solutions can be suggested:

- (1) In regions of distributed deformation, fault sets behave in accordance with unknown friction criteria.
- (2) The stress field is not homogeneous and stationary. Instead, it changes orientation from one domain to the next.
- (3) The stress field is homogeneous and stationary and the fault sets slip in accordance with friction criteria but in some domains blocks and faults rotate.

The answer most probably lies in a combination of these three extreme cases. Fault behaviour is most likely a function of the slip rate and the history of slip; the stress field must be inhomogeneous to some extent across a region of distributed deformation; rotation of blocks and faults must indeed occur when many domains of fault sets coexist.

In this paper, we restrict our attention to the third case: the rotation of faults and of the blocks between them. Accumulating paleomagnetic and structural evidence shows that in region of distributed deformation, many structural domains have rotated in the past, and some are rotating today (see Nur et al., 1986; Ron et al., 1988). Different block rotation mechanisms have been proposed (see Molnar, 1988). Here, we propose a 3D block rotation mechanism based on Nur et al. (1986) 2D model. For this reason, we first give a brief summary of the kinematics and mechanics of the 2D version.

## 2. Kinematics of block rotation in 2D

The kinematics of block rotation in strike-slip tectonic regimes, were originally proposed by Freund (1970; 1974) on the basis of structural data alone. He observed two sets of strike slip faults with an angle of  $145^\circ$  between them measured in the maximum compressional direction. He attributed this angular spread to the tendency of strike slip faults to rotate about a vertical axis away from the maximum compressional direction. In fact, rotation of faults as a mechanism for accommodating deformation, was first recognized in normal tectonic regimes (Ransome et al., 1910; see references in Jackson and White, 1989).

This rotation is illustrated schematically in Fig. 2. In this simple case, the vertical stress  $S_v = \sigma_1 = \text{gravity}$ , is the only stress acting. As the books slide on the shelf they rotate away from  $\sigma_1$ , the direction of maximum compression: in a counter-clockwise (CCW) sense (domain A) or clockwise (CW) sense (domain B) depending on the orientation of the books. From this example, one can see that—whether strike-slip or dip-slip—right-lateral fault motion leads to CCW sense of rotation, and left-lateral movement leads to CW sense of rotation of blocks and faults.

The block rotation model assumes that the rotating blocks are rigid. Luyendyk et al. (1985), Ron et al. (1984), Carter et al. (1987) and Terres and Luyendyk (1985) have validated this assumption. In the domains they studied, two significant correlations were found. The first one between the measured sense of

slip, the expected sense of rotation and the paleomagnetically inferred axis of rotation (as explained in Fig. 2); the second one between the known amount of total displacement across a fault set, the measured average spacing between sub-parallel faults, and the amount of rotation inferred paleomagnetically for a domain.

### 3. Mechanics of block rotation in 2D

In Freund's model, as faults slip, the blocks they bound rotate away from the direction of maximum compression. Nur et al. (1986) added a mechanical limit to this kinematic model for the case of vertical strike slip faults rotating in a strike-slip regime. In Nur's block rotation (BR) model, two additional constraints are introduced. One is given by the Coulomb criterion for sliding, and the second one by the Coulomb criterion for fracturing (eq. (1) and (2) in the Appendix).

Within a region of distributed deformation, where a single fault set orientation characterizes each domain, the first constraint implies that fault sets may remain active even if poorly oriented in the stress field, and the second constraint sets a limit on how poorly oriented the fault set may become. A fault is considered optimally oriented when the intermediate stress  $\sigma_2$  is contained in the plane of the fault and the shear stress required for slip along the fault is such that the  $\sigma_1 - \sigma_3$  Mohr circle is just tangent to the sliding line (Fig. 3).

In Nur's model, faults rotate within a stationary stress field. This implies that during rotation the stress magnitudes must change in a domain, for blocks and faults to continue to slip and rotate (Fig. 4). When the magnitude of the differential stress reaches the strength of the intact crust (the fracture line on the  $\sigma_n - \tau$  plot), a new set of more optimally oriented faults forms, and the old set becomes locked. As a result, a discrete range of fault orientations is predicted by the BR model. Only when sufficiently large rotations occur in a domain will cross-cutting generations of fault sets give rise to a complex pattern of faulting, such as those observed in situ (Angelier et al., 1985; Ron et al, in press).

The mechanical constraints of the BR model provide an important step toward quantitative estimates of the contribution of block rotation to distributed deformation in the Earth's crust. The relationship among friction, strength and the amount of rotation that a single set of faults can experience are detailed in Nur et al. (1986).

As Fig. 4 shows, block rotation can cause poor fault orientation. However, the 2D model is limited in its application since the intermediate principal stress  $\sigma_2$  must remain in the fault plane. This limitation prevents any change of faulting style during rotation. A 3D formulation is necessary to model the more common case of rotation along reactivated faults, where  $\sigma_2$  is not necessarily in the plane of the fault. Then, we can identify the conditions that allow a fault set to drastically change its behaviour as it rotates.

### 4. Block rotation in 3D

The focus of this paper is to understand distributed deformation and the relationship between fault slip and the rotation of faults and blocks in a three dimensional stress field. The fundamental strength and friction criteria proposed in the 2D model are preserved. In addition, the 3D model considers all faulting styles that can occur in a general stress field for any starting orientation of modeled faults.

We will first discuss the more fundamental assumptions that must be made when modeling distributed deformation and block rotation in a 3D stress field. Then, we will discuss the implications of combining the 3D stress Mohr circle

with friction criteria applied to the present-day tectonics of Southern California. In the main part of the paper, we will discuss the principles of the 3D BR model. As the results will show, even a simple 3D BR model can produce complicated faulting histories and complex distributed deformation geometries.

Because faults generally change their behaviour as they rotate in a stationary stress field, a model of faulting and rotation in 3D is fundamental to our understanding of this mechanism. In the final part of the paper, as a practical application of our model, we will compare the known rotation history of the Western Transverse Range domain in Southern California with the results of our model. We find encouraging similarities between our 3D BR model predictions and the complex structural and geological record of this domain.

## THE STATE OF STRESS

### 1. One principal stress assumed vertical

Following Anderson (1951), the vertical stress  $S_v$  is assumed to be a principal stress. The magnitude of  $S_v$  determines the tectonic stress regime: normal if  $S_v = \sigma_1$ , reverse if  $S_v = \sigma_3$ , and strike-slip if  $S_v = \sigma_2$  —where  $\sigma_1 > \sigma_2 > \sigma_3$  and compressive stresses are positive. Note that beyond Anderson's view, a given tectonic stress regime does not imply a specific faulting style. Particularly in regions of distributed deformation because they are characterized by domains of fault sets.

### 2. Stress models

As shown in Fig. 4 for the 2D case, stress magnitudes must change in a domain because we assume that faults and blocks rotate within a stationary stress field. Since we do not know how this change may take place, we must make a number of simplifying assumptions. One possible assumption is that the volume of the crust being deformed remains constant so that hydrostatic stress is constant

$$\sigma_1 + \sigma_2 + \sigma_3 = \text{constant}$$

Another possibility is that the stress ratio  $\phi$  remains unchanged

$$\phi = \frac{\sigma_2 - \sigma_3}{\sigma_1 - \sigma_3} = \text{constant}$$

The stress ratio  $\phi = (\sigma_2 - \sigma_3)/(\sigma_1 - \sigma_3)$  is often used as a dimensionless parameter to describe the 3D state of stress in the Earth's crust. It may vary from  $\phi = 0$  when  $\sigma_2 = \sigma_3$  to  $\phi = 1$  when  $\sigma_2 = \sigma_1$ .

### 3. Fault geometry representation in 3D

Whatever assumptions are made, we need a way of tracking fault plane orientations during rotation in a 3D space. In this paper, we use two representations: the Mohr circle, which plots the orientation of faults in a  $\sigma_n - \tau$  plane, and the Wulff-projection stereonet, that plots the orientation of fault planes in the principal stress axis reference.

## THE 3D MOHR CIRCLE

In 2D space, a single angle defines fault orientation. In 3D space, two angles are required to define a pole to a fault plane. Fig. 5a shows how these angles are

represented in the Mohr circle. For a more complete treatment of the 3D Mohr circle representation we refer the reader to Jaeger and Cook (Chp 2.6, 1969). Let us consider here only three extreme cases:

- (1) pole  $P_2$  which falls exactly on the  $\sigma_1 - \sigma_3$  circle: this is equivalent to the 2D representation in which  $\sigma_2$  is in the plane of the fault.
- (2) pole  $P_1$  which falls exactly on the  $\sigma_3 - \sigma_2$  circle: in this case  $\sigma_1$  is in the plane of the fault and
- (3) pole  $P_3$  which falls exactly on the  $\sigma_2 - \sigma_1$  circle: in this case  $\sigma_3$  is in the plane of the fault.

When a pole (P) falls in the shaded region in Fig. 5a, then all three principal stresses are off the plane of the fault. In this case  $\alpha_1$  and  $\alpha_3$ , the angles that the fault plane normal makes with  $\sigma_1$  and  $\sigma_3$  respectively, are calculated by drawing two circles concentric with the two small  $\sigma_1 - \sigma_2$  and  $\sigma_2 - \sigma_3$  circles and passing through the pole. Then the intersection of the  $\sigma_1 - \sigma_2$  concentric expansion with the  $\sigma_2 - \sigma_3$  circle defines  $\alpha_3$ , and the intersection of the  $\sigma_2 - \sigma_3$  concentric expansion with the  $\sigma_1 - \sigma_2$  circle defines  $\alpha_1$  as shown in Fig. 5a. The Mohr circle representation is powerful because it represents stress magnitudes, friction criteria and the geometry of faults in the stress field, all in one graph.

#### THE WULFF-PROJECTION

The same fault normals shown in Fig. 5a are plotted on a Wulff lower hemisphere projection in Fig. 5b:  $P_2$  plots on the line joining the  $\sigma_1 - \sigma_3$  directions,  $P_1$  plots on the line joining the  $\sigma_2 - \sigma_3$  directions and  $P_3$  plots on the line joining the  $\sigma_1 - \sigma_2$  directions. Depending on the stress regime, either  $\sigma_1$ ,  $\sigma_2$  or  $\sigma_3$  is represented in the down orientation throughout the paper. This type of representation is often used by structural geologists because it makes it easier to visualize the geometry of faults in the stress field.

#### 4. Choice of material parameters

Finally, we need to assume some values for the mechanical constraints of the BR model. The relationship between material parameters and block rotation is discussed in detail in Nur et al. (1986). As we will see for the case of the Western Transverse Range, the specific values do not affect the qualitative aspect of the results. In this paper, we are more concerned with the changing behaviour of faults as they rotate. In the model, we assume the following values for the material parameters (Handin, 1969): 1.0 for the coefficient of friction of intact rock (it could be much greater) and 0.6 for the coefficient of friction of preexisting faults (it could be less). 1000 bars for the cohesion of intact rock (could be greater) and 50 bars for the cohesion of preexisting faults (could be 0). Given these values, the stress limits (Coulomb criteria) employed in the model become:

- (1) The upper limit, representing the strength of the crust (the fracture line)

$$\tau_0 = 1000 + 1.0\sigma_n \quad (\text{in bars})$$

- (2) The lower limit, representing the strength of preexisting faults (the sliding line)

$$\tau_f = 50 + 0.6\sigma_n \quad (\text{in bars})$$

- (3) the tensile limit, assuming the crust cannot withstand any tensile stress

$$\sigma_3 \geq 0 \quad (\sigma_3 < \sigma_2 < \sigma_1)$$

#### 3D MOHR CIRCLE: A KEY TO MIXED STYLES OF FAULTING

In a three dimensional situation, the value of the intermediate stress plays a key role in determining the style of faulting. This contrast with the two dimensional one where  $\sigma_2$  is always in the fault plane. By itself, this result is not new ( Bott, 1959; McKenzie, 1969; and others). However, here we include  $\sigma_2$  specifically to allow us to understand how active faults become poorly oriented during 3D block rotation. Before considering block and fault rotation, let us first enlist the help of the Mohr circle to see when preexisting faults can be reactivated—and what this means for regionally distributed deformation in Southern California.

### 1. Friction criteria and the 3D Mohr circle

Clearly, reactivation of preexisting faults is constrained by the strength of the crust, the strength of the faults and the relative magnitudes of the three principal stresses. Jaeger and Rosengren (1969) discuss the influence of these parameters in more detail. Let us consider the material parameters values discussed in the previous section and a  $\sigma_3/\sigma_1$  ratio exceeding the sliding line but not the fracture line, as shown in Fig 6.

Consider only three sets of preexisting faults as sketched in Fig. 6: (a) set 1 which contains the  $\sigma_1$  direction, (b) set 2 which contains the  $\sigma_2$  direction and (c) set 3 which contains the  $\sigma_3$  direction. The faulting styles expected along each fault set are also sketched. They depend on the tectonic stress regime and the orientation of each fault set. The normals to actively slipping faults plot within the shaded region of the Mohr circle. The size of the shaded region depends on the  $\sigma_3/\sigma_1$  ratio and the  $\phi$  value. Assuming low  $\sigma_3/\sigma_1$  ratio, at lower  $\phi$  values, say less than 0.4, all three fault sets will be active. In the normal regime, set 1 will be reactivated as strike-slip faults, set 2 and set 3 as normal faults. In the reverse regime set 1 and set 2 will be reactivated as reverse faults and set 3 as strike-slip faults. In the strike-slip regime, set 1 will be reactivated as normal faults, set 2 as strike-slip faults and set 3 as reverse faults. At  $\phi$  values exceeding 0.4, fault set 3, which contains  $\sigma_3$  in its plane, will be locked, while the other two fault sets can be reactivated.

These cases represent the most extreme styles of faulting that can be expected in the three tectonic stress regimes. Clearly in a domain characterized by an obliquely slipping fault set, movement could occur if it plotted within the shaded region of the 3D Mohr circle. A summary table for the limiting cases is provided in Table 1.

Stress Ratio	Tectonic stress regime			Faults
	<i>normal</i> $S_v = \sigma_1$	<i>reverse</i> $S_v = \sigma_3$	<i>strike-slip</i> $S_v = \sigma_2$	
<i>low</i> $0. < \phi < 0.4$	normal	reverse	strike-slip	set 2
	strike-slip	reverse	normal	set 1
	normal	strike-slip	reverse	set 3
<i>high</i> $0.4 < \phi < 1.0$	normal	reverse	strike-slip	set 2
	strike-slip	reverse	normal	set 1

Table 1. *Limiting cases of faulting styles expected in three tectonic stress regimes as functions of the stress ratio  $\phi = (\sigma_2 - \sigma_3)/(\sigma_1 - \sigma_3)$ —for each of the three*

sets aligned with one of the principal stresses in their planes and for a low  $\sigma_3/\sigma_1$  ratio.

## 2. Southern California domains: an example of distributed deformation

Southern California is characterized by domains of faults separated by through-going boundary faults (Fig. 1). The shaded regions in Fig. 1 represent domains where block rotation has been inferred (Luyendyk et al., 1985) and therefore where we expect faults to be poorly oriented in the present-day stress field. Whatever the stress field orientation, we do observe a mixture of faulting styles. In the Western Transverse Range domain (WTR), high-angle reverse-oblique slip along E-W trending faults has been documented (Lee et al., 1979; Yerkes and Lee, 1979a,b). In the Mojave domain (MOJ), Sauber et al. (1986) have described right-lateral strike-slip along NW-SE trending vertical faults. In the East Transverse Range domain (ETR), activity is left-lateral strike-slip along E-W trending vertical faults (Jones, 1988; Powell, 1982).

Can this diverse fault behaviour be the result of a regionally stationary stress field—in accordance with friction criteria? Note first how the San Andreas strike-slip system dominates the region's tectonics. Consider next, from the arguments above and Table 1, that reverse and strike-slip faulting may coexist within a low  $\phi$  strike-slip stress regime and low  $\sigma_3/\sigma_1$  ratio. Lastly, we need an estimate of the  $\sigma_1$  direction and of the value of  $\mu_f$ , the coefficient of frictional sliding, to apply the 3D BR model to this region. Both, the  $\sigma_1$  direction and the  $\mu_f$  value, are constrained by the orientation of strike-slip faults in the MOJ domain and of high angle reverse faults in the WTR domain:  $\sigma_1$  must trend  $N20^\circ E$  and  $\mu_f = 0.4$  for MOJ and WTR faults to slip. Representative fault plane solutions shown in Fig. 1 are plotted on the 3D Mohr circle of Fig. 7. The plot is normalized by the value of  $\sigma_1$ , assuming a depth of faulting of 5–10 kms, an orientation of  $\sigma_1$  trending  $N20^\circ E$ , a  $\mu_f = 0.4$  and a  $\phi = 0.1$ . Faults of the ETR, as well as those of the WTR and MOJ domains, plot closely to the sliding line. Therefore, in our simple model of distributed deformation, faults sets in all three domains can slide in accordance with friction criteria in a regionally stationary strike-slip regime.

The BR model can not presently account for slip along domain bounding faults (Fig. 1). In fact, the model predicts that very little shear stress is resolved on the San Andreas fault, the major throughgoing boundary fault in this region. While this agrees with recent borehole findings at Cajon Pass (Zoback et al., 1987), questions remain concerning the mechanics of lithospheric faults, but they are beyond the scope of this study.

In summary, we see discrete fault orientations that separate into domains. In Southern California, even poorly oriented fault sets can slip in a  $\sigma_1 N20^\circ E$  directed strike-slip regime with  $\phi = 0.1$  and  $\mu_f = 0.4$ . We will return to these values in the final part of the paper when discussing the faulting history of the WTR domain.

A fundamental question must be considered at this point: how do faults that presumably form in a favorable orientation become poorly oriented? As mentioned previously, extensive paleomagnetic studies (references in Luyendyk et al., 1985 and Dokka, 1989) indicate that these domains have undergone a complex history of deformation characterized by rotations about a vertical axis. In the following section, we hope to demonstrate that block rotation in a 3D stationary stress field provides a simple mechanism to accommodate distributed deformation that explains, in accordance with friction criteria, those rotations

that have been documented.

### 3D BLOCK ROTATION

In the previous section, we defined conditions in a 3D stress field under which reactivation of poorly oriented faults can occur (Table 1). We showed that domains of poorly oriented faults can be active in a regionally stationary stress field if the limits for the differential stresses in the Earth's crust lie between the upper bound (rock strength) and the lower bound (fault strength).

We will now investigate a process which allows faults, to pass from optimal to poor orientation; this is the rotation of blocks and their associated faults. Block rotation was modeled kinematically in 2D by Freund (1974), Garfunkel (1974) and Ron et al. (1984) and mechanically in 2D by Nur et al (1986). In this paper we present a 3D mechanical modeling program. Given strength and friction values, our model computes both the maximum rotation possible for a given fault set, and the conditions needed to induce a change of faulting style for that set.

#### 1. The model

The block rotation model (BR) describes idealized domains of fault sets in situ. Faults in a set are typically sub-parallel, so it is reasonable to consider the rotation history of one fault to be representative of the entire set. In the BR model, we assume that all faults in a given set are active simultaneously. Thus, deformation remains uniform throughout the domain. We also assume that the rotating blocks are rigid. Faulting is therefore brittle. We expect a detachment at depth (ca. 15 kms), that decouples upper crustal rotations from lower crustal ductile shear.

In the brittle upper crust, we require four main assumptions for the 3D BR model. The first, a mechanical constraint, assumes that the Coulomb criterion controls sliding of faults in the set. The second assumes that fault slip is directed along the maximum resolved shear stress for the fault. The third, a kinematic constraint, assumes that both blocks and fault planes rotate away from the  $\sigma_1$  direction. The fourth and final assumption is the stationarity of the principal stress directions. Thus, once fault sets have slipped and blocks rotated, stress magnitudes must change to allow further slip and rotation.

To facilitate the analysis, we assume that the magnitude of the principal vertical stress  $S_v$  remains constant throughout rotation. The other two stress magnitudes vary to conserve stress ratio  $\phi$  (see Appendix for discussion). As mentioned earlier, more general stress histories are possible but they require additional information. Here, we present results for a constant  $\phi$  stress history only.

Given a stress model and a stationary direction of the stress field, we must keep track of the fault orientation during rotation. Two new concepts are introduced: the stress path and the rotation path of a rotating fault set. These concepts form the basis of the 3D BR model. Estevez et al. (1987) discussed the stress path concept in considerable detail. The derivation is summarized in the Appendix here. This paper will focus mainly on the rotation path concept. The rotation path of a rotating fault set can be represented on a Mohr circle, as the successive  $(\sigma_n, \tau)$  values of the fault set on the Coulomb sliding line, and on the Wulf-projection, as the subsequent positions of the fault set in the stress field.

#### 2. 2D rotation path

The rotation path, a fundamental concept of 3D fault rotation, is illustrated

schematically on a 2D Mohr circle in Fig. 8. Assume that a given domain contains one preexisting fault set with its normal aligned at  $\alpha_1$  from the  $\sigma_1$  direction (Fig. 8a, point 1). For the fault set to slip, the stress must rise from point 1 to point 2. By the Coulomb criterion, shear stress at point 2 can drive the fault set into motion. At slip, the fault set rotates, eventually assuming an orientation  $\alpha_2$  (Fig. 8b). The angles  $\alpha_1$  and  $\alpha_2$  represent fault normals! Therefore, as blocks and faults rotate away from  $\sigma_1$ , normals to faults approach the  $\sigma_1$  point along the  $\sigma_n$  axis—as shown earlier in Fig. 4. Thus during rotation fault normals move from point 2 to point 3. In time, with increasing stress, the fault normal will continue to rotate. When point 4 is reached (Fig. 8c), the Coulomb fracture criterion will come into play—the fault will be locked at position  $\alpha_3$ , and a new set of faults will be created (point 5 in Fig. 8c). The path followed from point 2 to point 4 is the rotation path for Nur's 2D model.

Unfortunately, a 2D model is limited to analysis of the special case where  $\sigma_2$  lies within the preexisting fault set. To model faults rotating more generally within the stress field, we must study the 3D case.

### 3. 3D rotation paths

Many rotation paths are possible in 3D, but we will consider only three limiting cases, shown in Fig. 9. As described earlier, faults slip and rotate in the BR model, as long as the stress limits and the Coulomb sliding criterion are satisfied. By assuming a constant  $\phi$  stress history, we can plot the rotation path of a fault set on Mohr circles normalized by  $\sigma_1$ . Thus, rotation paths plot as curved lines, reflecting the variation, with fault rotation, in the absolute magnitudes of the principal stresses.

For a given stress regime, we would like to determine the style of faulting exhibited at every point along the rotation path of a fault set. This style can be characterized by the rake, or the direction of slip of the fault's hanging wall along the footwall, as shown in Fig. 10. Because the fault plane itself is also rotating, we must track this change as defined by fault plane strike and dip, or more simply by the orientation of the fault normal in 3D space.

In the following section, we present the results of 3D BR modeling. We have assumed stationary stress orientations and constant  $\phi$  during rotation. Separately, we discuss modeled changes in faulting style (rake) and attitude (strike and dip) for the three specific fault sets, as functions of both the stress ratio  $\phi$  and the tectonic stress regime.

### **3D BLOCK ROTATION: RESULTS**

Rotation paths for the three limiting cases (Fig. 9) are summarized in Fig. 11 and Fig. 12. In each figure, results are shown for the three stress regimes, at low, intermediate and high  $\phi$  values. Fig. 11 displays changes in faulting style as a function of rotation in its nine *rotation/rake* plots. The columns represent the three  $\phi$  cases, and the rows represent the three tectonic regimes. The faulting style along the rotation path, that is the rake of a fault set, is determined by the fault set orientation and the  $\phi$  value: the higher the  $\phi$  value the more stable the rake becomes during rotation. This is illustrated by the Mohr circle plots (bottom row in Fig. 11): as the  $\sigma_2 - \sigma_3$  circle grows, the  $\sigma_1 - \sigma_2$  circle shrinks, and rotation paths stop farther away from the  $\sigma_1 - \sigma_2$  circle.

Fig. 12 displays the fault set attitude for the same rotation paths shown in Fig. 11. The columns still represent the three  $\phi$  cases, but Fig. 12a,b,c represent the normal, reverse and strike-slip regime separately. 3D motion is shown by plotting rake vs. strike, rake vs. dip and strike vs. dip along the rotation path. Rotation paths are plotted on Wulff-projections at the bottom of Fig. 12, to help

visualize the changing orientation of fault sets during rotation in a stationary,  $\phi = \text{constant}$  stress field. Notice, again, the stabilizing effect of high  $\phi$  values displayed by the shape of the rotation path. The dominant  $\sigma_1$  at  $\phi = 0.1$ , drives all three paths very close to its direction. Some curvature of the paths can be noticed at  $\phi = 0.5$ , while straight paths characterize the  $\phi = 0.9$  case—where  $\sigma_1$  and  $\sigma_2$  are nearly equal in magnitude.

Let us consider each rotation path in more detail. The initial orientation of pole 3 in Fig. 11 and 12, for example, closely contains the  $\sigma_2$  direction in the planes of its fault set. This makes it equivalent to the 2D block rotation case—the intermediate stress  $\sigma_2$  plays no part in this pole's rotation path. The rake (Fig. 11) remains unchanged during rotation under any value of  $\phi$ : normal regimes produce normal slip. Likewise, reverse and strike-slip regimes yield reverse and strike-slip motion, respectively. Thus, our assumption that one principal stress axis is vertical has precluded oblique slip in the 2D case of pole 3.

Pole 1 and pole 2, however, are influenced by  $\sigma_2$ . As a result, their faulting style changes under rotation—sometimes dramatically. Surprisingly complex patterns of nonlinear rotation paths are outlined for these fault sets in Fig. 11 and 12. Note that these changes take place under fixed  $\phi$  values and stationary principal stress directions.

### Changing faulting style—Rake

As mentioned earlier, higher  $\phi$  values have a stabilizing effect. Thus, rakes for the rotation paths of pole 1 and 2 in Fig. 11 are nearly constant during rotation in all three stress regimes. At lower values of  $\phi$ , however, the model yields surprising rake histories for the rotation paths of these poles. In the normal stress regime, strike-slip fault sets may rotate into pure normal fault sets. In the reverse stress regime oblique-slip fault sets with a large component of strike-slip may rotate into a reverse slip fault set (pole 2) or a strike-slip fault set (pole 1).

The strike-slip stress regime displays the most dynamic results of the 3D BR model. The results suggest that it is possible for pure normal fault sets (pole 1) to rotate into a strike-slip one, and subsequently into a reverse-oblique slip fault set—all within a strike-slip regime! Even at intermediate  $\phi$  values, dramatic changes take place in the rakes of pole 1 and 2, although they converge to strike-slip motion upon rotation. High  $\phi$  values limit rake changes during rotation, as always, but pole 2 does tend towards a more strike-slip motion.

The 3D BR model predicts rotations of up to  $75^\circ$  (each rotation step corresponds to  $5^\circ$  of rotation) for the most poorly oriented fault sets. By considering these limiting cases, we have modeled rotations much greater than those of Nur et al. (1986), and we have also found cases where the faulting style may reverse during the rotation path of a single fault set.

### Changing fault orientation—Strike and Dip

Fig. 12 has been designed to express 3D rotation about oblique axes as a function of dip, strike and rake—to better visualize fault rotation in 3D. Again the stabilizing effect of higher  $\phi$  values is observed in all three stress regimes (Fig. 12a,b,c).

Results of the model for the normal stress regime are detailed in Fig. 12a. Considering the low  $\phi$  column on the left, one can see how all three paths change mostly in dip. This horizontal axis of rotation is what one might typically expect for a normal stress regime, and the 3D BR model concurs. Intermediate  $\phi$  values suggest greater changes in strike during rotation, while at high  $\phi$  values the model predicts—surprisingly so—that strike changes more than dip, particularly

for pole 1. Vertical-axis rotation, usually associated with strike-slip regimes, is therefore possible in normal stress regimes as well.

The results for the reverse stress regime shown in Fig. 12b, predict rake changes throughout rotation at low  $\phi$  values. Poles 1 and 2 are expected to change more in strike than in dip. Again, we see how the 3D BR model predicts vertical-axis rotation of fault sets—this time in a reverse stress regime. Increasing  $\phi$  values induce predominantly steepening of the fault planes during rotation, resulting in the more familiar horizontal-axis rotations.

The results for the strike-slip stress regime shown in Fig. 12c, represent the most striking results of the 3D BR model. Interestingly, the low  $\phi$  case allows for decreasing dip during normal slip, followed by a steepening of the dip when the rake becomes reverse. In the strike-slip regime, the model predicts that most fault sets will follow an oblique axis of rotation. One notable exception, though, can be found in the  $\phi = 0.9$  case, where pole 1 rotates unexpectedly about a horizontal axis in a strike-slip regime.

To summarize the results of our model, three specific initial orientations of fault sets were studied in nine different combinations of  $\phi$  values ( $\phi = 0.1, 0.5, 0.9$ ) and stress regimes ( $S_v = \sigma_1, \sigma_2, \sigma_3$ ). In each case the predictions of the model were presented using the rotation path. Along this path we analyzed behaviour (rake) and attitude (strike and dip) of the fault set as it rotated in a stationary,  $\phi = \text{constant}$  stress field.

The most important conclusions of our results are: first, that for most cases the results predict an oblique axis of rotation, and second that during rotation, as faults change their orientation in the stress field, the style of faulting may change as well—sometimes dramatically.

A direct consequence of these result is that paleomagnetically inferred rotations may not be directly related back to a specific tectonic stress regime. Indeed, rotations about vertical axes, while usually found in strike-slip stress regimes (Hornafius, 1986; Kamerling and Luyendyk, 1985; and others), have been documented in normal stress regimes as well (Li et al., 1990; Pavlides et al., 1988; Hudson and Geissman, 1987; Kissel et al. 1986; Brown and Golombek, 1986; Jackson and McKenzie 1984; 1983). Paleomagnetism is an invaluable aid to decipher complex histories of rotation in regions of distributed deformation. Our 3D BR model provides a framework within which, paleomagnetic, structural and stress data can be combined to better understand complex rotation histories. We analyze such a case in the following section, to demonstrate the application of the 3D BR model to actual complex tectonic problems.

### **A 3D BLOCK ROTATION EXAMPLE: THE WESTERN TRANSVERSE RANGE**

The shear motion between the Pacific and the American plates in Southern California is distributed across a 200 km wide zone which consists of a complex array of block-faulted domains (Fig. 1; Luyendyk et al., 1985). In the first part of the paper, we showed (Fig. 7) how mixed styles of faulting observed today in this region can be explained in a stationary strike-slip stress regime. Now, we apply the results of the 3D BR model to the rotation history of one of these domains, namely the Western Transverse Ranges (WTR).

#### **1. Tectonic history**

The WTR domain is a region limited to the north by the Santa Ynez fault, to the south by the Malibu fault system, to the west by the Hosgri fault and to the east by the San Gabriel fault (see WTR in Fig. 1). The right-lateral shear between the Pacific and North American plates since Oligo-Miocene time

should have dominated the tectonic history of this domain. From the geological record alone, however, the tectonic history seems much more complex. This is documented by detailed stratigraphic and structural studies (Yerkes et al., 1981; Luyendyk et al., 1985; Yeats, 1987; Namson and Davis, 1988 and others). The following discussion is concerned with the most prominent deformational phases documented for this region—simplified for the purpose of this study.

Phase I: in late Oligocene to early Miocene time, there was deposition of sediments in elongate normal-fault controlled basins which are presently oriented east-northeast (Terres and Luyendyk, 1985).

Phase II: a mixture of strike-slip and normal faulting characterized the extensional tectonics of Miocene times (Yeats, 1987).

Phase III: a significant period of compression followed at the beginning of the Quaternary, overprinting all previous events. Structural evidence suggests (Yerkes and Lee, 1979a) that “at the present rates all the measured compressive deformation within the WTR could have occurred during the last 0.5 to 1 m.y.”. Namson and Davis (1988) describe this last phase of north-south convergence in detail.

This sequence of phases is shown schematically in Fig. 13: a rake of  $90^{\circ}$ , representing the normal faulting period—phase I is followed by a rake of  $0^{\circ}$ , representing the strike slip faulting period—phase II, leading to a rake of  $-65^{\circ}$ , representing the present day period of reverse oblique faulting—phase III.

With the advent of paleomagnetic studies carried out in many domains across Southern California (Luyendyk et al., 1980; Terres and Luyendyk, 1985; Hornafius, 1986; Carter, 1987), it appears that block rotation has been the predominant mechanism of deformation in this region. Paleomagnetic interpretations indicate that since mid-Miocene time, the Transverse Ranges have experienced significant block rotations about a vertical axis—particularly in the WTR domain, where up to  $90^{\circ}$  of rotation is estimated.

According to Luyendyk and his co-workers, the WTR clockwise rotations were associated with left-lateral slip on a set of vertical, strike-slip faults originally N-NE trending. The faults defined blocks about 100-200 kms long and 10 kms wide that rotated as rigid bodies away from the direction of compression.

The structural history for the WTR, as suggested by Terres and Luyendyk (1985), is explained by three separate set of faults formed under three different stress regimes (Fig. 13). A set of N-NE striking normal faults formed during the extensional phase (I), another set of strike slip faults, which rotated with the blocks, formed during the shearing phase (II), and yet another set of E-W striking high-angle reverse faults formed during the present-day compressional phase (III).

While kinematic knowledge has improved our understanding of the WTR structural history, the story it tells is complex. By combining the frictional constraints of the 3D BR model with paleomagnetic, structural and geological data, we can now show how one set of faults, preexisting and rotating in a stationary strike slip stress field, can account for all three deformational phases.

## 2. The 3D BR model for the WTR

How can we use the results of Fig. 11 and 12 to help us understand the history of rotation of the WTR? Let us start with the simplest assumption: the stress directions remained stationary, in the present day orientation, throughout the post-Oligocene deformation history of the domain. From the first part of the paper, we know that it is possible for the WTR fault set to slip in a oblique reverse motion in a strike-slip regime with  $\sigma_1$   $N20^{\circ}E$  directed, if  $\mu_f = 0.4$  and  $\phi = 0.1$ . Consequently, we can expect the modeled rotation path that best describes the deformation of the WTR domain to be similar to that of pole 1 in

Fig. 11, for the case of the strike slip regime and  $\phi = 0.1$ , where the final value of the rake is oblique reverse.

The results shown in Fig. 11 and 12 are for  $\mu_f = 0.6$ . To model the faults of the WTR domain we must re-run the program with  $\mu_f = 0.4$ . Fig. 14a shows the stress regime and the rotation path modeled for the WTR domain. Fig. 14b shows how lowering the coefficient of frictional sliding allows faults to rotate further away from  $\sigma_1$ . The shape of the rotation path remains the same, but the limits within which a fault set may rotate change. In our case, faults may rotate until a steeper dip is achieved (compare strike and dip for the final orientation of pole 1 in Fig. 12c and Fig. 14b).

But what does this rotation path tell us about previous fault behavior and previous geometries of faulting? Fig. 14b displays the structural history predicted by the model for this rotation path. The rake starts at an initial value near pure normal slip, a time of "extension" similar to phase I. Upon fault and block rotation, the rake becomes pure strike-slip, a time of predominantly vertical axis rotation similar to phase II, before reaching the present day "compressive" period of reverse-oblique faulting—phase III. The corresponding values for the dip and the strike of the rotating fault set are also shown. As the strike of the fault set rotates away from  $\sigma_1$  (I  $\rightarrow$  II in the plot), the dip flattens at first and then steepens as soon as the reverse slip field is reached (II  $\rightarrow$  III).

### 3. Agreement with the observations

Our goal was to demonstrate how deformation in the WTR could have occurred along a single set of faults, reactivated in middle Miocene time as block rotation began.

In agreement with the observations (Fig. 13), Fig. 15 displays the salient features predicted by the 3D BR model for the structural history of the WTR fault set. The original orientation of the fault set in the WTR domain must have been NNE striking, dipping  $55^\circ - 60^\circ$  to the West and slipping in a normal sense. Subsequently, the same fault set rotated away from the direction of maximum compression  $\sigma_1$  and became strike-slip in style with a dip between  $40^\circ$  and  $50^\circ$ . Finally, the fault set rotated into the E-W, high angle, reverse-oblique faults observed today. The results of our modeling show that along the rotation path, a single fault set went through three different faulting styles during its  $75^\circ$  clockwise rotation, while stress directions remained stationary with  $S_v = \sigma_2$ ,  $\sigma_1$  oriented  $N20^\circ E$ , and  $\phi = \text{constant}$  at a value of 0.1.

These simplifying assumptions are not necessary. If we most accurately modeled the tectonic history of the WTR domain, we should have accounted for changes in stress directions that presumably took place between the Miocene and the Present. Evidence of this is found in studies of plate motion (Cox and Engebretson, 1985) that indicate a clockwise change in relative plate motion  $\sim 5$  My ago. Incorporating this change would introduce an additional degree of freedom and allow a less restrained solution. The original orientation of faults could be even more N-S striking, and the amount of total rotation that could be achieved by one single set of faults would increase by an amount comparable to the change in plate motion.

The second constraining assumption, that of a constant  $\phi$  stress history, maintains a strike-slip stress regime during the rotation history of the faults. This need not be the case. A change of stress regime might occur during the history of rotation of a fault set, and it could reverse the sense of rotation of blocks and faults or allow them to rotate in another direction.

Nevertheless, it is encouraging that with our simple 3D BR model and simple assumptions, we have been able to predict a sequence of structural phases

consistent with the known structural history of the WTR. This example demonstrates that one need not always invoke complex regional and local changes in the stress regime or erratic changes in plate motions to account for alternate periods of compression and extension. The geometry of each domain of fault sets determines the style of faulting that will occur there. The regional stress regime may remain stationary.

## CONCLUSIONS

We have presented a generalized model of distributed deformation and block rotation that emphasizes faulting in 3 dimensions. The need for this model is dictated by the following observations:

- (1) Reactivated faults are usually poorly oriented relative to the stress field.
- (2) Obliquely slipping faults are found in many domains that have undergone rotation.
- (3) These same faults change their faulting style through time.

We propose that mechanical constraints of friction and strength combined with the 3D Mohr circle and the kinematics of block rotation can explain these observations.

### 1. Block rotation: the cause of poorly oriented faults

According to the existing 2D BR model, rotation of blocks and faults are caused by contemporaneous slip on fault sets in adjacent domains. Based on fracture mechanics and friction criteria, the orientation of faults sets with respect to the direction of maximum compression  $\sigma_1$  determines the sense of fault slip and thus the sense of rotation of the blocks in each domain. Consequently, faults that are initially in optimal orientations must rotate away from this optimal orientation in domains undergoing rotation. In this paper, we generalized these concepts into a 3D BR model.

With the 3D BR model, we are able to determine the range of orientations for faults that may slip as well as their style of faulting (i.e. rake). We can also determine the maximum amount of rotation blocks and faults may experience before a new set of faults may take over the deformation.

The results of our modeling show that the value of the  $\phi$  parameter plays a key role in identifying those faults that may be reactivated and in determining their style of faulting. At low  $\phi$  values, where  $\sigma_2$  is close in magnitude to  $\sigma_3$ , faults may be reactivated even if very poorly oriented. Thus, in different domains at the same point in time or within the same domain through time, contrasting styles of faulting can occur. In a normal stress regime, both pure strike-slip and pure normal faulting styles can occur. In a reverse stress regime, both pure strike-slip and pure reverse faulting styles can occur. In a strike-slip stress regime, pure strike-slip, pure normal and pure reverse faulting styles can all occur. At high  $\phi$  values, where  $\sigma_2$  is closer to  $\sigma_1$  in magnitude, faulting styles are limited to strike-slip and normal in both the normal and strike-slip stress regimes and only to reverse in the reverse stress regime.

When applied to the distributed deformation of Southern California, our model can explain the diverse faulting styles observed there by assuming a simple regional strike-slip stress regime with  $\sigma_1$  oriented  $N20^\circ E$ , a low  $\phi = 0.1$ , and a coefficient of sliding friction of 0.4.

### 2. Change of faulting style with rotation

The importance of the  $\phi$  parameter is also clearly demonstrated by the change in rake predicted by the 3D BR model as faults rotate in a stationary stress field. The results show that rake varies with rotation at low  $\phi$  values, but

remains relatively constant at high values. By analyzing dip and strike of faults throughout rotation, we found surprising results. At low  $\phi$  values in the reverse regime, originally poorly oriented faults may rotate about a vertical axis. On the other hand, at high  $\phi$  values, poorly oriented faults may rotate unexpectedly about a vertical axis in the normal stress regime, and about a horizontal axis in the strike-slip stress regime. Therefore, for the general case of originally poorly oriented sets of faults, oblique axes of rotations are predicted by our model for all stress regimes.

We applied the 3D BR model to the complex history of faulting as documented in the Western Transverse Ranges of Southern California. The best model results indicate that for the WTR domain, a single set of originally NNE striking faults could have accommodated the deformation. Assuming a low  $\phi$  strike-slip stress regime, a stationary  $N20^{\circ}E$  directed maximum compressive stress, and a value of 0.4 for the coefficient of sliding friction, these faults were reactivated as normal faults at the beginning of the rotation period. Subsequently, the same faults became more NE striking, left-lateral strike-slip faults until they finally rotated into the present day "compressive" period of E-W striking reverse faults.

In spite of its simplifying assumptions, the our model provides clues to earlier geometries of faults for the WTR that are consistent with the geological, geophysical and paleomagnetic records.

We believe that block rotation is a fundamental process in regions of distributed deformation where poorly oriented faults are widespread. When applied to actual geologic situations, the model provides a powerful, yet simple tool to interpret the complex faulting histories and complex fault geometries that characterize regions of distributed deformation.

#### **ACKNOWLEDGEMENTS**

This study was supported by the Geodynamics Program of NASA, through grant no.NAG5-926 Mod.Amend01.

## APPENDIX

### 1. Stress limits

A fault can slip and rotate when the Coulomb criterion for sliding is satisfied:

$$\tau_f = C_f + \mu_f \sigma_n \quad (1)$$

where  $\tau$  is the shear stress on the fault plane,  $\sigma_n$  is the normal stress across it,  $C_f$  is the cohesion and  $\mu_f$  is the coefficient of friction of the fault.

Prior to slip and rotation, it is necessary to check that the differential stress does not exceed the Coulomb fracture line:

$$\tau_0 = C_0 + \mu_0 \sigma_n \quad (2)$$

where  $C_0$  is the cohesion and  $\mu_0$  is the coefficient of friction of the intact crust. This line defines the upper limit for the magnitude of the differential stress ( $R$ ) in the earth's intact crust :

$$R = \frac{\sigma_1 - \sigma_3}{2} \leq R_{max} = \frac{1}{\sqrt{1 + \mu_0^2}} [C_0 + \frac{\mu_0}{2}(\sigma_1 + \sigma_3)] \quad (3)$$

Furthermore, it is necessary to ensure that:

$$\sigma_3 \geq 0 \quad (4)$$

because the crust cannot support tension.

### 2. Stress model and stress paths

The normal ( $\sigma_n$ ) and shear ( $\tau$ ) stresses across a plane are computed according to the following relations (Jaeger and Cook, 1969):

$$\sigma_n = \alpha_1^2 \sigma_1 + \alpha_2^2 \sigma_2 + \alpha_3^2 \sigma_3 \quad (5)$$

$$\tau^2 = \alpha_1^2 \sigma_1^2 + \alpha_2^2 \sigma_2^2 + \alpha_3^2 \sigma_3^2 - \sigma_n^2 \quad (6)$$

where  $\alpha_1, \alpha_2, \alpha_3$  are the direction cosines of the pole (fault normal) with respect to the principal stress axes,  $\sigma_1, \sigma_2, \sigma_3$ .

As principal stress magnitudes change to satisfy equation (1), the initial value ( $\sigma_n, \tau$ ) on a given fault plane will change to a new value ( $\sigma'_n, \tau'$ ). The sequence of ( $\sigma'_n, \tau'$ ) described by the pole is computed with  $\alpha_1, \alpha_2, \alpha_3 = \text{constant}$ , because during these stress changes and before any rotation event occurs, the fault plane itself remains fixed in stress space.

This sequence of ( $\sigma'_n, \tau'$ ) will be referred to as the stress path of a fault. It depends on the stress history chosen and on the initial conditions ( $\sigma_n, \tau, \sigma_1, \sigma_2, \sigma_3, \alpha_1, \alpha_2, \alpha_3$ ).

As explained in the text, this paper considers three stress regimes in which one of the principal stress axis is always assumed vertical ( $S_v$ ) and the stresses are assumed to change according to a  $\phi = (\sigma'_2 - \sigma'_3)/(\sigma'_1 - \sigma'_3) = \text{constant}$  model. For each stress regime, the stress path of a fault is computed as follows:

#### a. NORMAL STRESS REGIME ( $S_v = \sigma_1$ )

$$\sigma'_1 = \sigma_1 = \text{constant} \quad (7)$$

$$\sigma'_2 = \sigma_2 - r_N \Delta\sigma \quad (8)$$

$$\sigma'_3 = \sigma_3 - \Delta\sigma, \quad (9)$$

where

$$r_N = \frac{\sigma_1 - \sigma_2}{\sigma_1 - \sigma_3}. \quad (10)$$

b. REVERSE STRESS REGIME (  $S_v = \sigma_3$  )

$$\sigma'_1 = \sigma_1 + \Delta\sigma \quad (11)$$

$$\sigma'_2 = \sigma_2 + r_R \Delta\sigma \quad (12)$$

$$\sigma'_3 = \sigma_3 = \text{constant} \quad (13)$$

where

$$r_R = \frac{\sigma_2 - \sigma_3}{\sigma_1 - \sigma_3} \quad (14)$$

c. STRIKE-SLIP STRESS REGIME (  $S_v = \sigma_2$  )

$$\sigma'_1 = \sigma_1 + \Delta\sigma \quad (15)$$

$$\sigma'_2 = \sigma_2 = \text{constant} \quad (16)$$

$$\sigma'_3 = \sigma_3 - r_S \Delta\sigma \quad (17)$$

where

$$r_S = \frac{\sigma_2 - \sigma_3}{\sigma_1 - \sigma_2} \quad (18)$$

Substituting the values for  $\sigma'_i$  into equations (5) and (6), the stress paths that result from the above models are given by the following equations with  $\Delta\sigma$  as a parameter:

$$\sigma'_n = \sigma_n + a\Delta\sigma \quad (19)$$

$$\tau'^2 = \tau^2 + b\Delta\sigma + c(\Delta\sigma)^2 \quad (20)$$

where  $\sigma_1, \sigma_2, \sigma_3, \tau, \sigma_n$  are known initial values and  $\alpha_1, \alpha_2, \alpha_3$  are the constant direction cosines of the fault normal. The coefficients  $a, b$  and  $c$  assume different values depending on the stress regime considered (see Table A1).

Stress Regime	Coefficients		
	$a$	$b$	$c$
normal	$-(\alpha_3^2 + r_N \alpha_2^2)$	$-2[r_N \alpha_2^2(\sigma_2 - \sigma_n) + \alpha_3^2(\sigma_3 - \sigma_n)]$	$(1 - r_N)^2 \alpha_2^2 \alpha_3^2 + (\alpha_3^2 + r_N^2 \alpha_2^2) \alpha_1^2$
reverse	$\alpha_1^2 + r_R \alpha_2^2$	$2[\alpha_1^2(\sigma_1 - \sigma_n) + r_R \alpha_2^2(\sigma_2 - \sigma_n)]$	$(1 - r_R)^2 \alpha_1^2 \alpha_2^2 + (\alpha_1^2 + r_R^2 \alpha_2^2) \alpha_3^2$
strike-slip	$\alpha_1^2 - r_S \alpha_3^2$	$2[\alpha_1^2(\sigma_1 - \sigma_n) - r_S \alpha_3^2(\sigma_3 - \sigma_n)]$	$\alpha_1^2 + r_S^2 \alpha_3^2 - a^2$

Table A1.  $a, b$  and  $c$  are coefficients required to calculate the stress path of a fault. They depend on the orientation of the faults ( $\alpha_1, \alpha_2, \alpha_3$ ), the assumed stress model ( $r_N, r_R, r_S$ ) and the initial values of  $\sigma_1, \sigma_2$  and  $\sigma_3$ .

Replacing  $\Delta\sigma$  from (19) into (20), we get an explicit equation for the stress path

$$a^2 \tau'^2 = A \sigma_n'^2 + B \sigma_n' + C, \quad (21)$$

where

$$A = c \quad (22)$$

$$B = ab - 2c\sigma_n \quad (23)$$

$$C = a^2 \tau^2 - ab\sigma_n + c\sigma_n^2 \quad (24)$$

By combining equation(21) and equation(1), we obtain the coordinates  $\sigma_n', \tau'$  of the intersection between the pole's stress path and the Coulomb sliding line. There the fault plane can slip and rotate.

### 3. Rotation of fault planes

Consider a normal to a fault plane with unitary vector direction cosines  $\alpha_1, \alpha_2, \alpha_3$ . Once the shear stress  $\tau$  across the fault plane satisfies equation (1), the fault plane will slip and rotate in the direction of the resolved shear stress, represented by the unitary vector  $\tilde{r}$ .<sup>1</sup> The nature of this rotation is better understood in Fig. A1, where the horizontal plane represents the fault before rotation and  $\tilde{r}$  is its unit normal vector (same direction as  $\vec{\sigma}_n$ ).

Given the coordinates  $\alpha_1, \alpha_2, \alpha_3$  of the normal to the fault  $\tilde{r}$  and the coordinates of the total stress vector ( $\vec{\sigma}$ ) across it

$$[\vec{\sigma}]_1 = \alpha_1 \sigma_1 \quad (25)$$

$$[\vec{\sigma}]_2 = \alpha_2 \sigma_2 \quad (26)$$

<sup>1</sup>A tilde will denote a unitary vector

$$[\vec{\sigma}]_3 = \alpha_3 \sigma_3, \quad (27)$$

we can compute the coordinates of vectors  $\tilde{n}$ ,  $\tilde{r}$  and  $\tilde{\tau}$ . In order to compute  $\tilde{n}$  we first compute vector  $\vec{n} = \tilde{r} \times \vec{\sigma}$  with coordinates:

$$n_1 = \alpha_2 \alpha_3 (\sigma_3 - \sigma_2) \quad (28)$$

$$n_2 = \alpha_1 \alpha_3 (\sigma_1 - \sigma_3) \quad (29)$$

$$n_3 = \alpha_1 \alpha_2 (\sigma_2 - \sigma_1) \quad (30)$$

Vector  $\tilde{n}$  is then simply  $\vec{n}/|\vec{n}|$ . Similarly,  $\vec{\tau} = \vec{n} \times \tilde{r}$  and has coordinates:

$$\tau_1 = \alpha_1 \{ \alpha_3^2 (\sigma_1 - \sigma_3) - \alpha_2^2 (\sigma_2 - \sigma_1) \} \quad (31)$$

$$\tau_2 = \alpha_2 \{ \alpha_1^2 (\sigma_2 - \sigma_1) - \alpha_3^2 (\sigma_3 - \sigma_2) \} \quad (32)$$

$$\tau_3 = \alpha_3 \{ \alpha_2^2 (\sigma_3 - \sigma_2) - \alpha_1^2 (\sigma_1 - \sigma_3) \} \quad (33)$$

The direction cosines of the rotated plane will be the coordinates of the vector  $\tilde{r}'$ . Therefore, they must satisfy the following 3 equations:

$$\tilde{r}' \cdot \tilde{n} = 0 \implies \alpha'_1 n_1 + \alpha'_2 n_2 + \alpha'_3 n_3 = 0 \quad (34)$$

$$\tilde{r}' \cdot \tilde{r} = \cos \delta \rho \implies \alpha'_1 \alpha_1 + \alpha'_2 \alpha_2 + \alpha'_3 \alpha_3 = \cos \delta \rho \quad (35)$$

$$\tilde{r}' \cdot \vec{\tau} = \tilde{r}' \cdot \vec{\tau} / |\vec{\tau}| = \sin \delta \rho \implies \alpha'_1 \tau_1 + \alpha'_2 \tau_2 + \alpha'_3 \tau_3 = \sin \delta \rho \cdot |\vec{\tau}| \quad (36)$$

After rotation has occurred, principal stresses will drop and Mohr circles should “shrink”. The newly computed values of the rotated fault plane direction cosines  $(\alpha'_1, \alpha'_2, \alpha'_3)$  define a new stress path, along which the pole must move as the stresses change (after each rotation we can choose a different model for stress changes). No direct relationship exists yet between the amount of stress drop and the amount of rotation. Nonetheless, whatever the stress drop, the new pole must move along its stress path. Since the rotation path is fully defined by the intersection between the stress path and the sliding line, it is not necessary to know the stress drop (that is, how far the pole will move along its new path) to estimate the next rotation event.

## REFERENCES

- Anderson, E.M., 1951, The dynamics of faulting. Oliver and Boyd, Edinburgh, 206pp
- Angelier, J., Colletta, B. and Anderson R.E., 1985, Neogene paleostress changes in the Basin and Range: a case study at Hoover Dam, Nevada-Arizona, G.S.A.Bull, **96**, 347-361
- Bott, M.H.P., 1959, The mechanics of oblique slip faulting. Geol.Mag.,**XCVI**, 2
- Brown, L. and Golombek, P., 1986, Block rotations in the Rio Grande Rift, New Mexico, Tectonics, **5**, 3, 423-438
- Carter, J.N., Luyendyk, B.P. and Terres, R.R., 1987, Neogene clockwise tectonic rotation of the eastern Transverse Ranges, California, suggested by paleomagnetic vectors, G.S.A.Bull, **98**, 199-206
- Cox, A. and Engebretson, D., 1985, Change in plate motion of Pacific plate at 5Myr BP. Nature,**313**, 472-474
- Dokka R. K., 1989, The Mojave extensional belt of Southern California, Tectonics, **8**, 2, 363-390
- Estevez, R., Scotti, O. and Nur, A., 1987, Block rotation in 3D., Stanford Rock Physics Project, Unpublished manuscript
- Freund, R., 1970, Rotation of strike-slip faults in Sistan, Southeast Iran. J.Geol.,**78**, 188-200
- Freund, R., 1971, The Hope fault, a strike-slip fault in New Zealand, N.Z.Geol.Surv., Bull., **86**, 49pp.
- Freund, R. , 1974, Kinematics of transform and transcurrent faults. Tectonophysics,**21**, 93-134
- Garfunkel, Z., 1974, Model for the late Cenozoic tectonic history of the Mojave desert, California, and for its relation to adjacent regions. G.S.A.Bull, **85**, 1931-1944
- Handin, J., 1969, On the Coulomb-Mohr failure criterion. J.G.R.,**74**, 22
- Hornafius, J.S., Luyendyk, B.P., Terres, R.R. and Kamerling, M.J., 1986, Timing and extent of Neogene tectonic rotation in the western Transverse Ranges, California, G.S.A.Bull, **97**, 1476-1487
- Hudson M.R. and Geissman J.W., Paleomagnetic and structural evidence for middle Tertiary counterclockwise block rotation in the Dixie valley region, west-central Nevada, 1987, Geology **15**, 638-642
- Jackson J.A. and White, N.J., 1989, Normal faulting in the upper continental crust: observations from regions of active extension. Journal of Struct.

Geol., 11, 1/2, 15-36

- Jaeger, J.C. and Cook, N.G.W., 1969, Fundamentals of rock mechanics. Methuen and Co.Ltd, London, 515pp
- Jaeger, J.C. and Rosengren, K.J., 1969, Friction and sliding of Joints. Proc. Aust. Inst. Min. Met., **229**, 93-104
- Jennings, C.W, 1975, Fault Map of California, Calif.Div. of Mines and Geology
- Jones, L.M., 1988, Focal mechanisms and the state of stress on the San Andreas fault in Southern California. J.G.R., **93**, B8, 8869-8891
- Kamerling, M.J. and Luyendyk, B.P., 1985, Paleomagnetism and Neogene Tectonics of the Northern Channel Islands, California. JGR, **90**, B14, 12, 485-12, 502
- Kissel C., Laj C. and Mazaud A., 1986, First paleomagnetic results from Neogene formations in Evia, Skyros and the Volos region and the deformation of central Aegea., Geophy. Res. Lett., **13**, 13, 1446-1449
- Lee, W.H.K., Yerkes, R.F. and Simirenko, M., 1979, Recent earthquake activity and focal mechanisms in the Western Transverse Ranges, California. in U.S.Geological Survey, Map MF-1032
- Li Y., Geissman J., Nur A., Ron H. and Huang Q., 1990 Counterclockwise block rotation in the North Nevada Rift region: paleomagnetic evidence, Geology, **18**, 79-82
- Luyendyk, B.P., Kamerling, M.J. and Terres, R.R., 1980 Geometric model for Neogene crustal rotations in Southern California. GSA Bull, **91**, 211-217
- Luyendyk, B.P., Kamerling, M.J., Terres, R.R. and Hornafius J.S., 1985, Simple shear of Southern California during Neogene times suggested by paleomagnetic declinations. J.G.R., **90**, B14, 12, 454-12, 466
- Luyendyk, B.P. and Hornafius, J.S., 1987, Neogene crustal rotations, fault slip and basin development in Southern California, in Ingersoll R.V. and Ernst W. G. (eds.), Rubey Vol VI, Cenozoic basin development of coastal California,, 259
- McKenzie, D.P., 1969, The relation between fault plane solutions for earthquakes and the directions of principal stresses. B.S.S.A, **59**, 2, 591-601
- Jackson J. and McKenzie, D.P., 1983, The geometrical evolution of normal fault systems, J. struct. Geol., **5**, 471-482
- Jackson J. and McKenzie, D.P., 1984, Active tectonics of the Alpine-Himalayan Belt between western Turkey and Pakistan, Geophys. J. R. astr. Soc., **77**, 185-264
- Molnar, P., 1988, Continental tectonics in the aftermath of plate tectonics. Nature, **335**, 131-137

- Namson, J. and Davis, T., 1988, Structural transect of the western Transverse Ranges, California: Implications for lithospheric kinematics and seismic risk evaluation, *Geology*, **16**, 675-679
- Nur, A., Ron, H. and Scotti, O., 1986, Fault mechanics and the kinematics of block rotations. *Geology*, **14**, 746-749
- Pavlidis, S.B., Kondopoulou, D.P., Kiliyas, A.A. and Westphal M., 1988, Complex rotational deformations in the Serbo-Macedonian massif (north Greece): structural and paleomagnetic evidence, *Tectonophysics*, **145**, 329-335
- Powell, R.E., 1982, Crystalline basement terranes in the South-Eastern Transverse ranges, Southern California. in *Geological excursion in the Transverse Ranges*, edited by GSA Cordillera section, pp109-151
- Ransome, F.L., Emmons, W.H. and Garrey, G.H., 1910, Geology and ore deposit of the Bullfrog district, Nevada. *U.S.G.S. Bull.*, **407**, 1-130
- Ron, H., Freund, R., Garfunkel, Z. and Nur, A., 1984, Block-rotation by strike-slip faulting: structural and paleomagnetic evidence. *J. Geophy. Res.*, **89**, 6256-6270
- Ron, H., Nur, A., Aydin, A., 1989, Stress field rotation or block rotation: an example from the Lake Mead fault system, submitted to *Tectonics*
- Sauber, J.W., Tatcher, W. and Solomon, S.C., 1986, Geodetic measurements of deformation in the central Mojave Desert, California. *J. Geophy. Res.*, **91**, 12.683-12.693
- Terres, R.R. and Luyendyk, B.P., 1985, Neogene tectonic rotation of the San Gabriel region, California suggested by paleomagnetic vectors, *J.G.R.*, **90**, B14, 12, 467-12, 484
- Yeats R.S., 1987, Changing tectonic styles in Cenozoic basins of Southern California, in Ingersoll R.V. and Ernst W. G. (eds.), *Rubey Vol VI, Cenozoic basin development of coastal California*, 259
- Yerkes, R.F. and Lee, W.H., 1979a, Late quaternary deformation in the West Transverse ranges, California, *U.S. Geol. Survey Circular*. **799-B**, 27-37
- Yerkes, R.F. and Lee, W.H., 1979b Map showing faults and fault activity and epicenters, focal depths and focal mechanisms for 1970-1975 earthquakes, Western transverse Ranges, California. *U.S. Geol. Survey Misc. Field Studies*, Map MF-1032
- Yerkes, R.F. et al., 1981, Seismotectonic setting of the Santa Barbara channel area, Southern California. Map MF-1169
- Zoback, M.D. and Healy, J.H., 1984, Friction, faulting, and << in situ >> stress, *Annales Geophysicae*, **2**, 6, 689-698
- Zoback, M.D. et al., 1987, New evidence on the state of stress of the San Andreas fault system, *Science*, **238**, 1105-1111

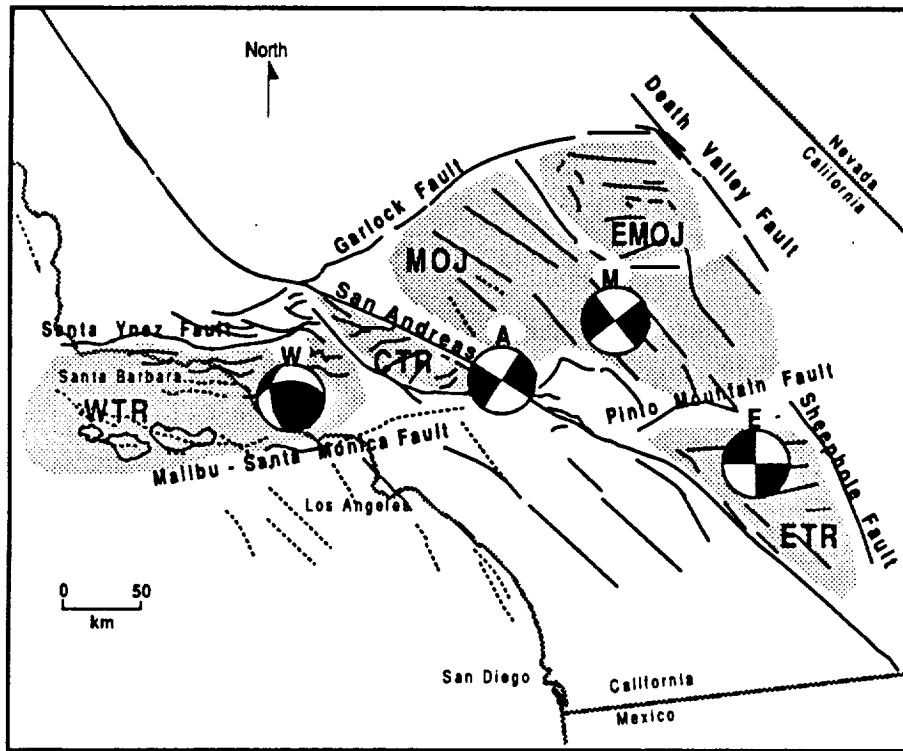


*Fig. 1 Structural domains in Southern California. Sub-parallel sets of faults (Quaternary in Age) of different orientations define structural domains: Mojave (MOJ) and East Mojave (EMOJ), West (WTR), Central (CTR) and East Transverse Ranges (ETR). Domains are separated by throughgoing boundary faults such as the San Andreas, Santa Ynez, and Garlock faults (base map adapted from Jennings, 1975). Representative fault plane solutions (W, E and M) for three domains and for the San Andreas fault (A) are also shown.*

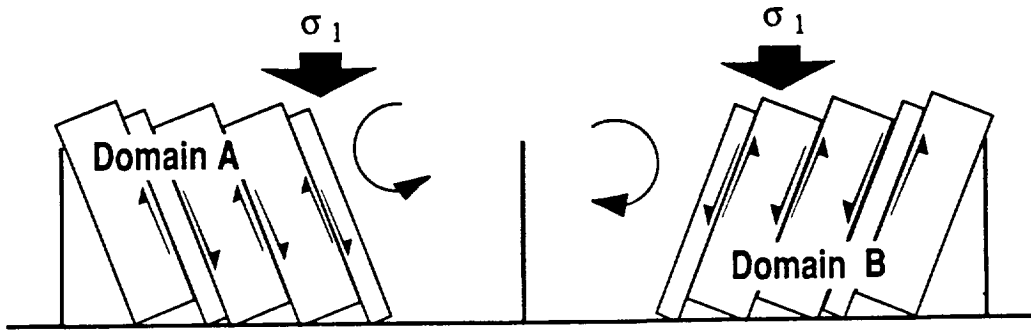


**Fig. 2 Kinematics of block rotation.** Blocks (books) of different orientations abut against boundary faults (shelf and book-holders). The orientation of the blocks with respect to the direction of maximum compression (in this case gravity) controls the sense of slip and therefore the sense of rotation of blocks.

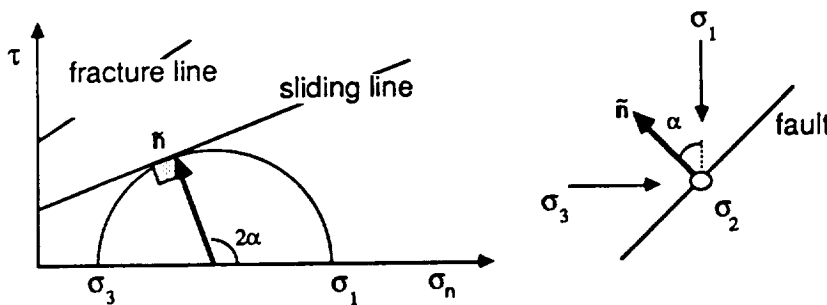


**Fig. 3 Optimally oriented fault.** According to *traditional* friction models (Zoback and Healy, 1984), active faults are generally optimally oriented in the principal stress axis. Therefore, when plotted on the Mohr circle, optimally oriented faults should be represented by a  $\sigma_1 - \sigma_3$  circle tangent to the sliding line, with the intermediate stress  $\sigma_2$  contained in the plane of the fault.

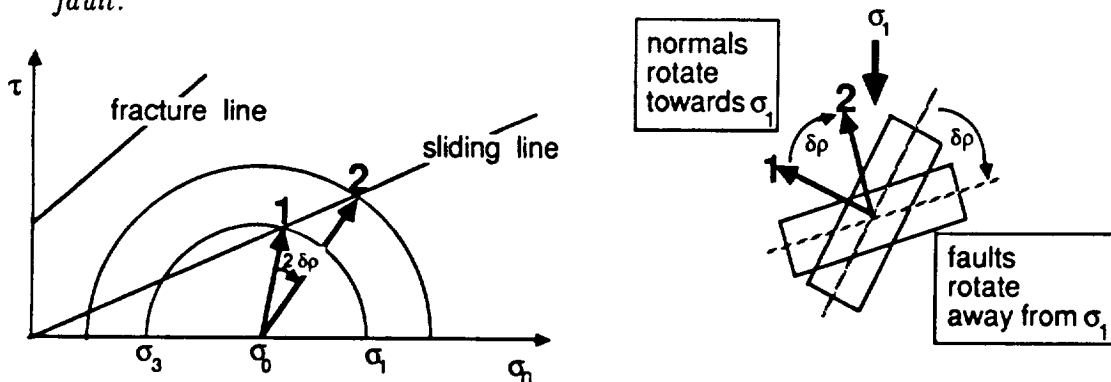


**Fig. 4 Mechanics of block rotation.** The 2D Mohr circles show values of  $\sigma_n$  and  $\tau$  required for the fault to slip, when its fault normal is at point 1, and when the fault rotated to a point 2, closer to the  $\sigma_1$  direction. The lines represent the Coulomb criterion for sliding along preexisting faults and the Coulomb criterion for fracturing an intact rock mass. As illustrated in the sketch to the right, faults rotate away from  $\sigma_1$ . Therefore, normals to faults (poles to fault planes) will rotate towards  $\sigma_1$ , on a Mohr circle.

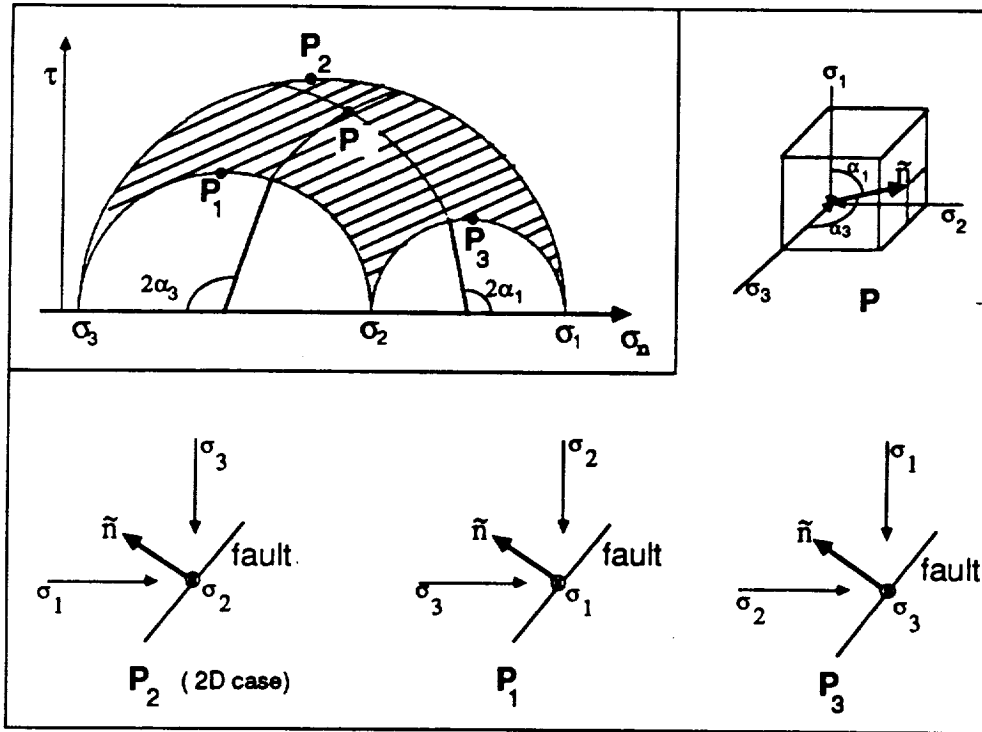


Fig. 5a The 3D Mohr circle is a 3-dimensional construction on a 2-dimensional  $\sigma_n - \tau$  plane. Any point in the shaded region represents the orientation of a fault plane in space. For example,  $\alpha_1$  and  $\alpha_3$  are the direction cosines of a pole ( $P$ ) relative to the  $\sigma_1$  and  $\sigma_3$  directions respectively. Three specific cases are shown: pole ( $P_2$ ) plotting on the  $\sigma_1 - \sigma_3$  circle with the  $\sigma_2$  direction contained in its fault plane, identical to the 2D case; pole ( $P_1$ ) plotting on the  $\sigma_2 - \sigma_3$  circle, with the  $\sigma_1$  direction in its fault plane and pole ( $P_3$ ) plotting on the  $\sigma_1 - \sigma_2$  circle, with the  $\sigma_3$  direction in the fault plane.

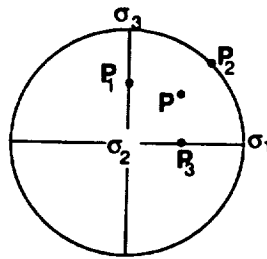


Fig. 5b Poles  $P$ ,  $P_1$ ,  $P_2$  and  $P_3$  of Fig. 5a are plotted in a lower hemisphere Wulff stereo projection. This is another way of plotting the orientation of poles to faults in a 3D space.

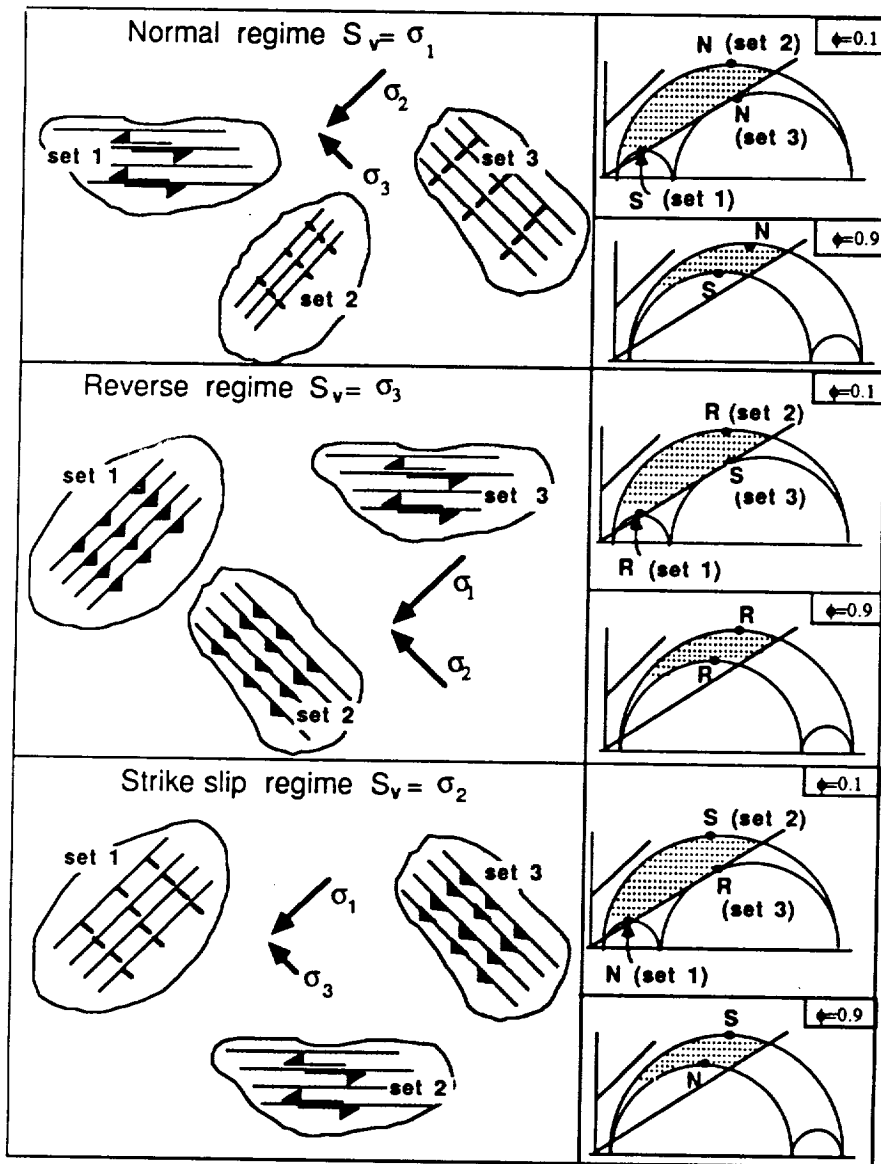


Fig. 6 Mohr circle, friction criteria and faulting styles. Different faulting styles ( $N$  = pure normal,  $R$  = pure reverse,  $S$  = pure strike-slip) may occur in a region of distributed deformation. It depends on the orientation of the fault sets, the tectonic stress regime and the stress ratio  $\phi$  as well as on the material parameters. Here we consider three sets of faults subjected to the three tectonic stress regimes (assuming 1.0 and .6 for the fracture and sliding coefficients respectively): set 2 which contains the  $\sigma_2$  direction in its plane (the 2D case), set 1 which contains the  $\sigma_1$  direction in its plane and, set 3 which contains the  $\sigma_3$  direction in its plane.

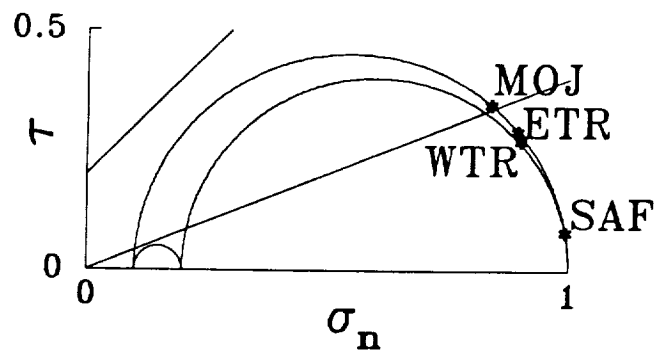


Fig. 7 Representative fault planes shown in Fig. 1 are plotted on a 3D Mohr circle (normalized by  $\sigma_1$ ). A slope of 0.4 for the sliding line, a value of  $\phi = 0.1$  for the stress ratio and a regional strike slip stress regime with  $\sigma_1$  N20°E directed are required to slip faults in the different domains. Notice that the San Andreas fault (SAF), a major throughgoing boundary fault, cannot slip in accordance with friction criteria assumed in this model.

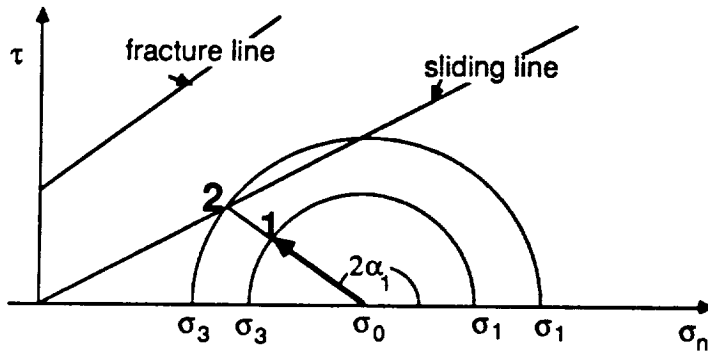


Fig. 8a. Assume a set of faults exists in a domain with an orientation  $\alpha_1$  to the  $\sigma_1$  direction. The  $\sigma_2$  direction is contained in the fault plane. Stress magnitudes must change ( $1 \rightarrow 2$ ) to allow sliding on the fault set. Assume that this change takes place by keeping the mean stress  $\sigma_0$  constant.

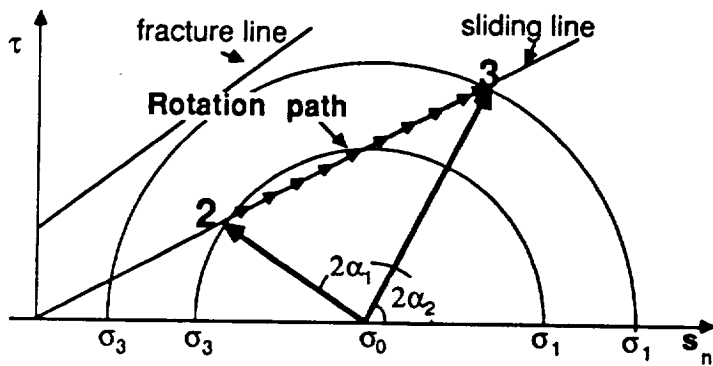


Fig. 8b. **The Rotation Path:** At point 2 there is sufficient shear stress to overcome friction. The faults of a set slip and rotate. On the Mohr circle poles to faults are plotted (see Fig. 4). Thus, as rotation proceeds, stress magnitudes change and the poles plot closer and closer to  $\sigma_1$  tracing a rotation path from 2 to 3 along the sliding line.

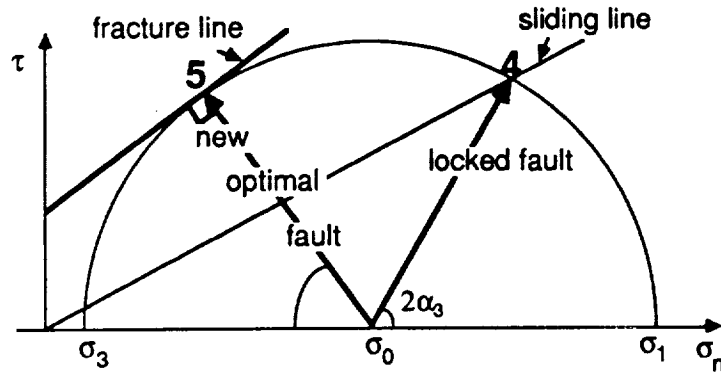


Fig. 8c At point 4 rotation along this set of faults ceases once stress magnitudes have reached the fracture line. Therefore a new, more optimally oriented set of faults forms, point 5, and the old set remains locked into an orientation  $\alpha_3$  relative to  $\sigma_1$ . In 2D, only fault orientations with the  $\sigma_2$  direction in their plane can be modeled. After each rotation step, faults plot on the  $\sigma_1 - \sigma_3$  circle. This results in only one rotation path and a constant fault behaviour.

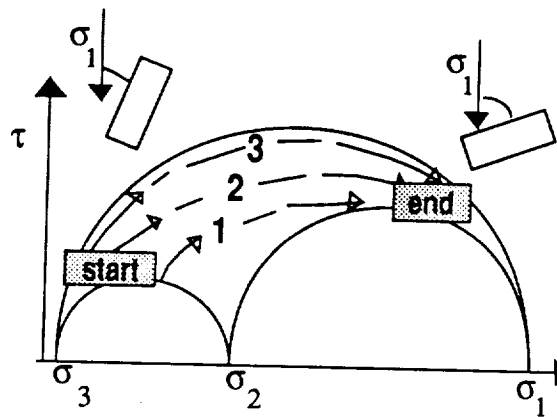


Fig. 9. In 3D there are many rotation paths. In this paper we consider three specific paths. They all start close to the  $\sigma_3$  direction but rotation path for pole 1 starts close to the  $\sigma_2 - \sigma_3$  circle, rotation path for pole 3 starts close to the  $\sigma_1 - \sigma_3$  circle, rotation path for pole 2 starts at an intermediate position between the two. Rotation paths shown in this figure and Fig. 11 are plotted on graphs normalized by the magnitude of  $\sigma_1$ . The stress ratio  $\phi$  remains constant throughout the rotation history of a fault set. Thus rotation paths will appear as curved lines.

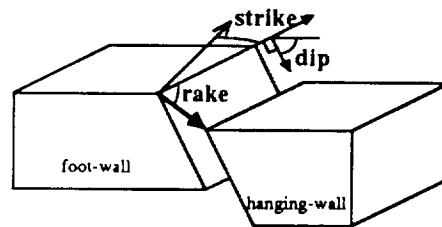


Fig. 10: The orientation of a fault set is given by the strike, or the azimuth of the fault with respect to a reference direction, and the dip, or the angle between the fault plane and the horizontal plane ( $0^{\circ}$  = horizontal;  $90^{\circ}$  = vertical). The style of faulting is determined by the rake, or the angle between the direction of fault slip and the horizontal ( $+90^{\circ}$  = pure normal;  $0^{\circ}$  = pure strike - slip;  $-90^{\circ}$  = pure reverse).

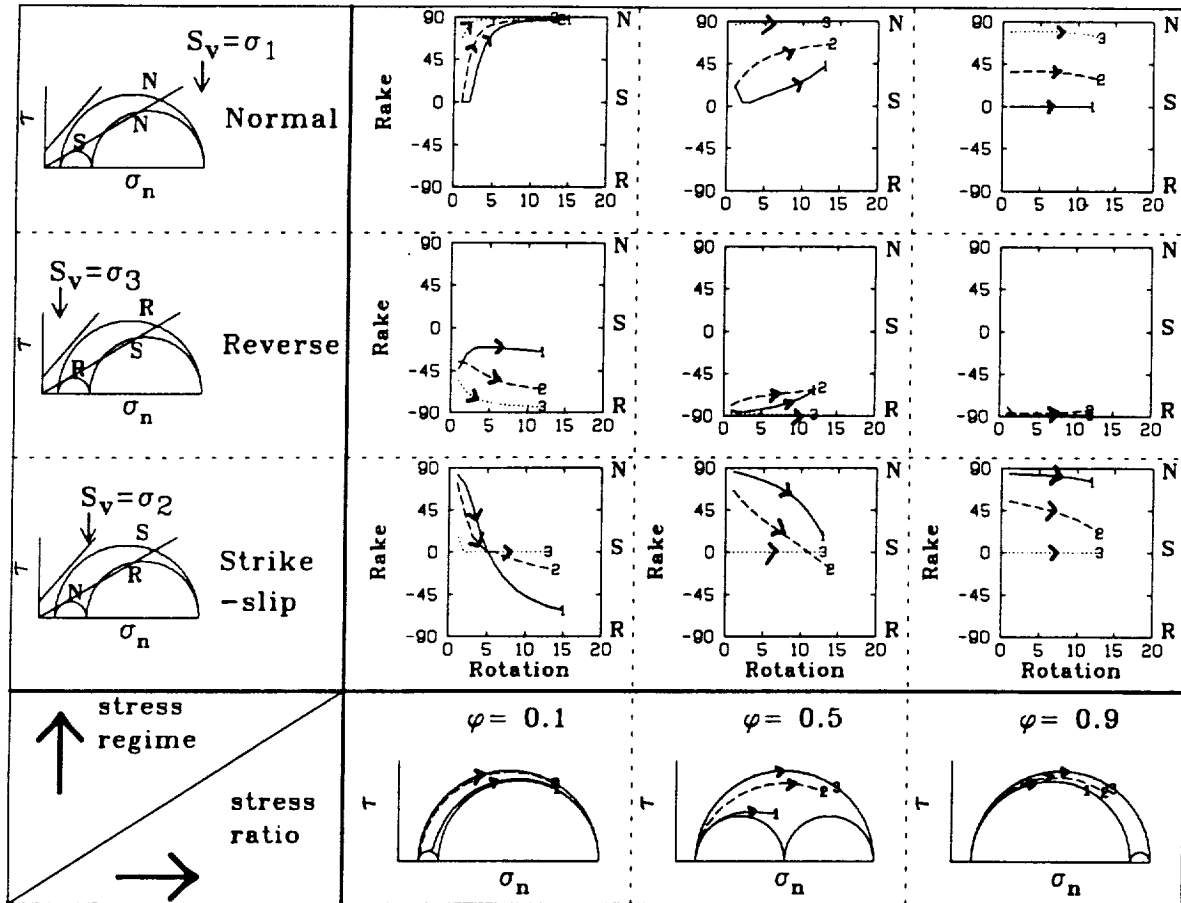


Fig. 11 Cross-plot of faulting styles for different stress regimes and  $\phi$  ratios. The faulting style evolves along various rotation paths in plots of rake vs. rotation. Strike-slip fault styles (S) are at  $0^\circ$ , normal (N) styles are at  $90^\circ$ , and reverse (R) styles are at  $-90^\circ$ . Fig. 9's case 1 plots with a solid line, case 2 with dashes, and case 3 with dots. Variations in rake with rotation are sensitive to  $\sigma_2$ . Low  $\phi$  values change the modeled rake dramatically while high values leave it largely unchanged along the rotation paths.

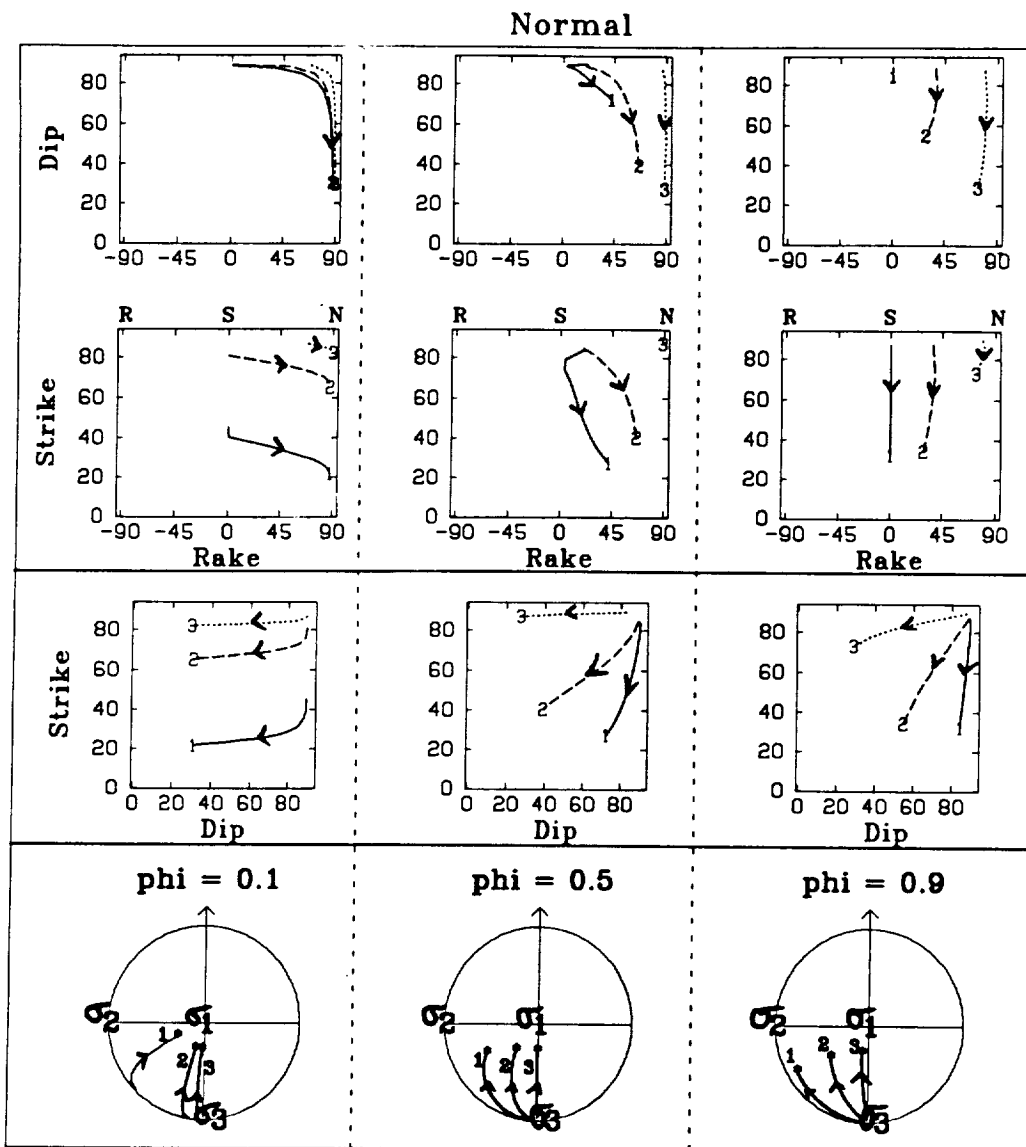
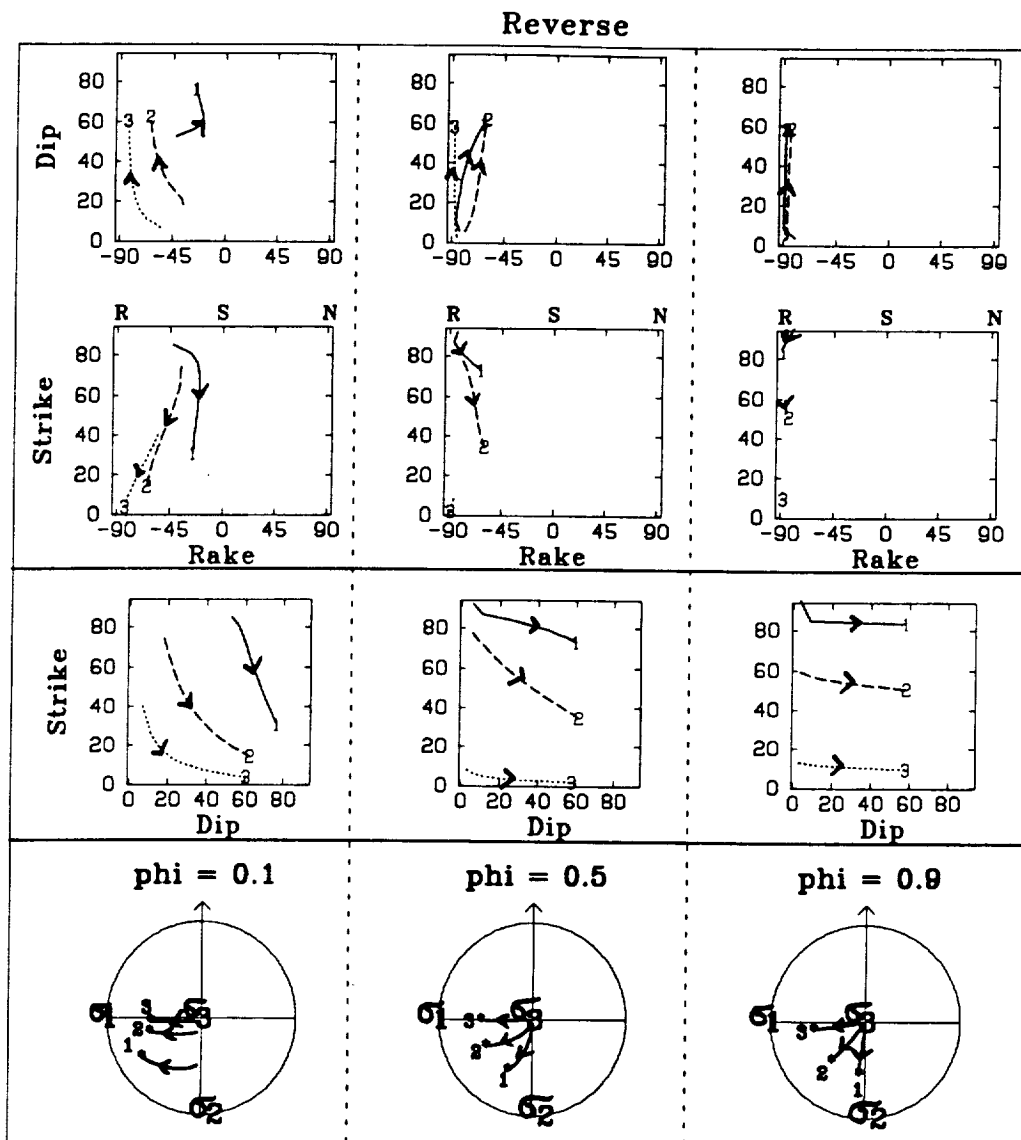


Fig. 12a Rake versus Dip, Rake versus Strike and Dip versus Strike are plotted for the three rotation paths (1, 2, 3) at different values of the stress ratio  $\phi$ . The arrows indicate the sense of rotation. Wulff stereo-projections for the three rotation paths are shown, for reference, at the bottom of each figure.

Normal stress regime,  $S_v = \sigma_1$ . The flattening of the dip decreases with increasing stress ratio. The rake changes from strike-slip to normal at low stress ratios ( $\phi = 0.1$ ) but remains constant at the initial value at high stress ratios. This is accompanied by an increase in vertical axis rotation with increasing stress ratio (see rotation paths 1 and 2): the strike is relatively constant at low stress ratios but changes considerably at high ratios ( $\sigma_3$  is at strike =  $0^\circ$ ).



*Fig. 12b Reverse stress regime,  $S_v = \sigma_3$ . The dip steepens throughout rotation for all fault planes at all stress ratios. The rake changes from oblique-strike-slip to oblique-reverse-slip (rotation path 1) or to strike-slip (rotation path 2) at low stress ratios but at intermediate and high stress ratios the rake is reverse along all rotation paths. This is accompanied by a vertical axis rotation at low  $\phi$  values (see rotation paths 1 and 2) where the strike changes considerably. At higher stress ratios, rotations occur predominantly about a horizontal axis ( $\sigma_2$  is at strike =  $0^\circ$ ).*

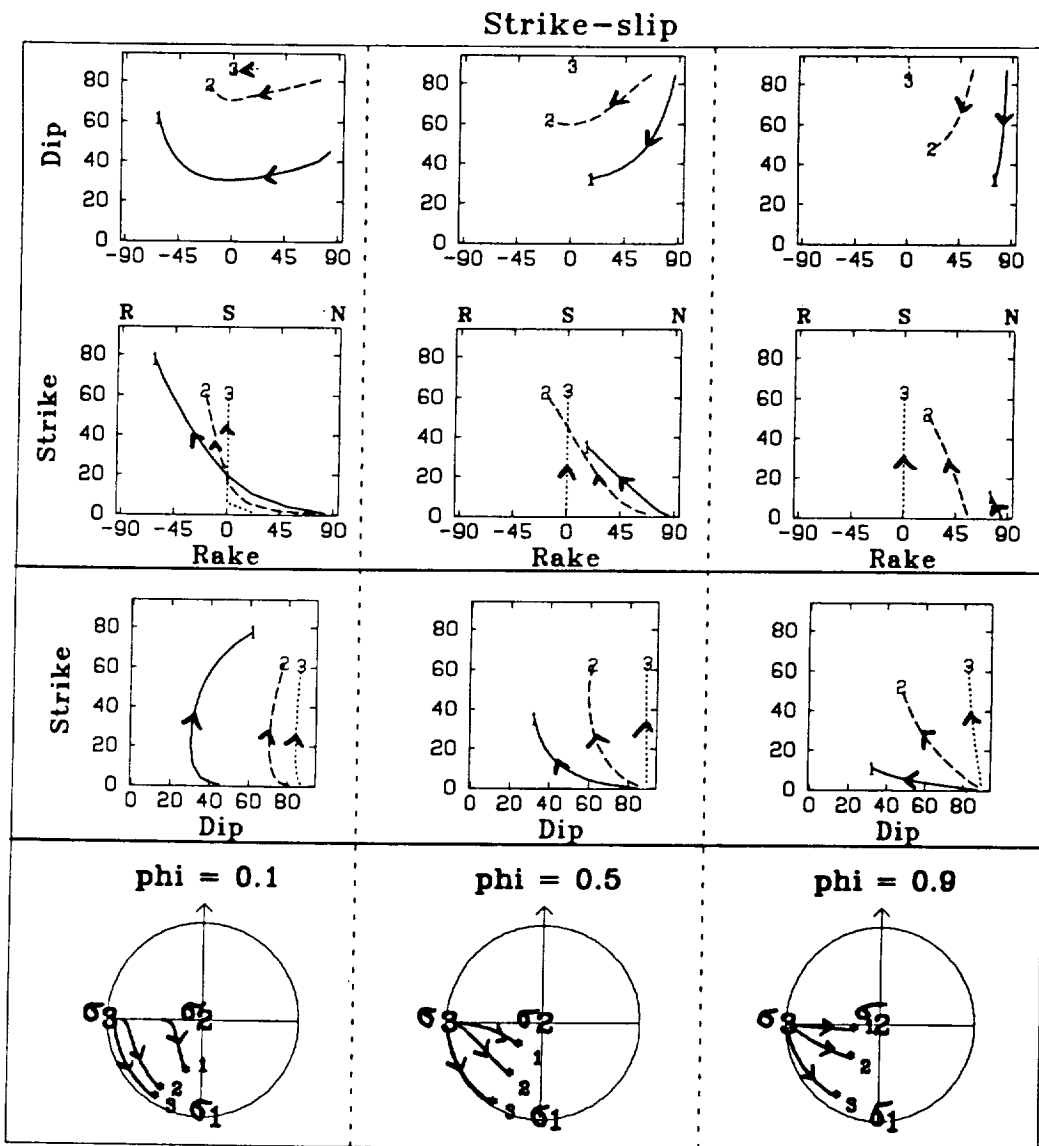


Fig. 12c Strike slip stress regime,  $S_v = \sigma_2$ . As the rake goes from normal, through strike-slip and then to reverse, the dip of the fault plane flattens at first and then steepens at low stress ratios ( $\phi = 0.1$ ). At higher stress ratios rotation stops before the reverse field is reached. The strike change is greater than the dip change, producing predominant vertical axis rotations in most cases ( $\sigma_1$  is at strike=0). An exception to this is rotation path for pole 1 at  $\phi = 0.9$ : the strike does not change, only the dip and therefore a purely horizontal axis rotation can occur in a strike-slip stress regime.

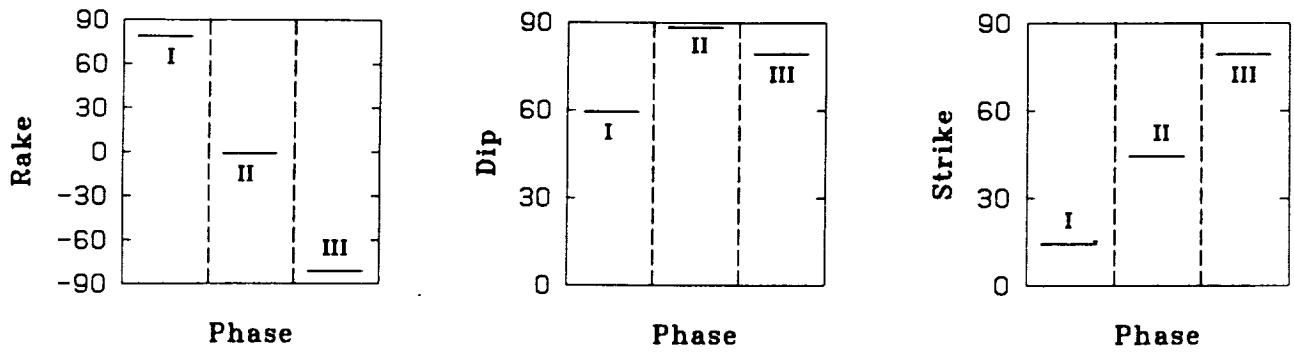


Fig. 13 Observed and inferred rake, dip and strike of the WTR fault set since Miocene times. Based on structural, geological and paleomagnetic data as discussed in the text.  $\sigma_1$  is assumed at  $N20^\circ E$  and is at strike =  $0^\circ$  on the plot.

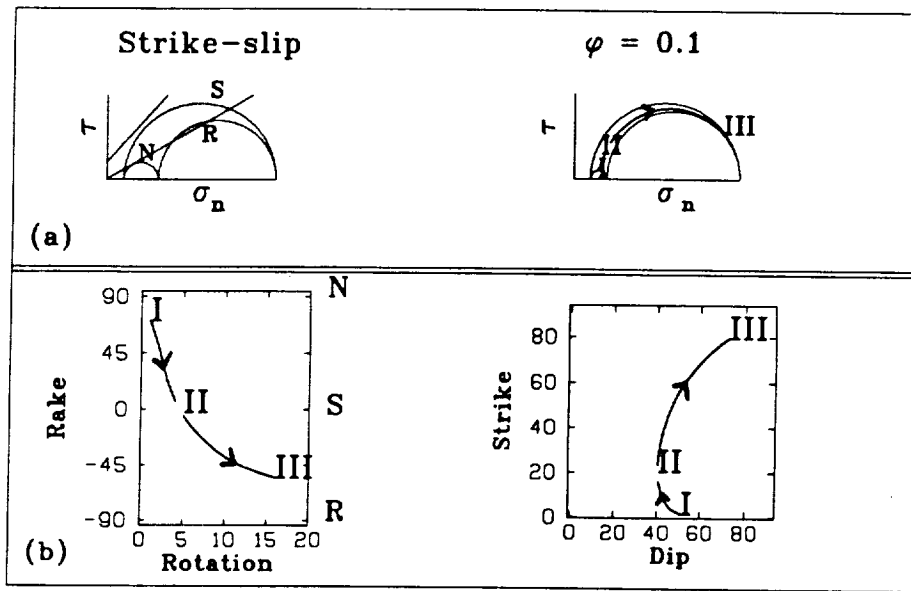


Fig. 14 Modeling 3D fault rotation in the West Transverse Ranges. (a) The rotation path predicted by the 3D BR model, assuming, as in Fig. 7, a strike slip stress regime with the maximum principal stress direction  $\sigma_1$   $N20^\circ E$ , a coefficient of friction  $\mu_f = 0.4$ , and a stress history with a constant stress ratio  $\phi = 0.1$ . (b) According to the 3D BR model, a single set of rotating faults may have accommodated the deformation of the WTR domain. The model predicts, in accordance with observations summarized in Fig. 13, three different phases of faulting styles since rotation began: normal-oblique faulting (I)  $\rightarrow$  strike-slip faulting (II)  $\rightarrow$  high angle reverse-oblique faulting (III).

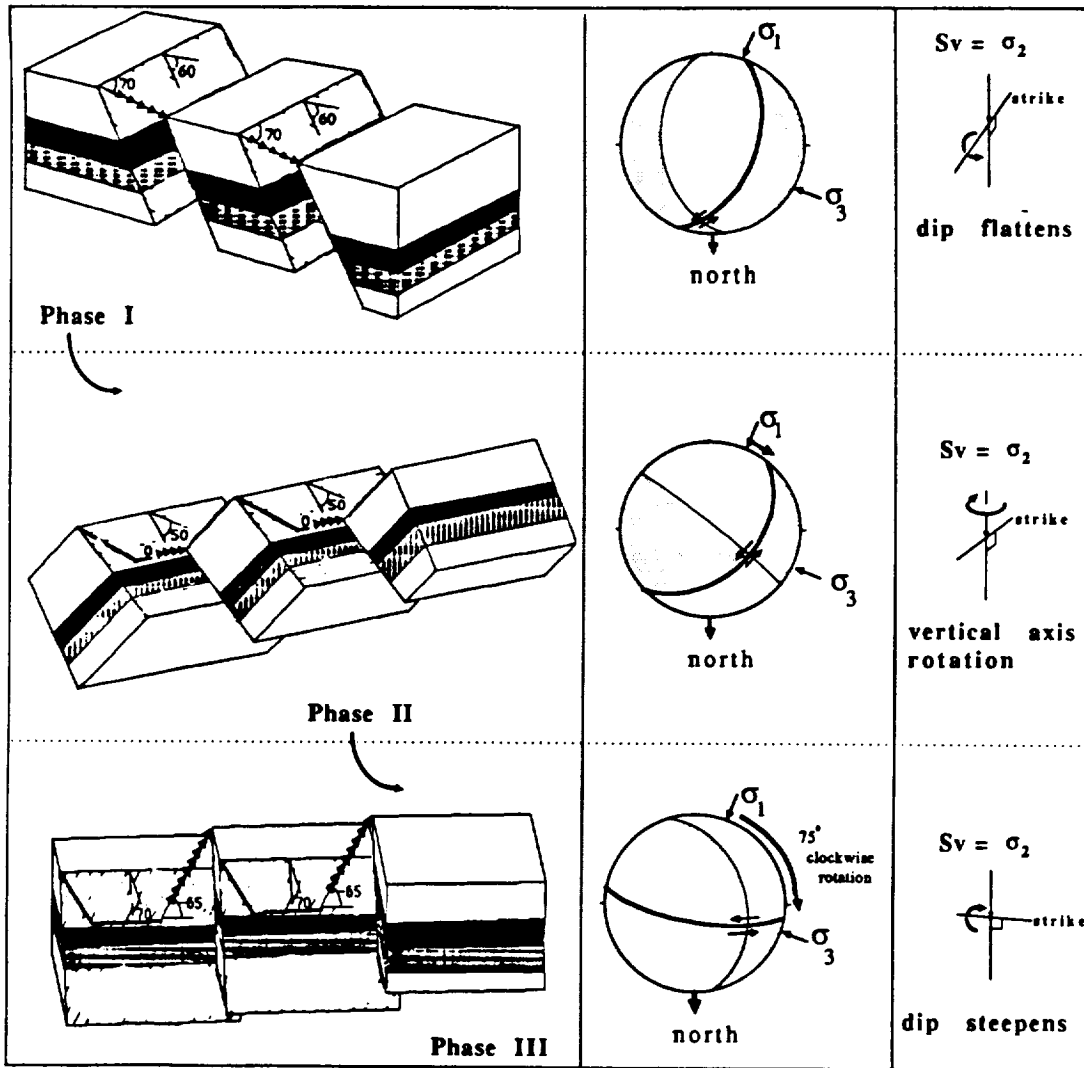
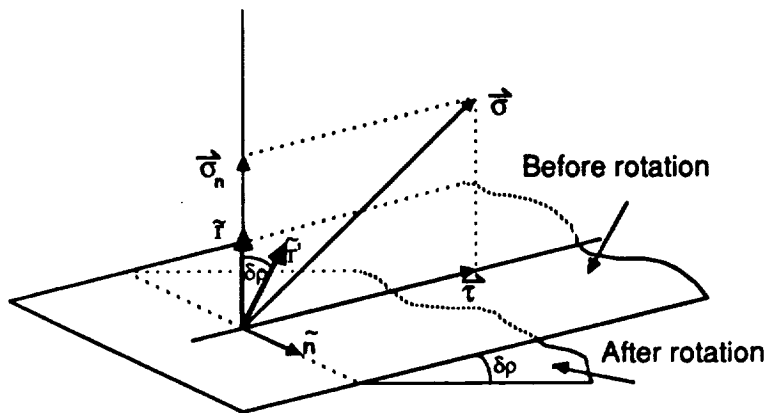


Fig. 145 The evolution of the rake, the dip, and the strike of the faults of the WTR through time. Each phase may be better visualized with idealized block diagrams and focal plane solutions (lower hemisphere projections). The sketches in the right column show the dominant axis of rotation, where  $S_v$  refers to the principal vertical stress axis and the strike of the fault is shown. When the strike of the fault is almost parallel to  $\sigma_1$ —phase I—the faults move in a normal-oblique (rake = +70) sense. When none of the principal stresses are parallel to the strike of the faults—phase II—the faults move in a strike-slip sense (rake = 0). Finally, when the strike of the fault becomes parallel with the  $\sigma_3$  direction—phase III—the faults move in a reverse-oblique sense (rake = -65).



*Fig. A1: Rotation of Fault Planes. The horizontal plane, with its normal vector  $\vec{r}$ , represents the initial orientation of the fault. During rotation, the normal  $\vec{r}$  will rotate through an angle  $\delta\rho$  within the plane (normal  $\vec{n}$ ) that contains  $\vec{\sigma}_n$ ,  $\vec{r}$ ,  $\vec{\sigma}$ ,  $\vec{r}$ , moving to a new position  $\vec{r}'$ , defined by direction cosines  $\alpha'_1, \alpha'_2, \alpha'_3$ .*

Final  
August 8, 1989

N 9 1 - 1 4 6 6 8

**STRESS FIELD ROTATION OR BLOCK ROTATION:  
AN EXAMPLE FROM THE LAKE MEAD FAULT SYSTEM**

by  
**Hagai Ron**  
The Institute for Petroleum Research and Geophysics  
Holon, Israel

**Amos Nur**  
Department of Geophysics  
Stanford University, Stanford, CA 94305-2215

**Atilla Aydin**  
Department of Geosciences  
Purdue University  
West Lafayette, Indiana 47907

**ABSTRACT**

The Coulomb criterion, as applied by Anderson (1951), has been widely used as the basis for inferring paleostresses from insitu fault slip data, assuming that faults are optimally oriented relative to the tectonic stress direction. Consequently if stress direction is fixed during deformation so must be the faults. Freund (1974) has shown however that faults, when arranged in sets, must generally rotate as they slip. Nur et al., (1986) showed how sufficiently large rotations require the development of new sets of faults which are more favorably oriented to the principal direction of stress. This leads to the appearance of multiple fault sets in which older faults are offset by younger ones, both having the same sense of slip. Consequently correct paleostress analysis must include the possible effect of fault and material rotation, in addition to stress field rotation.

The combined effects of stress field rotation and material rotation were investigated in the Lake Mead Fault System (LMFS) especially in the Hoover Dam area.

Fault inversion results imply an apparent 60° clockwise (CW) rotation of the stress field since mid-Miocene time. In contrast structural data from the rest of the Great Basin suggest only a 30° CW stress field rotation. By incorporating also paleomagnetic and seismic evidence, the 30° discrepancy can be neatly resolved. Based on paleomagnetic declination anomalies it is inferred that slip on NW trending right lateral faults caused a local 30° counterclockwise (CCW) rotation of blocks and faults in the Lake Mead area. Consequently the inferred 60° CW rotation of the stress field in the LMFS consists of an actual 30° CW rotation of the stress field (as for the entire Great Basin) plus a local 30° CCW material rotation of the LMFS fault blocks.

## INTRODUCTION

The Coulomb criterion, as applied by Anderson (1951) to faulting, gave rise to the widely used concepts of faulting mechanics in rocks. Accordingly faults form at angles of 45° or less (depending on the frictional properties of rocks) from the maximum compressive stress. It is the orientation of the principle stress axes relative to the earth's free surface which thus defines the three types of standard faults: Normal, reverse and strike slip.

Anderson's approach has provided the basis for methods to infer paleostress directions from insitu fault strike and dip, sense of slip, and related strain indicators (Choukroune, 1969; Hancock and Atiya, 1979; Zoback et al., 1981; Letouzey and Tremolieres, 1980; Marshak et al., 1983; Eyal and Reches, 1983 and others). Improved estimates were introduced during the last decade (Angelier, 1979, 1984; Michael, 1984; Ellsworth, 1982, and others) based on the added assumption that fault slip is in the direction of maximum shear stress resolved on the fault plane. Here fault slip data is used to determine that paleo orientation of the principle stresses which minimizes the angular deviations between the observed slip direction along a fault and the direction of the maximum resolved shear stress. Reches (1987) introduced a further improve-

ment in the fault's coefficient of friction and cohesion are also constrained.

## STRESS ROTATION VS. MATERIAL ROTATION

A key assumption in all the inversion methods mentioned above is that fault orientation remains unchanged relative to the principal stress directions during fault slip. However in a seminal paper, Freund (1974) explored the consequences of relaxing this assumption by adding rotation of crustal blocks bounded by slipping faults. On the basis of simple 2-D kinematic analysis Freund showed that rotations are not only possible, but generally unavoidable. Furthermore he showed that the sense of these rotations is directly controlled by the orientation of the faults (arranged in sets) relative to the direction of the principle tectonic shortening, and that the magnitude of the rotation of crustal blocks is controlled by the magnitude of the crustal shortening.

Significant evidence has accumulated by now to suggest that block and fault rotations due to crustal shortening and extension are widespread. For example Ron et al., (1984) showed that adjacent conjugate fault domains experienced both clockwise and counterclockwise rotations in a single tectonic setting of northern Israel. Similar interpretations were suggested for the Mojave area in California (Garfunkel, 1974), the Transverse Range, California (Terres and Luyendyk, 1985) central America (Manton, 1987), Alaska (Stamatakis et al., 1988), Lake Mead, Nevada region (Ron et al., 1986; Geissman, 1986,) and northern Greece (Pavlidis et al., 1988). According to Freund's (1974) model the blocks and their bounding faults always rotate away from the direction of shortening and toward the direction of elongation. Furthermore it was shown by Nur et al., (1986), that when rotation becomes sufficiently large, slip on the rotating faults ceases because the resolved shear stress on them has decreased and the normal stress has increased to the point where the frictional resistance is too great for further slip. If crustal deformation is to proceed further it must be accommodated by a set of new faults, more favorably oriented to the principle direction of the regional stress field

As a result, domains of multiple sets are formed in which the younger faults systematically offset the older ones. This relatively simple process of crustal deformation by multiple sets of rotating faults and blocks thus results in complex fault patterns which do not require stress field rotations. Consequently tectonic and structural analysis of complex fault systems, using fault plane inversion methods which exclude fault rotation, can lead to unduly complicated and often erroneously inferred paleostress histories. Although it is most probable that in many cases stress field rotations actually take place over geological time, these rotations are probably slow and gradual. As a result, much of the observed complexity of the fault pattern observed insitu could very well be due to multiple fault sets formed by material rotation of blocks and their bounding faults, not by stress field rotation.

To determine the relative importance of the two rotations - stress field rotation vs. material rotation they have to be determined independently. Stress rotations must be inferred indirectly from regional structural and tectonic features (e.g., Zoback et al., 1981). In contrast material rotations can be determined directly from paleomagnetic declination and inclination anomaly measurements.

The purpose of this short paper is to report on a probable case of combined material rotation and stress field rotation in the Lake Mead fault system, Nevada. The evidence is based on three types of information: Structural evidence (Zoback et al., 1981; Angelier et al., 1985), paleomagnetic data (Ron et al., 1986; Geissman, 1986), and seismicity (Rogers and Lee, 1976; Rogers et al., 1984).

## **DATA**

**Structures.** The 30 by 80 km Lake Mead fault system (figure 1) includes a few long northeast-trending left-lateral strike slip faults (set #1 in figure 1 & 2). Based on offsets of Late Neogene volcanic rocks (Anderson, 1973; Bohannon, 1983) the total slip across this system is approximately 65 km. Geological evidence shows that strike slip

faulting has begun 13.5 to 11.3 Ma ago and continued through Miocene to early Pliocene and possibly to Pleistocene times (Anderson, 1973; Bohannon, 1983). Bohannon (1983) suggests specifically that most of the left lateral faulting occurred during late Miocene time. This phase of intense faulting was followed by decreasing volcanic and plutonic activity and by normal faulting that formed broadly spaced basins and ranges (Anderson et al., 1972; Angelier et al., 1985). Results by Ron et al., (1986) and by Li (personal communication, 1989) suggest that sets of smaller faults, trending NW and showing right lateral slip are bounded by the larger NE trending faults.

A more detailed and local study of the geometry and nature of faulting of the LMFS was completed by Angelier et al., (1985) in a small area near Hoover Dam. The data, in the form of density distributions (the numbers of faults in a given set) have shown that (a) the most prominent fault set is the one striking northwest (Anglier et al., 1985, Figure 6); (b) the rake distribution of this NW trending fault set is bimodal, with groups of dip slip and right-lateral strike slip faults striking  $290^{\circ}$  -  $325^{\circ}$  (northwest)(Angelier et. al., 1985 figure 6 and 9); (c) a few left-lateral faults striking  $350^{\circ}$  -  $30^{\circ}$  (north to northeast) are also found here (Anglier et. al., figure 9).

Together these results suggest that the northwest-trending right lateral faults (set #2 in figure 1 & 2) probably accommodated most of the internal deformation of the LMFS region and are therefore reliable stress indicators in this region.

Angelier et al., (1985) used the fault data above to determine the paleostress history of the Southern Great Basin. Assuming that any one cluster of fault orientations is associated with a corresponding orientation of the stress field (and excluding material rotation) Anglier et. al., (1985) inferred a clockwise (CW) stress field rotation of about  $60^{\circ}$  since mid-Miocene time. Although the CW sense of this paleostress rotation is very consistent with the sense of stress rotation proposed for the entire Basin and Range (Ekren, 1977; Zoback et al., 1981), the magnitude of this stress rotation is in

remarkable disagreement with values elsewhere: Zoback et al., (1981) suggested a 30° CW rotation of the principal paleostress direction since mid-Miocene throughout the Basin and Range, whereas the results by Anglier et al., (1985) seemingly imply a 60° CW stress field rotation for the Hoover Dam and presumably the entire Lake Mead area. The resulting 30° discrepancy led Anglier and co-workers to actually suggest that rocks in the Hoover Dam study area may have experienced, in addition to the regional Basin and Range stress field rotation, also some local material rotation, associated with shearing along the Lake Mead fault system.

**Seismicity.** Rogers & Lee (1976) inferred from fault plane solutions for earthquakes in the Lake Mead region that many faults are right handed strike slip in nature, with north-south strikes (set #3 figures 1 & 2). It is noteworthy that this seismic activity is not associated with the large northeast left-lateral strike slip faults (set # 1), nor is it associated with the shorter NW trending right lateral faults (set #2). From the prevalence of the NW trending, now inactive faults (set #2) and the N trending seismic faults (set #3) we have suggested (Ron, et. al.,1986) that active crustal deformation in this area was and is still being accommodated by the sets of the smaller fault with right-lateral strike slip, situated within the larger left-lateral shear zones. The tension or extension direction inferred from the seismically active fault plane solutions is oriented northwest-southeast, in agreement with the direction of the current least horizontal principal stress throughout the entire Basin and Range Province (Zoback et al., 1981; Carr, 1984).

**Paleomagnetism.** Two paleomagnetic data sets are directly relevant to our analysis, one from the Hamblin-Cleopatra volcano area (Ron et al., 1986), a second from the Hoover Dam area (Geissman 1986). Supporting evidence is found also in Wells and Hillhouse (1989). The Hamblin-Cleopatra volcano area results, according to Ron et al.,(1986) show that

(1) Based on in situ field inclination data, paleomagnetic analysis yields negligible local block rotation about horizontal axis. This implies insignificant tilting by normal faults.

(2) The in situ field data revealed a declination anomaly of  $-29.4^{\circ} \pm 8.5^{\circ}$ . This implies a counterclockwise rotation of blocks in this area about a vertical axis of about  $30^{\circ}$ .

Similarly, paleomagnetic data collected by Geissman (1986) in the same Hoover Dam area, where Angelier et al (1985) obtained their structural data, imply that

(1) Paleomagnetic declination data imply a counterclockwise rotation of approximately  $30^{\circ}$  of the Hoover Dam area relative to the unrotated region to southeast. This rotation - is close both in sense and magnitude to Ron's et al., (1986) results for the Hamblin-Cleopatra area.

(2) The tilting of fault blocks in the Hoover Dam and adjacent areas as inferred from inclination data occurred most probably prior to the left-lateral strike slip faulting of the Lake Mead system. This is in good agreement with Angelier et al., (1985) who suggested on the basis of independent structural evidence that tilting occurred before or very early in the strike slip faulting history.

Wells and Hillhouse (1989) also report on CCW rotations of  $\sim 10^{\circ}$  presumably on NW trending left lateral faults at the SW end of the LMFS, about 40 km away from the Hoover Dam area.

## DISCUSSION

The results reviewed above can be summarized as follows:

(1) The structural data suggests that the shorter NW trending right-lateral faults (set #2 in figure 1 & 2) accommodated much of the deformation of the region (Angelier et al, 1985).

(2) The seismic data shows that current fault slip takes place along short north-

south trending right-lateral strike slip faults (set #3) (Rogers and Lee, 1976; Rogers et al., 1984) and not along the NW older trending ones, or the major NE faults.

(3) The paleomagnetic data reveals that the NW trending right-lateral strike slip faults (set #2) were most probably involved in a 30° counterclockwise material rotation of blocks and faults (Figure 2). This has led us to suggest (Ron et al., 1986) that the original orientation of these faults was approximately north-south as shown in figure 3. Presumably, as a consequence of their rotation they locked up, and a new, NS trending set of currently seismically active faults has developed.

(4) As shown in figure 4 the structural paleostress indicators from the Lake Mead fault system yield, assuming no material rotation, a 60° clockwise stress field rotation since mid-Miocene (Angelier et al., 1985). In contrast, paleostress indicators throughout the Basin and Range suggest only a 30° clockwise stress field rotation (Anderson and Ekren, 1977; Zoback et al., 1981).

(5) The current maximum horizontal stress as inferred from earthquakes fault plane solutions, is oriented N30° E. This direction is in good agreement with stress orientation derived from post mid-Miocene structures in other parts of the Great Basin.

Figure 3 presents our proposed model for the fault geometry, the sense of horizontal slip, and the nature of block rotation in the study area (Ron et al., 1986) beginning about 11 My ago and still in progress today: overall left-lateral shear in Miocene times caused right-lateral strike slip displacement on set #2 of local faults, initially trending north-south. The strike slip on these faults lead to their counterclockwise rotation together with the intervening blocks. The faults locked up following the 30° CCW rotation from their initial direction (Nur et al., 1986). Assuming that the stress field orientation remained constant over 11 My (Zoback et al., 1981) subsequent crustal deformation was and is still being accommodated by the new set #3 of the more favorably oriented north-south trending right-lateral strike slip faults.

Taken together, these results provide a neat and simple explanation for the puzzling discrepancy between the apparent 60° clockwise **stress field rotation** inferred from the Angelier et al., (1985) data for the Hoover Dam area, and the known 30° clockwise stress field rotation established for the entire Basin and Range province. We suggest that the 60° rotation consists of a 30° CW stress field rotation plus a 30° CCW material rotation. Consequently local **material rotation** in the LMFS it has been superimposed on the regional Basin and Range stress field rotation. This local rotation obeys the rules of the kinematics. (Freund 1974; Ron et al., 1984), and mechanics (Nur et al., 1986) of block and fault rotation model. In this model, simultaneous strike slip faulting and rigid block rotation about the vertical axis take place. A key feature is that the sense of rotation is opposite to the sense of slip (e.g., counterclockwise rotation associated with right-lateral slip and clockwise rotation associated with left lateral slip). Equivalently the material rotation is always away from the direction of maximum compression. Consequently, when structural markers are used to infer rotation, a **clockwise stress field rotation** is indistinguishable from a **counterclockwise material rotation**, and vice versa.

#### SUMMARY

We suggest that the Lake Mead - Hoover Dam area experienced the same 30° CW tectonic **stress field rotation** that presumably affected the entire basin and range province (Zoback et al., 1981). In addition this region has also experienced a 30° CCW **material rotation** of blocks and faults (Figure 4) giving rise to the apparent discrepancy between the stress history of the LMFS and the rest of the Basin and Range province.

There must exist other regions where the tectonic history involved both paleo-stress field rotation and material rotation. Consequently our analysis here may prove effective in solving faulting complexities elsewhere: Examples include central Japan (Angelier & Huchon, 1987), where large differential paleomagnetic rotations have

been found (Yasuto, 1988), in northern Greece (Pavrides and Kiliias, 1987, Pavrides et al., 1988) southern California (Nicholson et al., 1986), and New Zealand (Walcott, 1988), to name but a few.

#### **ACKNOWLEDGEMENT**

This research was supported by a grant from NASA to Amos Nur. We are grateful for discussions and comments by John Geissman, Oona Scotti, and Yanping Li.

## FIGURE CAPTIONS

Figure 1. The main fault sets in the Lake Mead Fault System (modified after Rogers & Lee, 1976): (1) Large NE trending left lateral strike slip faults, (set #1); (2) Shorter NW trending right lateral strike slip faults (sets #2); and (3) N trending seismically active faults (set #3) Although these faults are mapped as normal faults, the fault plane solution indicate right handed strike slip.

Figure 2. Structural interpretation of paleomagnetic data in the Hamblin-Cleopatra area (Ron et. al., 1986) and the Hoover Dam area (Geissman, 1986). In both areas, a 30° paleomagnetic declination anomaly was found, suggesting a 30° counterclockwise material rotation. Assuming that Freund's (1974) model applies, this rotation was accommodated by the NW trending strike slip fault (set #2). According to this model the major faults of set #1 have remained unrotated.

Figure 3. Structural model for the development of multiple faults due to the material rotation in the Lake Mead fault zone: Left slip on the irrational faults of set #1 caused right slip on the faults of set #2, as well as rotation of the blocks bounded by these faults. When these right handed faults rotated approximately 30° CW away from the direction of maximum compression  $\sigma_1$ , they locked up. Further deformation is now accommodated by the new set #3 of right handed faults. Presumably, when these fault will reach a CCW rotation of 30° in the future, they will lockup, and another set of rotating faults may have to develop.

Figure 4. Combined material rotation and stress field rotation in the Lake Mead Fault system vs. stress field rotation only in the basin and range province: (a) old (090°) and new (120°) extension directions in the basin and range province, according to Zoback et. al., (1981). (b) Expected old and new optimal directions of strike slip faults in the basin and range province subject to the stresses in (a). Note that the angle between them should be 30°; (c) Directions of old and new strike slip faults observed in the

Lake Mead Fault zone (MFZ) and Hoover Dam area (set #2 and #3 respectively of figure 1 & 2). The angle between them is close to  $60^\circ$ , not  $30^\circ$  as expected from (a) and (b); (d) explaining the LMFZ  $60^\circ$  apparent rotation as a combination of a  $30^\circ$  clockwise stress field rotation plus a  $30^\circ$  counterclockwise material rotation, as inferred from the paleomagnetic declination anomalies of Ron et. al., (1986) and Geissman (1986).

## REFERENCES

- Anderson, E. M., 1951, The dynamics of faulting: Oliver and Boyd, Edinburgh, p. 206.
- Anderson, R. E., 1973, Large-magnitude late tertiary strike slip faulting north of Lake Mead, Nevada: U.S. Geological Survey Professional Paper 794.
- Anderson, R. E., and Ekren, E. B., 1977, Comment on Late Cenozoic fault patterns and stress field in the Great Basin and westward displacement of the Sierra Nevada block: *Geology* V5, #7, p. 388-389.
- Anderson, R. E., Longwell, R. C., Armstrong, R. L., and Marvin, R. F., 1972, Significance of K-Ar ages of tertiary rocks from the Lake Mead region, Nevada-Arizona: *Geological Society of America Bulletin*, V83, p. 273-288.
- Angelier, J., 1979, Determination of the mean principal directions of stress for a given fault population: *Tectonophysics*, 56, T17-T26.
- Angelier, J., 1984, Tectonic analysis of fault slip data sets: *J. Geophys. Res.*, 89, p. 5835-5848.
- Angelier, J., Barrier, E., and Chu, H. T., 1986, Plate collision and paleostress trajectories in a fold-thrust belt: the Foothills of Taiwan: *Tectonophysics*, 125 p. 161-178.
- Angelier, J., Collette, B., and Anderson, E. R., 1985, Neogene paleostress changes in the Basin and Range: A case study at Hoover Dam, Nevada-Arizona: *Geological Society of American Bulletin*, V96, p. 347-361.
- Angelier, J., and Huchon, P., 1987, Tectonic record of convergence changes in a collision area; the Boso and Miura peninsulas, central Japan: *Earth and Planetary Science Letter*, 81, p. 3997-408.
- Bohannon, R. G., 1983, Geologic map, tectonic map and structure sections of the Muddy and northern Black mountains, Clark County, Nevada: U. S. Geological Survey Miscellaneous Investigation Series, Map I-1406.
- Carr, W. J., 1984, Regional structural setting of Yucca Mountain, southwestern Great Basin. Nevada and California: U. S. Geological Survey Open-File Report 84-854.
- Choukroune, P., 1969, Un exemple d'analyse microtectonique d'une serie calcaire affectee de plis isopaques ("concentrique"): *Tectonophysics*, 7, p. 57-70.

- Ellsworth, W. L., 1982, A general theory for determining the state of stress in the earth from fault slip measurements: *Terra Cognita*, 2(2), p. 170.
- Eyal, Y., and Reches, Z., 1983, Tectonic analysis of the Dead Sea Rift region since the Late Cretaceous based on mesostructures: *Tectonophysics*, 2, p. 167-185.
- Freund, R., 1974, Kinematics of transform and transcurrent faults: *Tectonophysics*, V21, p. 93-134.
- Frizzell, V. A. Jr., and Zoback, M. L., 1987, Stress orientation determined from fault slip data in Hampel Wash. area, Nevada, and its relation to contemporary regional stress field: *Tectonics*, V6, No2, p. 89-98.
- Garfunkel, Z., 1974, Model for the late Cenozoic tectonic history of the Mojave Desert, California, and for its relation to adjacent regions: *Geological Society of America Bulletin*, v85, p. 1931-1944.
- Geissman, W. J., 1986, Paleomagnetism and strike slip tectonism in the Hoover Dam area, southeast extension of the Lake Mead Fault Zone, Nevada and Arizona: *EOS* V67, No.44 p. 922.
- Hancock, P. L., and Atiya, M. S., 1979, Tectonic significance of the mesofractures systems associated with the Lebanese segment of the Dead Sea transform fault: *Journal of Structural Geology*, 1, p. 143-153.
- Letouzey, J., and Tremolieres, P., 1980, Paleostress around the Mediterranean since the Mesozoic from microtectonic: Comparison with plate tectonic data: *Rock Mech.*, 9, p. 173-192.
- Manton, W. I., 1987, Tectonic interpretation of the morphology of Honduras: *Tectonics*, V6, No5, p. 533-651.
- Marshak, S., Geiser, P. A., Alvarez, W., and Engelder, T., 1983, Mesoscopic fault array of the northern Umbrian Apennine fold belt, Italy: Reactivation of joints by pressure-solution slip: *Geological Society of America Bulletin*, V93, p. 1013-1022.
- Michael, A. J., 1984, Determination of stress from slip data: *Faults and folds: J. Geophys. Res.*, V.89, No11, p. 517-526.
- Nicholson, C., Seeber, L., Williams, P., and Sydes, L. R., 1986, Seismic evidence for conjugate slip and block rotation within the San Andreas Fault system, Southern California: *Tectonics*, V5, No4, p. 629-648.
- Nur, A., Ron, H., and Scotti, O., 1986, Fault mechanics and the kinematics of block

- rotations; *Geology*, V14, p. 746-749.
- Pavrides, S. B., and Kiliyas, A. A., 1987, Neotectonic and active faults along the Serbomacedonian zone (SE Chalkidiki, northern Greece): *Annales Tectonicae*, V1, No2, p. 97-104.
- Pavrides, S. B., Kondopoulou, D. P., Kiliyas, A. A., and Wetphal, M., 1988, Complex deformations in the Serbo-Macedonian assif: Structural and paleomagnetic evidence; *Tectonophysics* 145, p. 329-335.
- Reches, Z., 1987, Determination of the tectonic stress tensor from slip along faults that obey the Coulomb yield condition: *Tectonics*, V6, No6, p. 849-861.
- Rogers, A. M. Harmsen, S. C., Carr, W. J., and Spence, W., 1983, Southern Great Basin seismological data report from 1981 and preliminary data analysis: U. S. Geological Survey, Open File Report 83-669.
- Rogers, A. M., and Lee, W. H. K., 1976, Seismic study of earthquakes in the Lake Mead, Nevada-Arizona region: *Bulletin of the Seismological Society of America*, V66, #5, p. 1657-1631.
- Ron, H., Aydin, A., and Nur, A., 1986, Strike slip faulting and block rotation in the Lake Mead Fault System: *Geology*, V14, p. 1024-1026.
- Ron, H., Freund, R., Garfunkel, Z., and Nur, A., 1984, Block rotation by strike slip faulting: Structural and paleomagnetic evidence: *Journal of Geophysical Research*, V89, NoB7, p. 6256-6270.
- Stamataakos, J. A., Kodama, K. P., and Pavlis, T. L., 1988, Paleomagnetism of Eocene plutonic rocks, Matanuska Valley, Alaska: *Geology*, V16, p. 618-622.
- Wells, Ray. E., and Hillhouse, John, W., 1989, Paleomagnetism and tectonic rotation of the lower Miocene Peach Springs Tuff: Colorado Plateau, Arizona, to Barstow, California.
- Yasuto, I., 1988, Differential rotation of the eastern part of southwest Japan inferred from paleomagnetism of Cretaceous and Neogene rocks: *Journal of Geophysical Research*, V93, No.B4, p. 3401-3411.
- Zoback, M. L., Anderson, R. E., and Thompson, G. A. 1981, Cainozoic evolution of the state of stress and style of tectonism of the Basin and Range province of the western United States: in Vine, F. J. and Smith, A. G., organizers *Extensional tectonics associated with convergent plate boundaries*, Royal Society of London Proceedings, p. 189-216.

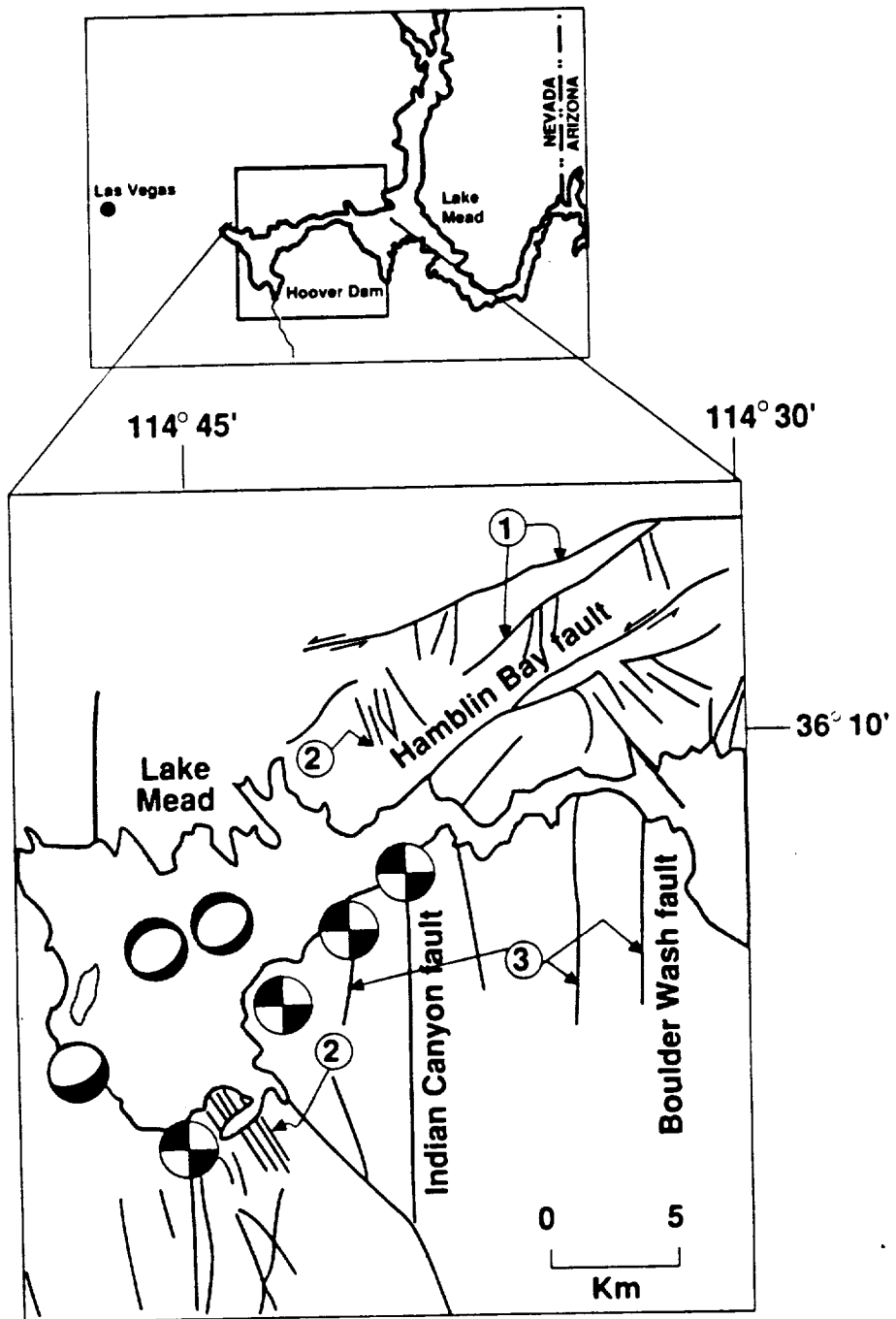
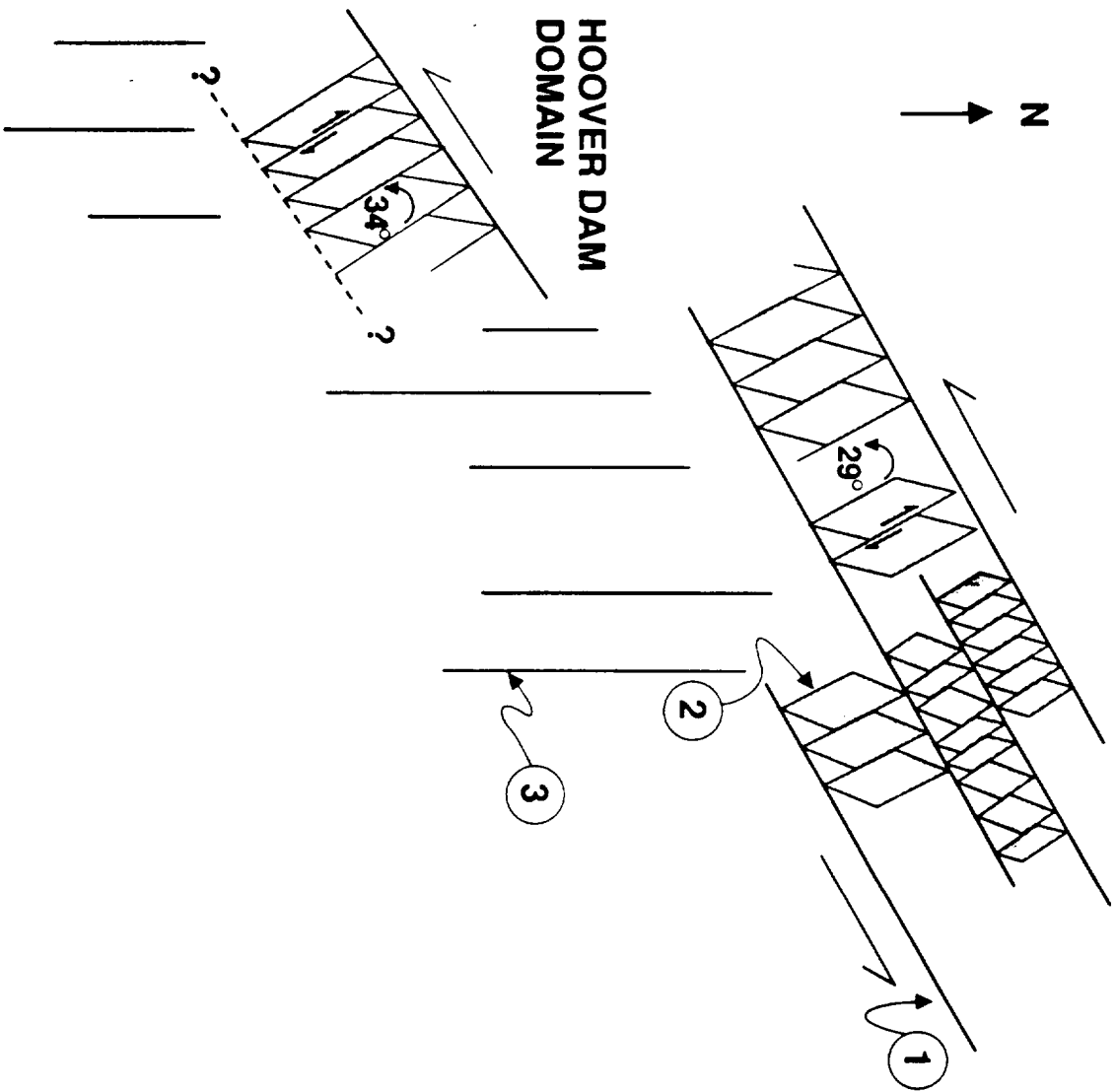
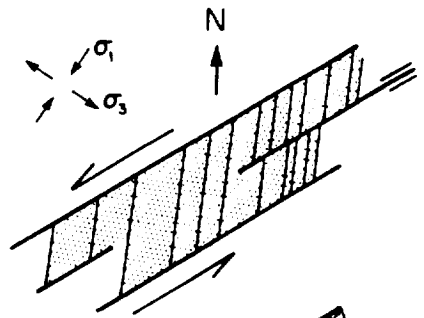


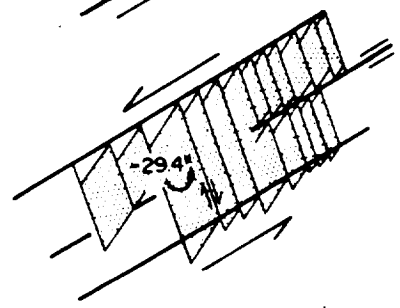
fig 1

# HAMBLIN-CLEOPATRA DOMAINS

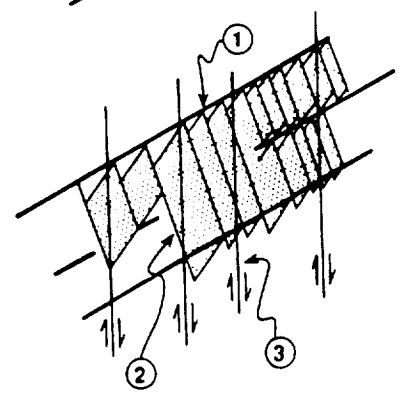




A



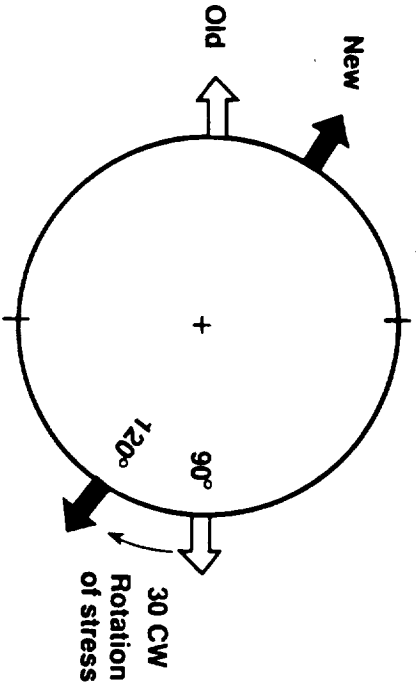
B



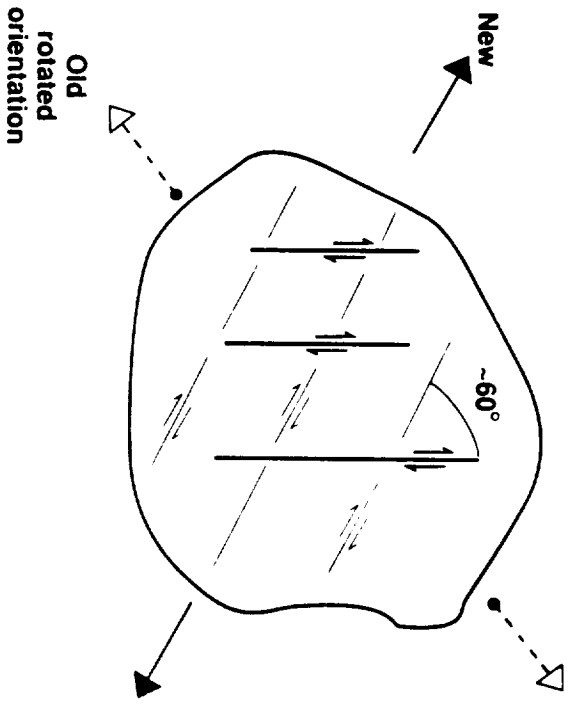
C

fig.

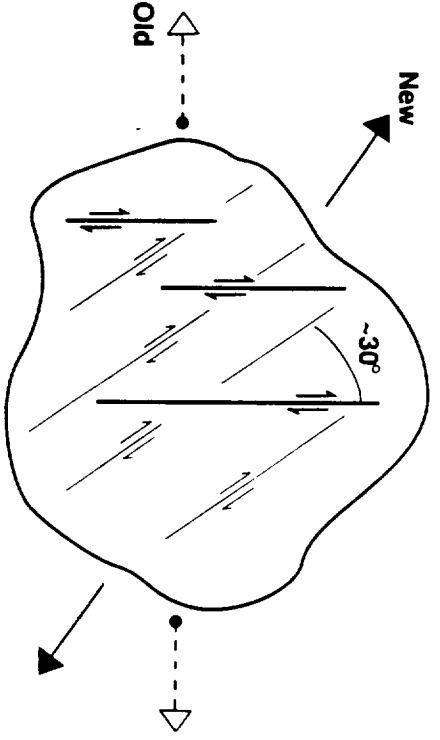
(a) ZOBACK ET AL (1981)



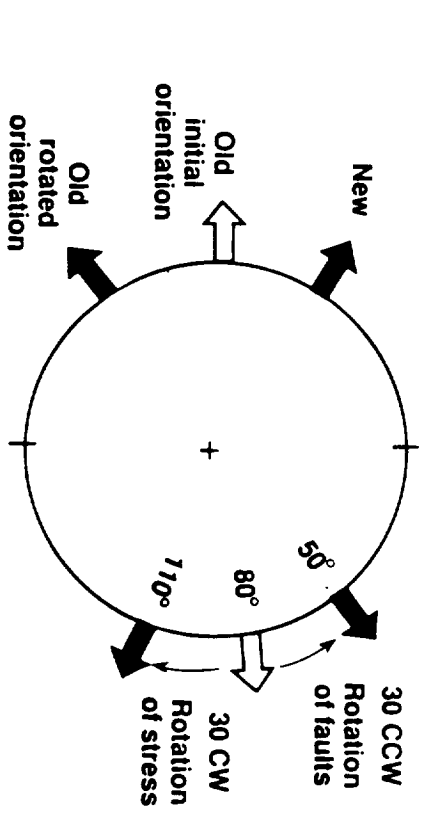
(c) HOOVER DAM AREA  
OF LAKE MEAD FAULT SYSTEM



(b) GENERAL BASIN AND RANGE



(d) INTERPRETATION OF  
ANGELIER ET AL (1985) DATA



294585

259

Submitted to Tectonics - February 14, 1989

N91-14669

**MULTIPLE STRIKE SLIP FAULTS SETS:**

**A CASE STUDY FROM THE DEAD SEA TRANSFORM**

Hagai Ron

The Institute for Petroleum Research and Geophysics

Holon, Israel

Amos Nur

Department of Geophysics, Stanford University, California, USA

Y. Eyal

Department of Geology, Beer Sheva University, Israel

*IK376030*

*307-11-16*

*32-4-1664*

## ABSTRACT

In many strike slip tectonic settings, large rotations of crust blocks about vertical axes have been inferred from paleomagnetic data. These blocks are bounded by sets of parallel faults which presumably accommodate the relative motion between the blocks as regional deformation progress. A mechanical model by Nur et al., (1986) suggests that rotations greater than  $\phi_c = 25^\circ$  to  $45^\circ$  must be accommodated by more than one set of faults, with angle  $\phi_c$  between their direction, consequently the sum of the angles between sets must be roughly equal to the total tectonic material rotation. To test this model we investigated the fault geometry and field relation of fault sets in the Mt. Hermon area in northern Israel, where paleomagnetic declination implies data  $69^\circ \pm 13^\circ$  counterclockwise block rotation. The statistical and field relation analysis of over 315 faults shows that the faulting is predominantly right lateral strike slip consisting of three distinct sets. The oldest set strikes  $253^\circ$ , the second oldest set strikes  $293^\circ$  and the youngest strikes  $339^\circ$ . This last direction is consistent also with the current north-south direction of the maximum principle stress axis. The angle  $\phi_c$  between the first and second sets is  $39^\circ$  and between the second and third sets  $46^\circ$ , in good agreement with the  $\phi_c$  angle predicted from mechanical considerations. The sum of the two angles is  $85^\circ$  CCW, in good agreement with the  $69^\circ \pm 13^\circ$  CCW paleomagnetically derived rotation. The results suggest specifically that the sequential development of multiple intersecting fault sets is responsible for the faulting in the Mt. Herman area; and generally that the model of block rotation with multiple faults provides very good simple rules for analyzing very complex fault patterns.

## INTRODUCTION

In a seminal paper, Freund (1974) explored the kinematics of rotations of crustal blocks bounded by faults in sets. In his analysis, Freund has shown that the *sense* of

these rotations is controlled by the orientation of the faults within a given set relative to the principal direction of tectonic shortening, whereas the *magnitude* of the rotation of crustal blocks and their bounding faults is related to the magnitude of crustal shortening or extension.

There is growing evidence that block rotation due to crustal shortening and extension is widespread: For example, Ron et al. (1984) showed that adjacent domains of clockwise and counterclockwise rotations occur in the same tectonic setting of northern Israel, depending on the orientation of the active faults. Similar models were given for the Mojave area in California (Garfunkel, 1974), central America, (Manton, 1987), Alaska (Stamatokos et al., 1988), the Lake Mead, Nevada, region (Ron et al., 1986).

Freund's model implies that as blocks rotate, their bounding faults rotate away from their optimal direction of slip. When this rotation becomes sufficiently large, these faults lock up (Nur et al., 1986). Further crustal deformation must then be accommodated by a set of new faults, more favorably oriented to the principal direction of regional deformation. As a result, domains of multiple sets must form in which the younger faults systematically offset the older ones. The existence of such multiple sets thus provides a rigorous test for Freund's block rotation model. Although a few cases of multiple sets have been studied (Nur et al., 1986, Ron et al., 1986, Nur et al., in press), the evidence is still sparse. The purpose of this paper is to report on a new case of multiple fault sets and the evidence that they were formed sequentially through the process of large rotations of blocks in domains.

## KINEMATICS AND STRESS ON ROTATING FAULTS

A key aspect of Freund's model is that blocks rotate counterclockwise (CCW) when slip is right handed, and clockwise (CW) when slip is left handed. When several

domains of fault sets exist - left and right handed, the model predicts relative rotations between the CCW and CW domains. It was shown by Nur et al., (1986) that when a fault set rotates away from the original and optimal direction of failure  $\varnothing_0$  relative to the maximum stress, the shear stress acting on the fault plane decreases and the normal stress increases until it becomes locked. Thus, beyond a critical angle of rotation  $\varnothing_c$  a new fault set is required more favorably oriented relative to the stationary direction of maximum stress. The faults in this new set will offset (Figure 1) the now locked faults of the older set.

The value of the predicted angle  $\varnothing_c$  between the old and new fault directions was shown by Nur et al., (1986) to fall in the range of  $25^\circ$  up to  $45^\circ$ , for the extreme cases of coefficient of friction  $\mu = 0$  or fracture strength to rock strength ratio  $S_1/S_0 = 0$ . The value  $\varnothing_c = 45^\circ$  is the upper premissible limit of block rotation (from the optimal failure direction which can be accommodated by a single set of faults).

The values  $\varnothing_c = 25^\circ$  to  $45^\circ$  are significantly lower than many reported rotations inferred for rocks insitu from paleomagnetic declination anomalies. If the analysis of Nur et al., (1986) is correct, than paleomagnetically derived rotations larger than  $45^\circ$  must involve more than one set of rotating faults. The existence of multiple sets in situ would, therefore, provide a direct test of the entire block rotation concept.

To test the model, we have carried out a detailed structural study of a carefully selected area in the Mt. Hermon region of northern Israel. Previously obtained paleomagnetic declination data in this region (Ron 1987) indicate a  $69^\circ \pm 13^\circ$  counter-clockwise rotation. The hypothesis to be tested in this paper is whether the deformation associated with this rotation was accommodated by more than one set of faults. These faults must show right lateral strike slip and angles  $\varnothing_c$  between them must fall in the range  $25^\circ$  to  $45^\circ$  or so.

## REVIEW OF PALEOMAGNETIC RESULTS

Paleomagnetic results from the Mt. Hermon regions at the restraining bend of the Dead Sea transform plate margins were obtained by Gregor (1974) and Ron (1987) repetitively. The results have clearly demonstrated that crustal deformation was accommodated by horizontal fault and block rotation (Figure 2a). The data was obtained from both sides of the plate boundary: Paleomagnetic results from Early Cretaceous volcanic rocks obtained from Lebanon to the west, reveal anomalous paleomagnetic declinations which imply  $55.6^{\circ} \pm 10.4^{\circ}$  *counterclockwise* rotation about a vertical axis (Gregor et al., 1974) - Ron's (1987) study in the Mt. Hermon area to the east yield a similar anomalous paleomagnetic declination with a  $69^{\circ} \pm 13^{\circ}$  *counterclockwise* rotation about a vertical axis.

Two relevant links to the multiple fault set model are obvious: If block rotate a la Freund then the counterclockwise *sense* of rotation must be associated with right lateral strike slip (Freund, 1974, Ron et al., 1984), and the larger than  $25^{\circ}$  to  $45^{\circ}$  *magnitude* of rotation requires that more than one set of right lateral faults is involved in the rotation (Nur et. al., 1986).

## STRUCTURAL STUDY

Mt. Hermon is situated at an oblique segment of the Dead Sea transform (Figure 2a) in a configuration similar to the transverse ranges in Southern California. This geometry gives rise to a transpressive regime normal to the plate boundary (Freund et al., 1970; Hancock and Atiya, 1979, Garfunkel, 1981) involving both folds and faults. The magnitude of shortening achieved by folding is only about 10% of the total shortening anticipated as a consequence of the left lateral displacement along the north-south Dead Sea transform colliding against the northeast trending Yammuneh segment (Figure 2a). Most of the deformation has presumably been accommodated by the

intricate network of west to north-west trending right lateral strike slip faults (Figures 2b, c; Ron, 1987). Because of good fault exposure and the existence of paleomagnetic data, this area was selected by us for a detailed study to determine in situ fault plane orientations, fault rakes (slip vectors), and the sense of displacements, to determine whether faulting here is by multiple sets of faults which cross cut each other as expected from the block rotation model.

Data obtained from 315 faults include fault plane dip and strike, trend and plunge of the fault rake (fault slip vector) and sense of displacement whenever possible using field criteria such as discussed by Eyal and Reches (1983) and Angelier et al., (1985).

### GEOMETRICAL ANALYSIS OF FAULT PATTERNS

We consider four aspects of the fault population data (a) the lower hemisphere projection of normals to the fault planes; (b) rose diagrams of pole trends; (c) rose diagrams of fault dips; and (d) rose diagram of fault rakes (Figure 3, a to d).

The results show that over 80% of the mapped faults are vertical or subvertical with horizontal or subhorizontal rakes, and are therefore strike slip faults. The orientation distribution (Figure 3a, b) however, does not reveal clear clustering of fault types. Consequently we have next deleted all those faults for which the sense of slip is unknown. The remaining faults were then separated statistically into right slip and left slip groups. Fault normal distribution for the right lateral (Figure 4a) and for the left lateral (Figure 6a) faults were next plotted to show the number and orientation distribution of these faults. The trend distributions of both the right lateral (Figure 4b) and left lateral (Figure 6b) faults reveal that each group consists of three distinct sub groups or sets: The orientation and the statistical parameters of each right lateral fault sub group, calculated using Fisher's (1953) statistics are summarized in Figures 5 and 7 and in Table 1.

The results reveal that the right lateral faults make up over 70% of all the mapped faults, suggesting that most of the deformation in this area was accommodated by right lateral slip. This is in good agreement with the earlier model by Ron (1987) which requires that the dominant crustal deformation here is by right lateral slip on distributed fault sets. The results are of course consistent also with paleomagnetic data which imply from declination anomalies counterclockwise rotation (Figure 2b, c).

### CROSS CUTTING RELATIONS

How are the three sets of right lateral strike slip faults related? The presence of three distinct sets of right lateral strike slip faults (Figure 10a) does not by itself verify that they are multiple sets. To fit our definition of multiple sets the following relations exist insitu:

- a) cross-cutting between the sets must be sequential as illustrated in Figure 1.
- b) The angle between the youngest and oldest sets must have the same sense and the same magnitude as the paleomagnetically inferred total rotation.

To nail down the time relationship between the sets we chose an exceptionally well exposed outcrop near Neve Ativ, (NA) of about 500 m<sup>2</sup> in which excellent fault data were collected. Analysis of the faults in this outcrop was performed (Figures 8 and 9 and Table 1) yielding very similar results (Figure 10b). to the entire Mt. Hermon area (Figure 10a), This suggests that the outcrop is fairly representative of the entire region, the cross-cutting relations of the three right lateral sets of faults NA1, NA2, and NA3 in this outcrop were carefully determined:

- a) The faults in the 256° trending set (NA-1) are always offset by the faults of the 333° trending set (NA-3).

b) The faults in 283° trending set (NA-2) offset the faults of the 256° trending set (NA-1) and form boudins of calcite fill of these faults.

These cross cutting relations imply that the oldest of the sets strikes 256°, the second oldest strikes 283° and the youngest strikes 333°. Furthermore the orientation of the youngest set is coincident with the optimal present direction of faulting associated with the current north-south maximum horizontal compression (Ben Menahem et al, 1976; Joffe and Garfunkel, 1987).

As shown earlier, Nur's et al., (1986) block rotation model predicts that the angle between two consecutive sets of faults should fall in the range of 25° to 45°. Our field results yield a mean angle  $\phi_{12} = 39^\circ$  between the first and second sets, and the  $\phi_{23} = 46^\circ$  between the second and third sets (see Table 1) in good agreement with the values predicted by the mechanical model of rotating faults. It is noteworthy that the angle between the second and third sets is about the maximum value permitted. This high value may be due to low effective normal stress, perhaps associated with high pore pressure during this deformational phase.

Finally, the sum of the two angles  $\phi_{12}$  and  $\phi_{23}$  is 85°, a value which is in reasonable agreement with the paleomagnetically derived total rotation of  $69^\circ \pm 13^\circ$  (Ron, 1987).

## SUMMARY

In the study reported here we combined paleomagnetic and structural data to test in the Mt. Hermon area the validity of our model for the formation of multiple sets by the rotation of faults and blocks. The model predicts four features to the study area.

- a) Crustal deformation is accommodated by right lateral strike slip faults
- b) The observed paleomagnetic rotation requires at least two, and possibly three, sets of faults.

- c) The angle  $\theta_c$  between the sets of faults should be in the range of  $25^\circ$  to  $45^\circ$ .
- d) The angle between the oldest and youngest sets of faults has the same sense of, and is equal to the measured paleomagnetically derived total rotation.

The structural data show that fault slip is predominantly right lateral strike slip, consisting of three fault sets, with an angle of  $39^\circ$  between sets 1 and 2 and  $46^\circ$  between sets 2 and 3. The total structural rotation which is the sum of these two angles, is  $85^\circ$ . This value compares favorably with the  $69^\circ \pm 13^\circ$  of counterclockwise paleomagnetically derived rotation.

We conclude that the seemingly complex distributed strike slip fault pattern in the Mt. Hermon area is the result of large block rotations, which gave rise to three consecutive multiple fault sets. In this process older faults are systematically offset by younger sets, having identical slip sense.

The results are probably indicative of a general process of formation of multiple intersecting fault sets in the earth's crust. The multiple set model provides a simple and rational method for analyzing some very intricate fault patterns which, at first glance, appear very complicated and are often assumed to require an incredibly complex stress history to explain their formation.

## REFERENCES

- Angelier, J., 1985, Tectonic analysis of fault slip data sets. *J. Geophys. Res.*, 89, p. 5835-5848.
- Ben Menhem, A., Nur, A., and Vered, M., 1976, Tectonics, seismicity and structure of the Afro-Eurasian junction - the breaching of an incoherent plate. *Phy. of the Earth and Planet. Inter.*, 12, p. 1-50.
- Byerlee, J. D., 1978, Friction of rock. *Pure and Appl. Geophys.*, 116, p. 615-626.
- Eyal, Y., and Reches, Z., 1983, Tectonic analysis of the Dead Sea Rift region since the Late Cretaceous based on mesostructures. *Tectonics*, 2, p. 167-185.
- Fisher, R. A., 1953, Dispersion on a sphere. *Proc. R. Soc., London, Ser. A*, 217, p. 295-305.
- Freund, R., Garafunkel, Z., Zak, I., Goldberg, M., Weissbrod, T., and Derin, B., 1970, The shear along the Dead Sea Rift. *Philos. Trans. R. Soc., London, Ser. A.*, A267, p. 107-130.
- Freund, R., 1974, Kinematics of transform and transcurrent fault. *Tectonophysics*, 21, p. 93-134.
- Gans, P. D., and Miller, E. I., 1983, Style of mid-Tertiary extension in east central Nevada, in Guidebook part 1, Geological Society of American Rock

Mountain and Cordilleran Section Meeting, Utah. Geology and Mining Survey Special studies, V. 59, p. 107-160.

Garfunkel, Z., 1974, Model for the late Cenozoic tectonic history of the Mojave Desert, California and its relation to adjacent areas. Geological Society of America Bulletin, V.85, p. 1931-1944.

Garfunkel, Z., 1981, Internal structure of the Dead Sea leaky transform (rift) in relation to plate kinematics. Tectonophysics, 80 (1-4), p. 84-108.

Gregor, C. B., Mertzman, S., Narin, A. E. M., and Negendank, J., 1974, Paleomagnetism of some Mesozoic and Cenozoic volcanic rocks from the Lebanon. Tectonophysics, 21, p. 375-395.

Hancock, P. L., and Atyla, M. S., 1979, Tectonic significance of the mesofractures systems associated with the Lebanese segment of the Dead Sea Transform Fault. J. Struct., Geol., 1, p. 143-153.

Jaeger, J. D., and Cook, N. G. W., 1976, Fundamentals of rock mechanics. John Wiley & Sons Inc., New York, p. 585.

Joffe, S., and Garfunkel, Z., 1987, Plate kinematics of the circum Red Sea; a re-evaluation. Tectonophysics, 141, p. 5-22.

Menton, W. I., 1987, Tectonic interpretation of the morphology of Honduras. Tectonics, V. 6, No.5, p. 633-651.

- Nicholson, C., Seeber, L., Williams, P. L., and Sykes, L. R., 1986, Seismicity and fault kinematics through the eastern Transverse Range, California block rotation, strike slip faulting and low angle thrusts. *Journal of Geophysical Research*, V. 91, p. 4891-4898.
- Nur, A., Ron, H., and Scotti, O., 1986, Fault mechanics and the kinematics of block rotation, *Geology*, 14, p. 746-749.
- Proffett, J. M., Jr., 1977, Cenozoic geology of the Yerington district, Nevada and implications for the nature and origin of Basin and Range faulting. *Geological Soc., of American Bull.*, 88, p. 247-266.
- Ron, H., 1987, deformation along the Yammuneh, the restraining bend of the Dead Sea. Transform; paleomagnetic and kinematic implications. *Tectonics*, 6, p. 653-666.
- Ron, H., Aydin, A., and Nur, A., 1986, Strike-slip faulting and block rotation in the Lake Fault system. *Geology*, V.14, p. 1020-1023.
- Ron, H., Freund, R., Garfunkel, Z., and Nur, A., 1984, Block rotation by strike slip faulting; structural and paleomagnetic evidence. *Journal of Geophysical Research*, 89, p. 6265-6270.
- Stamatakos, J. A., Kodama, K. P., and Pavlis, T. L., 1988, Paleomagnetism of Eocene plutonic rocks, Matanusak Valley, Alaska. *Geology*, V.16, p. 618-622.

Terres, R. R., and Luyendyk, B. P., 1985, Neogene tectonic rotation of the San Gabriel region, California, suggested by paleomagnetic vector. *Journal of Geophysical Research*, V. 90, p. 12467-12484.

## FIGURE CAPTIONS

Figure 1. Block rotation model of multiple strike slip sets, showing a new fault set required to accommodate block rotation greater than  $45^\circ$ . The angle  $\varphi_0$  is the initial angle of the first set and  $\varphi_c$  is the angle between the first and second new sets (after Nur et. al., 1986).

Figure 2. General plate tectonic setting of the study area (a) and conceptual geometrical reconstruction of faulting and rotation of the investigated area (b) before fault slip and (c) after fault slip.

Figure 3. Equal area projection of poles and rose diagrams of all faults in the Mt. Hermon area.

Figure 4. Equal area projection and rose diagram of all right lateral strike slip faults in Mt. Hermon area.

Figure 5. Equal area projection of all right lateral strike slip faults in the Mt. Hermon area after separation into three distinct populations.

Figure 6. Equal area projection and rose diagram of all left lateral strike slip faults in the Mt. Hermon area. All faults and planes were projected to the west.

Figure 7. Equal area projection of all left lateral strike slip faults in the Mt. Hermon area after separation into three distinct populations.

**Figure 8. Equal area projection and rose diagram of all right lateral strike slip faults in Neve Ativ (NA) outcrops.**

**Figure 9. Equal area projection of all right lateral strike slip faults in Neve Ativ (NA) area after separation into three distinct populations. Separation was based on crosscut field relation of the faults.**

**Figure 10. Mean plane for the three right lateral fault population of (a) NA outcrop and (b) Mt. Hermon area. Mean poles were plotted with the circle of A95 confidence.  $\varnothing_c$  is the angle between the fault sets.**

## SUMMARY OF STRUCTURAL DATA

AREA	FAULT SET	FAULT STRIKE	FAULT DIP	A95	ANGLUAR SD	N	$\phi_c$
<b>REGIONAL</b>							
Hermon	1st.	253	89	6	20	49	39
Hermon	2nd.	293	86	6	20	49	46
Hermon	3rd.	339	83	7	24	51	
<b>LOCAL</b>							
NA1	1st.	256	82	5	22	26	27
NA2	2nd.	283	88	10	21	25	47
NA3	3rd.	330	80	7	16	15	

Table 1. Statistical parameters of the right lateral strike slip faults on the study area. N is the number of faults in each population. A95 is the 95% confidence about the mean and  $\phi_c$  is the angle between the fault sets. Hermon-regional includes all right lateral faults in the study area. Neve Ativ-local includes only faults of this local outcrop.

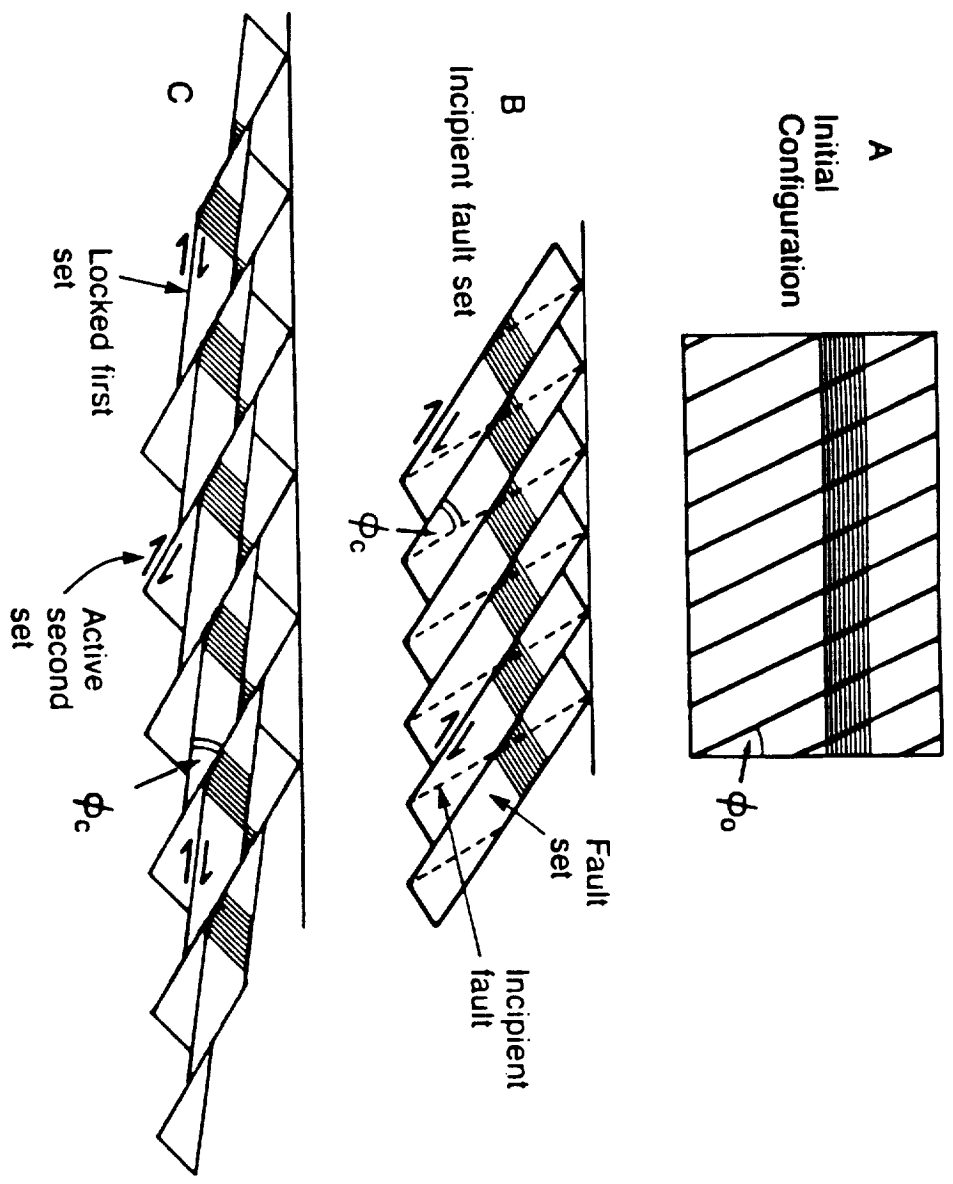


Fig 1

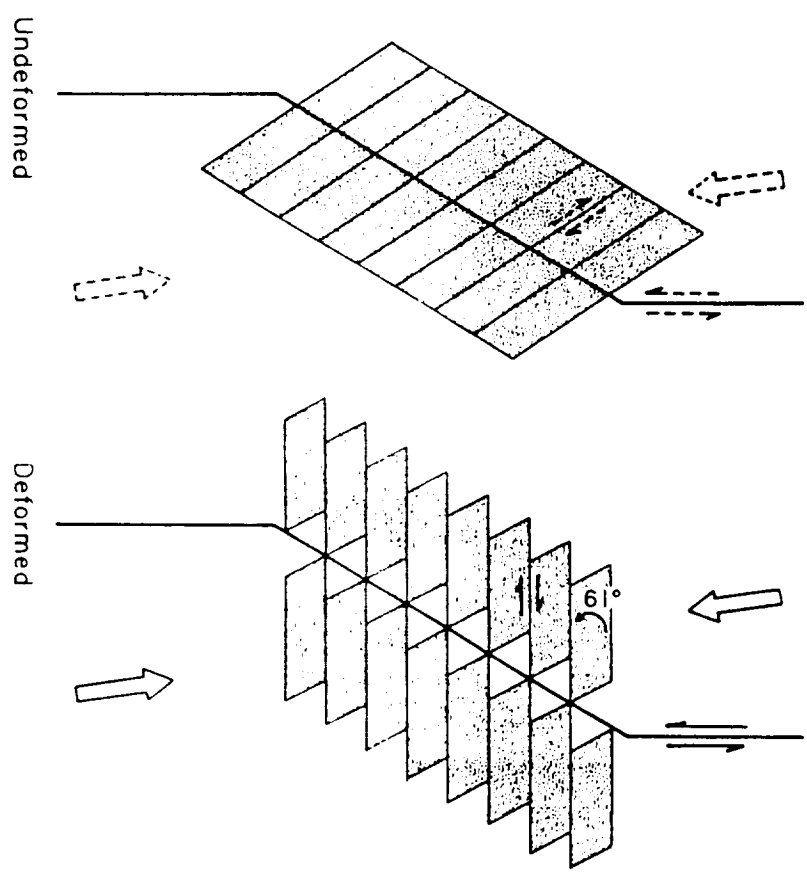
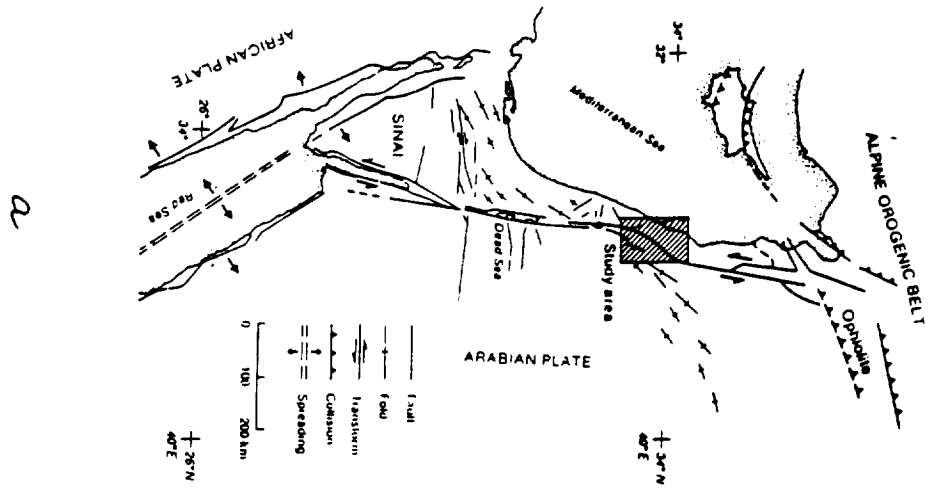
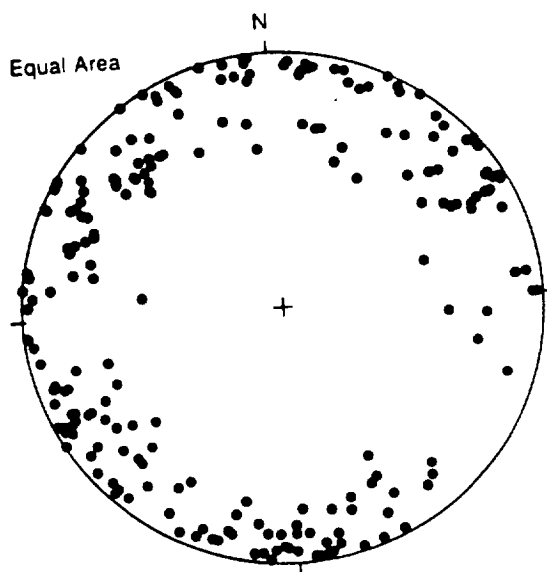
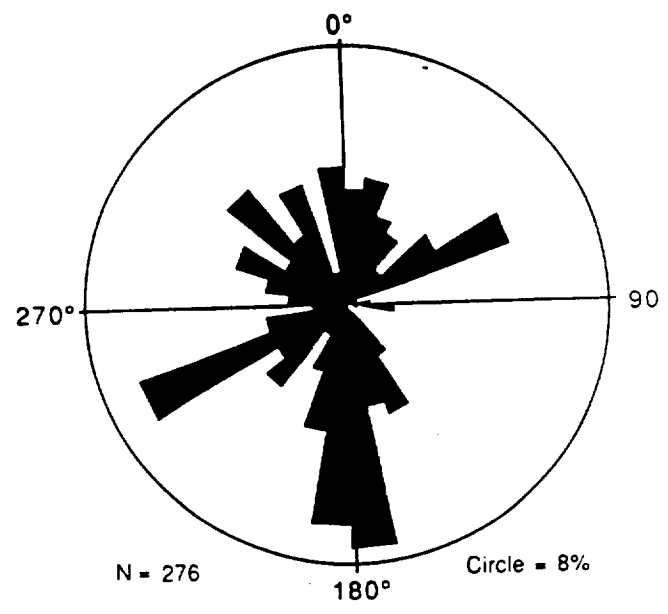


Fig 2

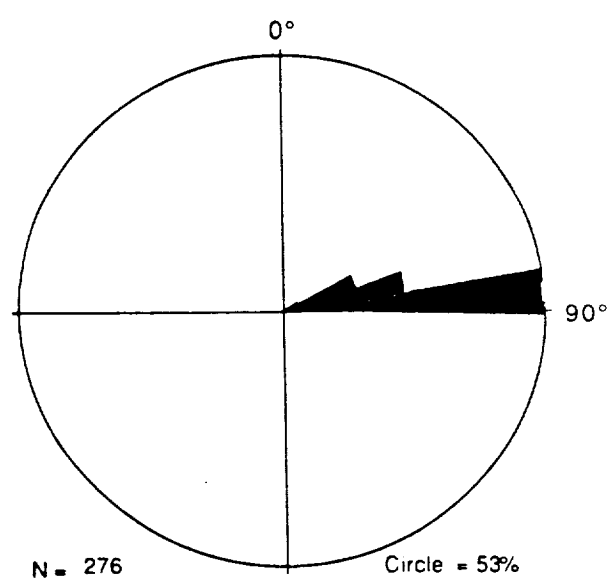
ORIGINAL PAGE IS OF POOR QUALITY



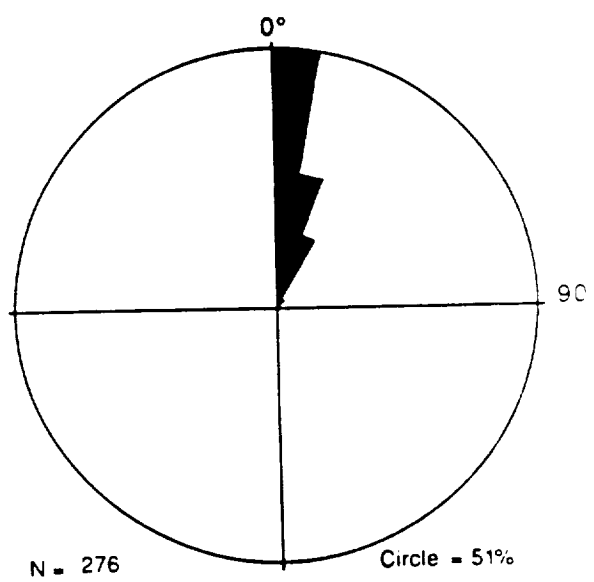
HERMON - POLE DISTRIBUTION OF ALL FAULTS



ROSE DIAGRAM OF POLE TREND: HERMON - ALL FAULTS



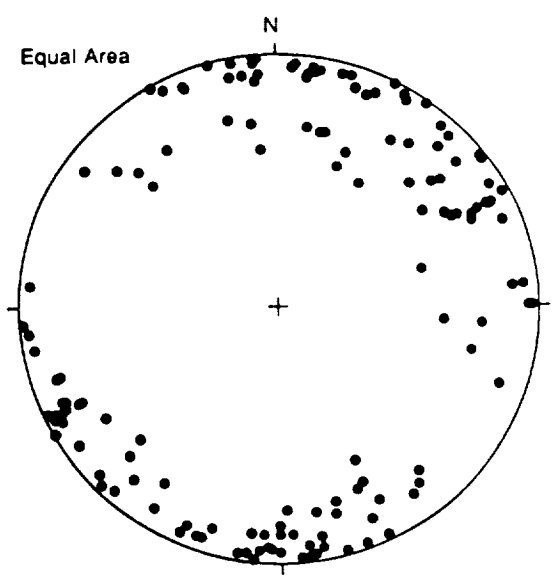
ROSE DIAGRAM OF DIP ANGLE FOR HERMON - ALL FAULT PLANES



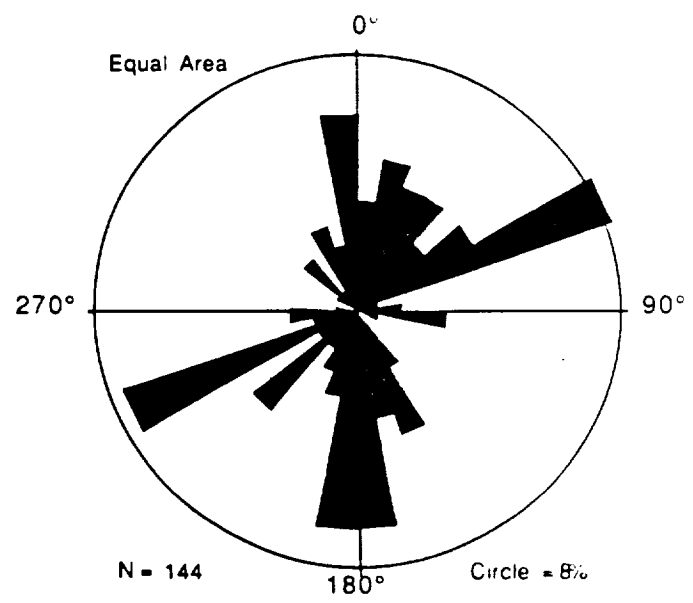
ROSE DIAGRAM OF DIP ANGLE FOR HERMON - RAKE OF ALL FAULTS

fig 3

ORIGINAL PAGE IS OF POOR QUALITY



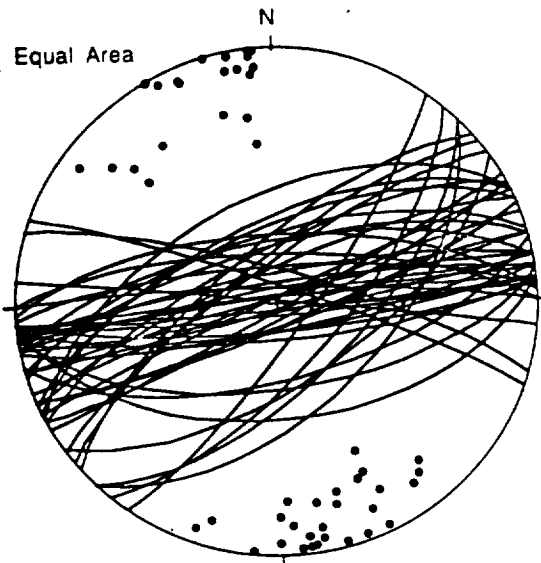
DISTRIBUTION OF POLE FOR  
HERMON - ALL RIGHT LATERAL SSF



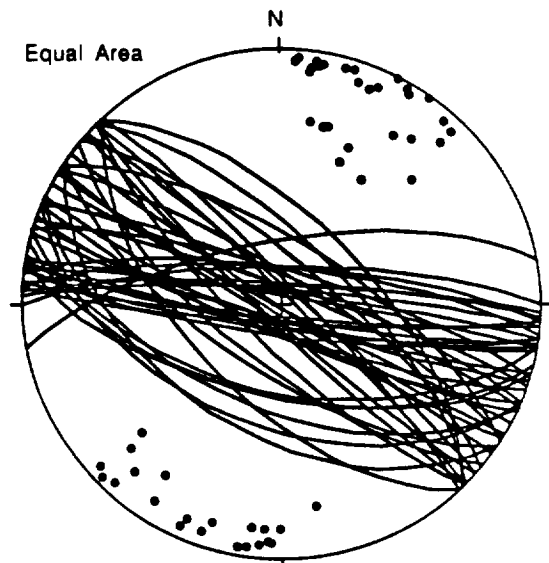
ROSE DIAGRAM OF POLE TREND FOR  
HERMON - ALL RIGHT LATERAL SSF

ORIGINAL PAGE IS  
OF POOR QUALITY

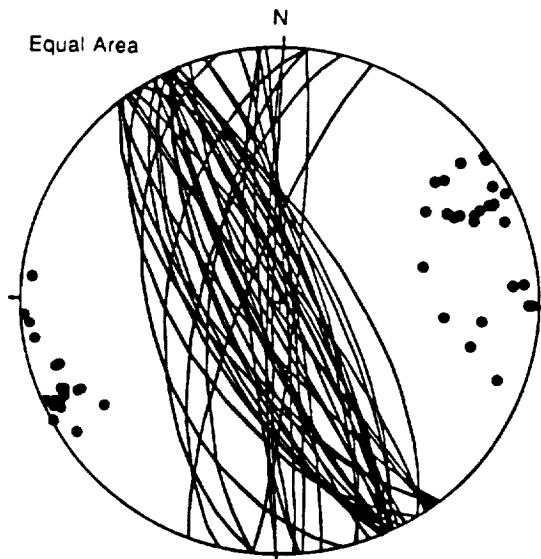
fig 4



DISTRIBUTION OF PLANES AND POLES FOR:  
HERMON - 1ST SET OF RIGHT LATERAL SSF



DISTRIBUTION OF PLANES AND POLES FOR:  
HERMON - 2ND SET OF RIGHT LATERAL SSF



DISTRIBUTION OF PLANES AND POLES FOR:  
HERMON - 3RD SET OF RIGHT LATERAL SSF

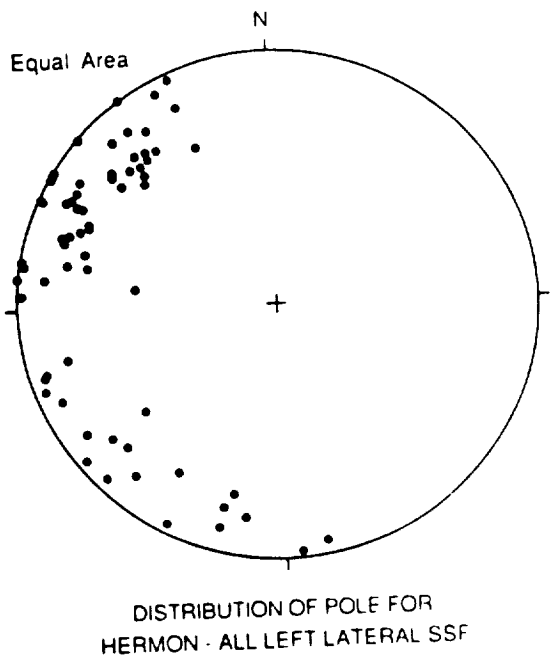
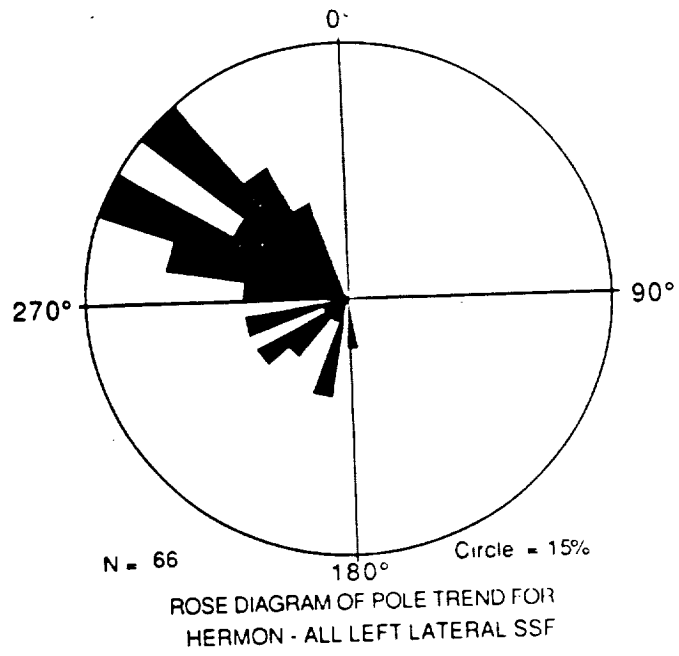
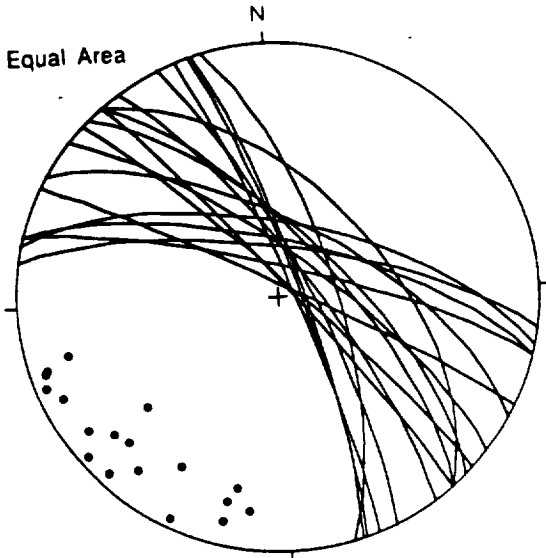
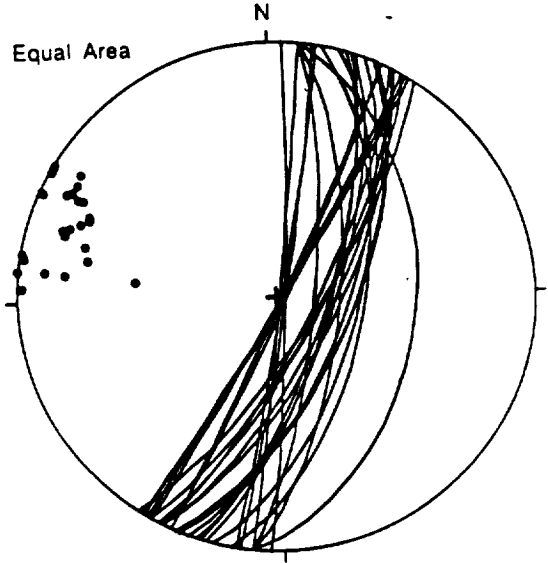


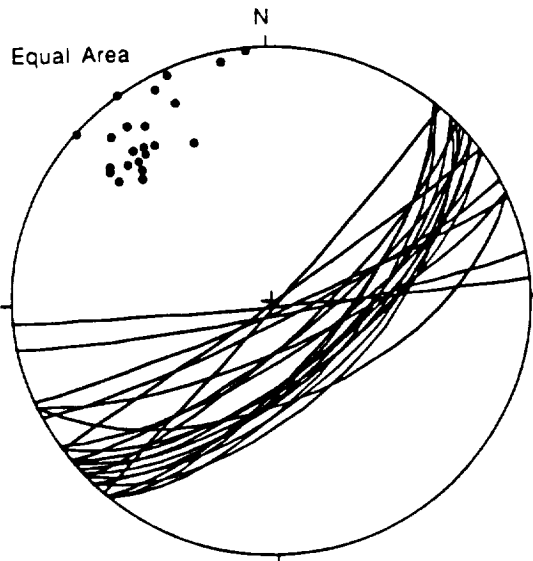
fig 6



DISTRIBUTION OF PLANES AND POLES FOR:  
HERMON - 1ST SET OF LEFT LATERAL SSF

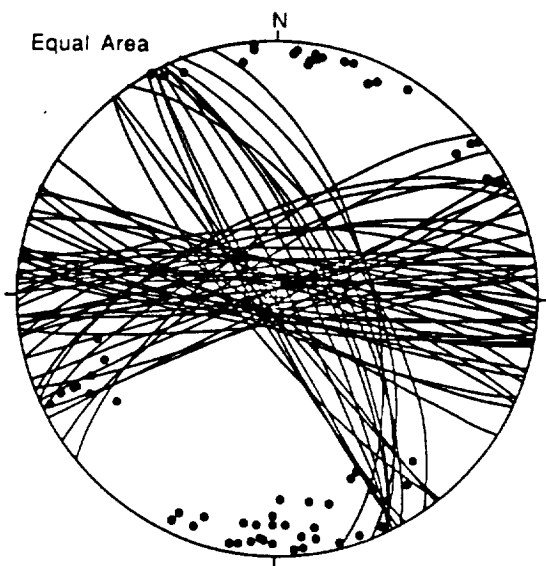


DISTRIBUTION OF PLANES AND POLES FOR:  
HERMON - 2ND SET OF LEFT LATERAL SSF

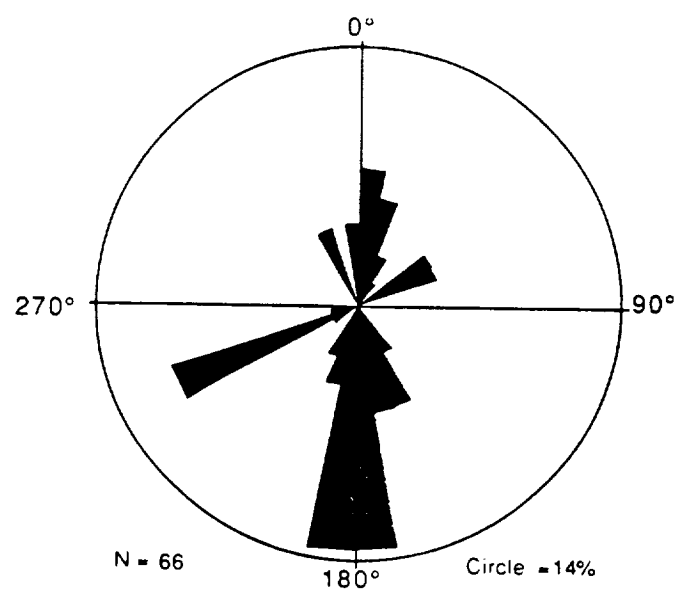


DISTRIBUTION OF PLANES AND POLES FOR:  
HERMON - 3RD SET OF LEFT LATERAL SSF

fig 7

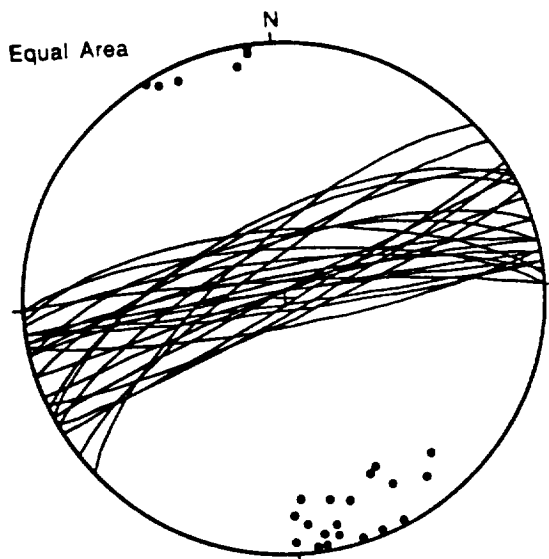


DISTRIBUTION OF PLANES AND POLES FOR:  
NEVE ATIV - ALL RIGHT LATERAL SSF

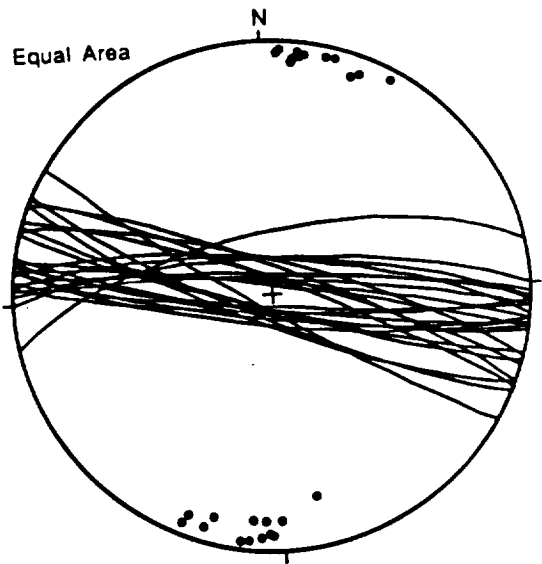


ROSE DIAGRAM OF POLE TREND DISTRIBUTION:  
NEVE ATIV - ALL RIGHT LATERAL SSF

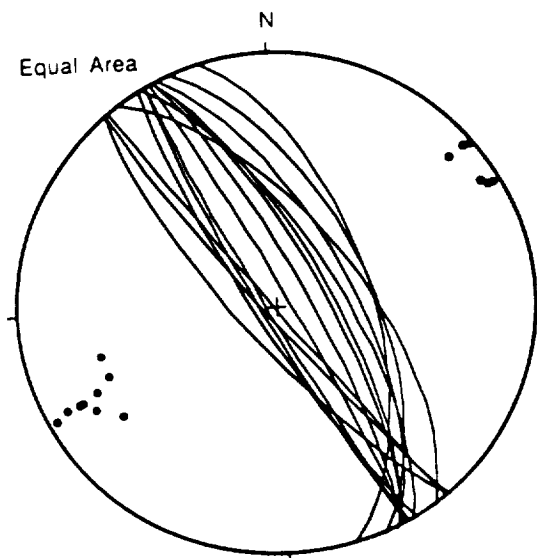
*fig 8*



DISTRIBUTION OF PLANES AND POLES FOR:  
NEVE ATIV - 1ST SET OF RIGHT LATERAL SSF



DISTRIBUTION OF PLANES AND POLES FOR:  
NEVE ATIV - 2ND SET OF RIGHT LATERAL SSF



DISTRIBUTION OF PLANES AND POLES FOR:  
NEVE ATIV - 3RD SET OF RIGHT LATERAL SSF